



HAL
open science

Human postural stability analysis : application to Parkinsonian subjects

Khaled Safi

► **To cite this version:**

Khaled Safi. Human postural stability analysis : application to Parkinsonian subjects. Signal and Image Processing. Université Paris-Est; Université Libanaise, 2016. English. NNT : 2016PESC1066 . tel-01546084

HAL Id: tel-01546084

<https://theses.hal.science/tel-01546084>

Submitted on 23 Jun 2017

HAL is a multi-disciplinary open access archive for the deposit and dissemination of scientific research documents, whether they are published or not. The documents may come from teaching and research institutions in France or abroad, or from public or private research centers.

L'archive ouverte pluridisciplinaire **HAL**, est destinée au dépôt et à la diffusion de documents scientifiques de niveau recherche, publiés ou non, émanant des établissements d'enseignement et de recherche français ou étrangers, des laboratoires publics ou privés.



École doctorale MSTIC & École doctorale EDST
Laboratoire LISSI & Centre AZM pour la recherche en
biotechnologie

THÈSE EN COTUTELLE

présentée en vue de l'obtention du grade de
**DOCTEUR DE L'UNIVERSITÉ PARIS-EST &
L'UNIVERSITÉ LIBANAISE**

Par
Khaled SAFI

**Méthodes d'analyse de la stabilité posturale chez l'homme. Application aux
sujets Parkinsoniens**

Human Postural Stability Analysis. Application to Parkinsonian Subjects

Spécialité : Image, signal, automatique & Bioinformatique

Soutenue publiquement le 14 Décembre 2016, devant le jury composé de :

Rapporteur	Prof. Eric Moreau	Université de Toulon
Rapporteur	Prof. Jean-Luc Zarader	Université Pierre et Marie CURIE
Examinatrice	Prof. Catherine Marque	Université de Technologie de Compiègne
Examinatrice	Prof. Latifa Oukhellou	IFSTTAR
Co-encadrant	Dr. Samer Mohammed	Université Paris Est Créteil
Co-directeur	Prof. Mohamad Khalil	Université Libanaise
Directeur	Prof. Yacine Amirat	Université Paris Est Créteil

Acknowledgements

First, and before i begin to write this manuscript, i would like with sincere gratitude to thank everyone who encourages me to complete my studies and pave the way to my success.

I express my sincere appreciation to the committee members Mrs. Catherine Marque, professor in the UTC university, Mr. Jean-Luc Zarader Professor at UPMC university, Mr. Eric Moreau professor at university of Toulon, and Mrs. Latifa Oukhellou, research director at IFSTTAR, for having accepted to judge this research work as rapporteurs and examiners on the jury.

A profound thanks to my directors "Prof. Yacine Amirat & Prof. Mohamad Khalil" who played a pivotal role to complete this project. I would like also to thank them for their welcome, patience, guidance, encouragement and for the information they have provided.

Special thanks to my supervisor "Dr. Samer Mohammed" whose goals always aim for our success and advancement. Also, i thank him for his acceptance and encouragement to press ahead with this project despite its importance and difficulty. Many thanks to "Dr. Ferhat Attal" for his support in the machine learning field.

Foremost, we would like to acknowledge the LASER for their financial support, for which we are truly grateful. We also appreciate the financial aid given by the Danniyeh municipalities union, the doctorate school ED-MSTIC of Paris-Est University and the campus France.

Thanks also go to my friends and colleagues Firas, Youssof, Ahmad, Said, Yacine, and Nicolas for their support and for the good times we spent together during these years. Its great to have friends like you joining my way and life.

Finally, my deepest gratitude goes to my parents for their continuing support, encouragement and inspiration throughout my studies. I hope for all of them an eternal happiness, health and continuous donation.

Khaled Safi

Table des matières

Acknowledgements	i
List of Figures	v
List of Tables	vii
Abbreviations	ix
1 GENERAL INTRODUCTION	4
2 THE HUMAN POSTURAL STABILITY ANALYSIS	9
2.1 Introduction	10
2.2 The human postural system	10
2.2.1 Definition	10
2.2.2 The main components of the postural system	11
2.2.2.1 Ocular sensor	11
2.2.2.2 Vestibular system	12
2.2.2.3 The base of support : the foot	13
2.2.2.4 Central regulation system	14
2.2.2.5 Motor response	15
2.2.3 The primary strategies to maintain stability	15
2.3 Tools for evaluating postural stability	16
2.3.1 Postural recording systems	16
2.3.1.1 Video-based methods	17
2.3.1.2 Body-worn inertial sensors-based methods	18
2.3.1.3 Force platform-baed methods : the stabilometer	19
2.3.2 Protocols for COP displacements recordings	22
2.3.3 Clinical stabilometry standardization	23
2.4 Postural stability analysis techniques	24
2.5 Conclusion	29
3 EMD-BASED APPROACH FOR POSTURE ANALYSIS	32
3.1 Introduction	33
3.2 Stabilometric data acquisition protocol	33
3.3 Empirical Mode Decomposition and its variant Ensemble Empirical Mode decomposition	36
3.3.1 EMD basics	37

3.3.2	Sifting process	38
3.3.3	Stopping criteria	38
3.3.4	Ensemble Empirical Model Decomposition	41
3.4	Stabilogram-diffusion analysis	42
3.4.1	Brownian motion	42
3.4.2	Mean square displacement	42
3.5	EMD-based approach for posture analysis	43
3.5.1	Diffusion curves modeling	44
3.6	Results and discussions	46
3.6.1	Balance analysis : classical approach	46
3.6.2	Balance analysis using EMD	47
3.6.2.1	Gain analysis	48
3.6.2.2	CP analysis	53
3.7	Conclusion	56
4	EMD-BASED FEATURE EXTRACTION AND SELECTION FOR SUBJECTS CLASSIFICATION	58
4.1	Introduction	59
4.2	Classification techniques	60
4.2.1	K Nearest Neighbors	60
4.2.2	Classification and regression tree (CART)	61
4.2.3	Random Forest	61
4.2.4	Support Vector Machine	62
4.3	Feature extraction and selection for subjects classification	65
4.3.1	Feature extraction	66
4.4	Experimental results	69
4.4.1	Performance evaluation	69
4.4.2	Results and discussions	71
4.4.2.1	Obtained results using data collected from all conditions	71
4.4.2.2	Obtained results using data collected from each condition (IMFs data)	73
4.4.2.3	Obtained results using data collected from each condition (Raw data)	76
4.5	Conclusion	78
5	HMM-BASED CLASSIFICATION APPROACH	80
5.1	Introduction	81
5.2	Hidden Markov Models	81
5.2.1	Introduction	81
5.2.2	Markov Chain	81
5.2.3	Discrete HMM	83
5.2.4	Gaussian HMM	87
5.3	HMM-based classification approach	88
5.4	Results and discussions	89
5.5	Conclusion	93
6	HMM REGRESSION-BASED APPROACH FOR AUTOMATIC SEGMENTATION OF STABILOMETRIC SIGNALS	95

6.1	Introduction	96
6.2	Hidden Markov Model Regression	96
6.2.1	Simple Hidden Markov Model Regression	97
6.2.1.1	Parameter estimation	97
6.2.2	Multiple Hidden Markov Model Regression	98
6.2.2.1	Parameter estimation	99
6.3	HMM Regression-based approach for automatic segmentation of stabilometric signals	101
6.4	Results and discussions	102
6.4.1	Segmentation based on feet and visual conditions of healthy subjects	103
6.4.2	Segmentation based on feet and visual conditions of PD subjects .	107
6.5	Conclusion	109
7	GENERAL CONCLUSION AND PERSPECTIVES	112
7.1	Conclusion	113
7.2	Perspectives	115
	 Bibliographie	 116

Table des figures

2.1	Eye components [14]	12
2.2	Inner ear [17]	13
2.3	Feet polygon	14
2.4	Movements strategies [23]	16
2.5	First stabilometric recordings [24]	17
2.6	Vicon camera system [34]	18
2.7	Multicamera system (According to Maeva Le Goic)	18
2.8	Force platform connected to a PC. The three axes (x, y, z) represent, respectively, the anteroposterior (AP), mediolateral (ML) and the vertical axes.	19
2.9	Planar illustration of COP displacements (Mondor stabilometric data)	20
2.10	Temporal representation of ML and AP displacements	21
2.11	Spectral representation of ML and AP displacements	21
2.12	Feet positions : (A) feet together, (B) feet apart, (C) semi tandem, (D) full tandem, (E) single foot	22
2.13	Normalized parameters values vs. sampling frequency [48]	23
2.14	Normalized parameters values vs. testing time [48]	24
2.15	Preferred feet position for young and elderly subjects [49]	24
2.16	A schematic diagram of the auto-regressive model [70].	28
3.1	ML and AP directions of human body	34
3.2	Stabilometric signals in ML direction for FAEC, FAEO, FTEC and FTEO conditions.	35
3.3	Stabilometric signals in AP direction for FAEC, FAEO, FTEC and FTEO conditions.	35
3.4	Planar representation of ML and AP signals for FAEC, FAEO, FTEC and FTEO conditions.	36
3.5	Upper, lower and mean envelopes of a signal	39
3.6	Block diagram of EMD	40
3.7	Diffusion curve of a stabilometric signal	43
3.8	The proposed methodology	44
3.9	ML stabilometric signal and its EMD decomposition for FAEO condition	45
3.10	AP stabilometric signal and its EMD decomposition for FAEO condition	46
3.11	Natural frequencies (ω_n) Vs Gain (G) : means + STDs	49
3.12	Diffusion curve of an IMF (mode)	53
4.1	Classification of new individual using KNN with K=5	61
4.2	Linear and non-linear hyperplanes of SVM classifier	63

4.3	Healthy and PD subjects classification process	66
4.4	AP stabilometric signal and its first eight IMFs for a healthy subject in FAEO condition	67
4.5	ML stabilometric signal and its first eight IMFs for a healthy subject in FAEO condition	68
4.6	AP stabilometric signal and its first eight IMFs for a PD subject in FAEO condition	69
4.7	ML stabilometric signal and its first eight IMFs for a PD subject in FAEO condition	70
4.8	Obtained results in terms of recognition rate for each classifier using extracted/selected features from EMD, Raw and EMD& Raw data.	72
4.9	Obtained results in terms of recognition rate for each classifier using extracted/selected features from IMFs data for each condition.	74
4.10	Obtained results in terms of recognition rate for each classifier using extracted/selected features from raw data for each condition.	76
5.1	An example of a Markov Chain model	82
5.2	An example of a discrete hidden Markov model	84
5.3	An example of a Gaussian hidden Markov model	88
5.4	The block diagram of the proposed classification approach	89
5.5	The log-likelihood maximization process of the HMM models for healthy and PD subjects (a) AP direction (b) ML direction (c) AP/ML directions.	92
6.1	The input and the output of the HMMR model for the discrimination between visual and feet conditions	103
6.2	Results obtained in the case of HMMR (left) and HMM (right) for AP direction with k=1 : FAEC, k=2 :FTEC, k=3 : FAEO, and k=4 : FTFO.	104
6.3	Results obtained in the case of HMMR (left) and HMM (right) for ML direction with k=1 : FAEC, k=2 :FTEC, k=3 : FAEO, and k=4 : FTFO.	105
6.4	Results obtained with HMMR (b) and HMM (c) for multi-input AP and ML directions (a) for healthy subjects with k=1 : FAEC, k=2 :FTEC, k=3 : FAEO, and k=4 : FTFO.	108
6.5	Results obtained with HMMR (b) and HMM (c) for multi-input AP and ML directions (a) for PD subjects with k=1 : FAEC, k=2 :FTEC, k=3 : FAEO, and k=4 : FTFO.	109

Liste des tableaux

3.1	Subjects information are expressed in mean±standard deviation [min-max] values.	34
3.2	Characteristics comparison between Fourier, wavelet and EMD methods	37
3.3	Stabilometric results	47
3.4	Effect of age, gender, feet position and vision for the COP excursion and the mean velocity parameters	48
3.5	Mean (STD) of gain parameters	50
3.6	Effect of age, gender, feet position and vision on EMD results.	51
3.7	Mean (STD) of CP parameters	54
3.8	Repeated measures ANOVA analysis of CP parameters	55
4.1	F_1 -measure per class, F_1 -measure, precision, recall, and average of accuracy rates (R) and its standard deviation (std) using IMFs data	72
4.2	F_1 -measure per class, F_1 -measure, precision, recall, and average of accuracy rates (R) and its standard deviation (std) using Raw data	72
4.3	F_1 -measure per class, F_1 -measure, precision, recall, and average of accuracy rates (R) and its standard deviation (std) using EMD and Raw data	73
4.4	F_1 -measure per class, F_1 -measure, precision, recall, and average of accuracy rates (R) and its standard deviation (std) for FAEC condition	74
4.5	F_1 -measure per class, F_1 -measure, precision, recall, and average of accuracy rates (R) and its standard deviation (std) for FAEO condition	74
4.6	F_1 -measure per class, F_1 -measure, precision, recall, and average of accuracy rates (R) and its standard deviation (std) for FTEC condition	75
4.7	F_1 -measure per class, F_1 -measure, precision, recall, and average of accuracy rates (R) and its standard deviation (std) for FTEO condition	75
4.8	F_1 -measure per class, F_1 -measure, precision, recall, and average of accuracy rates (R) and its standard deviation (std) for FAEC condition	77
4.9	F_1 -measure per class, F_1 -measure, precision, recall, and average of accuracy rates (R) and its standard deviation (std) for FAEO condition	77
4.10	F_1 -measure per class, F_1 -measure, precision, recall, and average of accuracy rates (R) and its standard deviation (std) for FTEC condition	77
4.11	F_1 -measure per class, F_1 -measure, precision, recall, and average of accuracy rates (R) and its standard deviation (std) for FTEO condition	78
5.1	Classification rates with different numbers of states	90
5.2	Classification rates with different numbers of Gaussian mixtures	90
5.3	Performances of the proposed classification approach for differentiating between healthy and PD subjects using both ML and AP signals	91

5.4	Performances of the proposed classification approach for differentiating between healthy and PD subjects using AP signals	91
5.5	Performances of the proposed classification approach for differentiating between healthy and PD subjects using ML signals	91
6.1	Confusion Matrix for AP direction	106
6.2	Confusion Matrix for ML direction	106
6.3	Confusion Matrix for both AP and ML directions	106
6.4	Correct classification rates (%) obtained with the different methods . . .	106
6.5	Correct classification rates (%) obtained with PD subjects using HMM and HMMR.	107
6.6	Confusion Matrix for both AP and ML directions (Planar) for PD subjects	107

Abbreviations

ANN	A rtificial N eural N etwork
ANOVA	A nalysis O f V ariance
AP	A nterio P osterior
CART	C lassification A nd R egression T ree
CHMM	C ontinuous H idden M arkov M odel
CoM	C enter o f M ass
CoP	C enter o f P ressure
DHMM	D iscret H idden M arkov M odel
EM	E xpectation M aximization
EEMD	E nsemble E mperical M ode D ecomposition
EMD	E mperical M ode D ecomposition
GMM	G aussian M ixture M odel
H	H irst exponent
HHT	H ilbert H uang T ransform
HMM	H idden M arkov M odel
HT	H ilbert T ransform
IF	I ntantaneous F requency
IMF	I ntrinsic M ode F unction
KNN	K Nearest Neighbor
ML	M edio L ateral
RF	R andom F orest
ROC	R eceiver O perating C haracteristic
SDA	S tabilogram D iffusion A nalysis
SVM	S upport V ector M achine

Resumé

L'analyse de la stabilité posturale chez l'homme a fait l'objet, ces dernières années, d'un intérêt grandissant au sein de la communauté scientifique. Le système postural permet de maintenir la stabilité du corps humain en posture statique ou dynamique. Cette capacité à maintenir cette stabilité devient critique dans le cas des sujets Parkinsoniens. La maladie de Parkinson a en effet une forte incidence sur la stabilité posturale. Un moyen efficace pour évaluer l'équilibre postural consiste à analyser les déplacements dans le plan horizontal du centre de pression du corps humain en posture orthostatique ; les trajectoires mesurées dans la direction medio-latérale (ML) et la direction Antéro-postérieure (AP) sont appelées signaux stabilométriques. Dans cette thèse, nous visons le développement de méthodes efficaces pour l'analyse de l'équilibre en posture orthostatique sous différentes conditions liées, l'entrée visuelle (yeux ouverts/yeux fermés), la position des pieds (pieds joints/pieds écartés), et en considérant d'autres facteurs comme le genre et l'âge. Dans ce cadre, nous proposons, tout d'abord, une méthode exploitant la variante EEMD (Ensemble Empirical Mode Decomposition) de la décomposition en modes empiriques (EMD) et l'analyse de la diffusion du stabilogramme. Dans le contexte du diagnostic de la maladie de Parkinson, la discrimination entre sujets sains et sujets Parkinsoniens est très importante, de même que l'évaluation du stade de la maladie pour les sujets atteints. Dans ce cadre, deux méthodes sont proposées. La première consiste tout d'abord en une extraction et sélection de caractéristiques temporelles et spectrales, à partir des signaux stabilométriques bruts ou des modes de fonctions intrinsèques dérivés de la décomposition EEMD. Des méthodes standards de type KNN, CART, RF et SVM sont ensuite appliquées pour reconnaître les sujets Parkinsoniens. La deuxième méthode proposée, est une approche de classification qui repose sur l'emploi des modèles de Markov cachée (HMMs) construits en utilisant les signaux stabilométriques bruts dans les directions ML, AP et ML/AP. Enfin, une dernière méthode est proposée pour la segmentation automatique des signaux stabilométriques sous différentes conditions (entrée visuelle, position des pieds). Pour ce faire, un modèle de régression régi par une chaîne de Markov cachée (HMMR) est utilisé pour détecter automatiquement les variations des structures des signaux stabilométriques entre ces conditions. Les résultats obtenus montrent clairement la supériorité des performances des méthodes proposées par rapport aux approches standards, aussi bien, en termes d'analyse de l'équilibre postural que de diagnostic de sujets Parkinsoniens.

Mots clés : Analyse posturale, stabilométrie, décomposition du signal, classification, HMM, HMMR, maladie de Parkinson. .

Chapitre 1

GENERAL INTRODUCTION

In recent years, human balance control analysis has received an increasing interest from the research community. This is mainly due to the necessity of understanding the complex mechanisms of the human postural system, which contribute to the development of efficient solutions for unstable postures in terms of orientation and equilibrium and to help decrease the high rate of falls among elderly and patients. The human postural system maintains the stability of the body both in the static posture (quiet standing) and during locomotion by considering external perturbations. It successfully keeps the human body in the upright position through the interactions among the central nervous system, the musculoskeletal system, and three sensory systems : vestibular, visual and proprioception systems.

The ability to maintain postural stability becomes a difficult task with aging and when suffering from some pathologies that affect the human stability such as Parkinson's disease (PD), cerebellar disease and vestibular deficits. Stability disorders of the elderly may lead to sudden falls with important orthopedic complications. Parkinson's disease is one of the most common degenerative movement disorders which is characterized by the progressive loss of specific neurons in the brain. It has a strong impact on postural stability during quiet standing situations, and during locomotion. This disease is the second most common neuro-degenerative disease in France, after Alzheimer's disease. According to the national institute of health and medical research, between 100,000 and 120,000 people are affected in France, and about 8000 new cases occur each year. One effective way to assess human stability is to analyze the postural sway during

quiet standing. This can be performed by quantifying the center of pressure (CoP) displacements of the human body during the quiet standing. The CoP displacements are recorded in the medio-lateral (ML) and antero-posterior (AP) directions over time, and the resulting signals are called stabilometric signals. Many classical parameters, such as, the mean velocity, the range, the swept area, the root mean square distance, are generally extracted from the stabilometric signals in order to analyze and compare stability under different conditions, such as the visual input and feet position.

The work of this thesis aims to develop efficient approaches in order to :

(1) Analyze the postural stability under different visual and feet position conditions, and between gender and age groups. In other words, the goal is to analyze the effect of the aforementioned conditions on the human stability using stabilometric signals. This is achieved using the Ensemble Empirical Mode Decomposition (EEMD) method for non-linear signals decomposition. This method does not use any a priori, and allows to decompose the original signal into a finite number of intrinsic mode functions (IMFs) based on frequency bands decomposition. Compared to classical approaches used in the literature, the EEMD method allows better analysis of the stabilometric signals. The analysis of each IMF, provides further information in depth about the human postural behaviors. The proposed method is compared favorably to standard stabilometric analysis that is often used to assess the human stability.

(2) Discriminate healthy from PD subjects. This discrimination is very important for diagnosing Parkinson's disease, as well as for evaluating the patient's disease level. Two approaches are proposed to address this problem. The first approach consists of an EMD-based temporal and spectral feature extraction/selection from the stabilometric signals. The EMD method allows to decompose the stabilometric signal into several components based on the frequency bands. Standard classification techniques were used to discriminate healthy from Parkinsonian subjects. This approach guarantees a better characterisation of the stabilometric signal through the analysis of the features resulting from the different generated IMFs. The second approach to discriminate healthy from PD subjects is based on a Hidden Markov model (HMM). The raw stabilometric data are used directly as input for the HMM model. The HMM model is an efficient tool to analyze temporal and sequential data. Compared to classical approaches, the proposed

approach allows accurate discrimination between healthy and PD subjects based on the sequential structure of their stabilometric signals.

(3) Segment the stabilometric signals recorded under four different conditions related to vision and feet position. A Hidden Markov Model Regression (HMMR)-based approach is used to carry out the segmentation between the different conditions using simple and multiple regression processes. The problem of condition recognition is formulated as one of a joint segmentation of multidimensional time series, in which each segment is associated with one condition. The proposed approach performs in an unsupervised context, which avoids data labeling phase, that is often time-consuming especially in the case of massive databases.

This manuscript is organized as follows :

Chapter 2 provides an exhaustive study about human postural stability. The postural system and its components in the human body are first presented. The second part of the chapter describes the primary tools commonly used to record and evaluate human postural sway in quiet standing. In the third part, the most relevant studies in the literature are presented and analyzed to highlight their performances and limitations.

Chapter 3 presents a new approach to analyze the human stability during orthostatic posture. The protocol used for measuring the stabilometric signals is first described, and then, the EMD method and its extension Ensemble EMD (EEMD) are presented. The principal of the Stabilogram-diffusion analysis technique, and the EMD-based proposed approach for a better assessment of the human posture, are then presented. Finally, the performances of the proposed approach are presented and discussed.

Chapter 4 proposes a novel approach to distinguish healthy subjects from PD ones using an EMD-based temporal and spectral feature extraction. The first part of this chapter describes the supervised classification methods used in this study. The proposed framework for discriminating between healthy and PD subjects using stabilometric data is then presented. Finally, the last part of the chapter presents the experimental results and discussions of this study.

Chapter 5 presents another classification approach to discriminate healthy subjects from PD subjects using the Hidden Markov model (HMM) method. The raw stabilometric data in ML, AP, and ML/AP directions, are used directly as model's input. The

first part of this chapter describes the hidden Markov models used in this study. The proposed approach for classifying healthy and PD subjects is then detailed in the second part. Finally, the performances of this approach are presented and discussed in the last part of the chapter.

Chapter 6 addresses the problem of the automatic segmentation of stabilometric signals recorded under four different conditions related to vision and feet position. This is achieved for both healthy subjects and PD subjects. A Hidden Markov Model Regression (HMMR)-based approach is used to carry out the segmentation between the different conditions using simple and multiple regression processes. The first part of this chapter describes the HMM regression model used in this study. The HMMR-based approach, proposed for automatic segmentation of stabilometric signals, is then detailed in the second part of the chapter. The performances of this approach are presented and discussed in the last part of the chapter.

Chapter 7 consists of a general conclusion, in addition to open perspectives from algorithmic and application points of view.

Chapitre 2

THE HUMAN POSTURAL STABILITY ANALYSIS

2.1 Introduction

The tonic postural system guarantees the equilibrium of the human body in static and dynamic standing situations, as well as during locomotion activities. We can say that such a system is in a balance state when the sum of all forces and all moments acting on this system is null. In case of static posture, static balance is achieved when two conditions are considered : first, the weight applied to the center of mass and the reaction forces of support applied to the center of pressure of the contact surface are equal and opposite; second, the center of gravity and the center of pressure are aligned on the same vertical line.

In the present chapter, an exhaustive study of human postural stability is presented. The first part describes the human postural system and its components. The primary tools to record and evaluate human sways in static posture are then presented. In the last part, the most relevant studies in the literature are shown and analyzed by highlighting the performances and limitations of the proposed techniques.

2.2 The human postural system

2.2.1 Definition

The tonic postural system is considered as a complex organization which involves several internal systems and has multiple sources of information. This system controls the human body sways and provides the human body equilibrium whatever the external environment status.

In case of standing in stable position with or without external disturbances, it is impossible for the human body to remain perfectly immobile [1]. This fact is due to several reasons mainly coming from neuromuscular adjustments [2], respiration [1], insufficient sensitivity of sensory receptors [3], or from the blood circulation [4].

The interaction between three principal systems including sensory, motor and central nervous systems insures the stability of the human body. The postural system uses information sourced from visual, vestibular and proprioceptive sensors [5] to estimate the center of mass position in the three directions of space. The variation of the center of

mass position is captured by these sensors which send information to the central nervous system (vestibular nuclei, the spine, and the cerebellum). The central nervous system sends commands to the skeletal muscles and to all other body muscles (motor system) to provide again the postural equilibrium.

The feet are the base of support of the human body which plays the main role in the balance control [6]. The size, strength and position of the feet affect strongly the human postural stability. The visual input helps also the postural system to maintain its stability and provides external information about the human body environment [7]. Aging population suffers from stability problems more than young population due to the decrease in some internal function abilities or due to the appearance of some specific diseases, such as the Parkinsons disease (PD) [8–12]. In contrast, internal and external factors can affect the functions of the postural system, and therefore, the human body stability.

2.2.2 The main components of the postural system

The tonic postural system has two types of entries. The input related to external information and those related to interior information. The sensory input provides the observed information, the body orientation, as well as the external environment status. The postural system takes into account the information related to the position of each body segment with respect to others as well as the whole body position with respect to its environment. In the following subsections, the components of the tonic postural system are presented. (1) the cephalic sensors including the ocular sensor and vestibular system; (2) the primary sensory organ of equilibrium (the foot); (3) the central regulation system and motor response.

2.2.2.1 Ocular sensor

The ocular sensor provides two different types of information. The first type is purely visual information, when the retinal picture is transmitted to the central nervous system. The second type of information is related to the tension of the external oculomotor muscles (Figure 2.1).

The retina provides information about the position and the movement of the body in space. This is achieved thanks to the retina sensory receptors which transmits foveal and peripheral visual information. The foveal vision allows the identification of objects and provides the main directions, i.e. the vertical and horizontal ones. The peripheral vision gives information about the situation of the subject with respect to its environment. This type of vision is involved in the dynamic equilibrium [13].

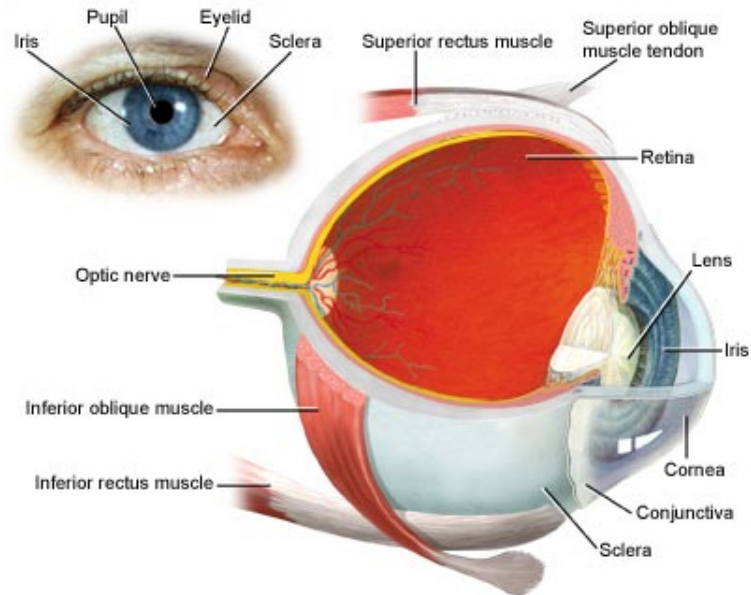


FIGURE 2.1: Eye components [14]

2.2.2.2 Vestibular system

The vestibular system is one from the essential sensory systems that provide and maintain the human body stability. It is located in the inner ear as a 3D motion detector (Figure 2.2). The inner ear consists of two distinguished parts, the first one has a neurosensory canal for the hearing function. The second part is the vestibule which is the responsible of the equilibrium function. The vestibule has three semicircular canals positioned at right angles to each other in the superior, posterior and horizontal positions. These canals are very sensitive during body movements and detect any displacement in the three planes of the space. The first canal detects the displacements on the horizontal plane, the second one detects the displacements on the frontal plane, and the last one, the displacements on the sagittal plane. These canals are attached to the utricle which

communicates with the saccule. These two organs controls the positions of the head, in the horizontal and vertical planes respectively [5, 15, 16].

The three canals are filled with a fluid called endolymph. When the head rotates, the endolymphatic fluid within the concerned canal lags behind because of inertia, and exerts pressure that deflects the cupula in the opposite direction. This deflection stimulates the hair cells by bending their stereocilia in the opposite direction. The receptor then sends impulses to the brain about movement from the specific canal that is stimulated. When the vestibular organs on both sides of the head are functioning properly, they send symmetrical impulses to the brain (Figure 2.2).

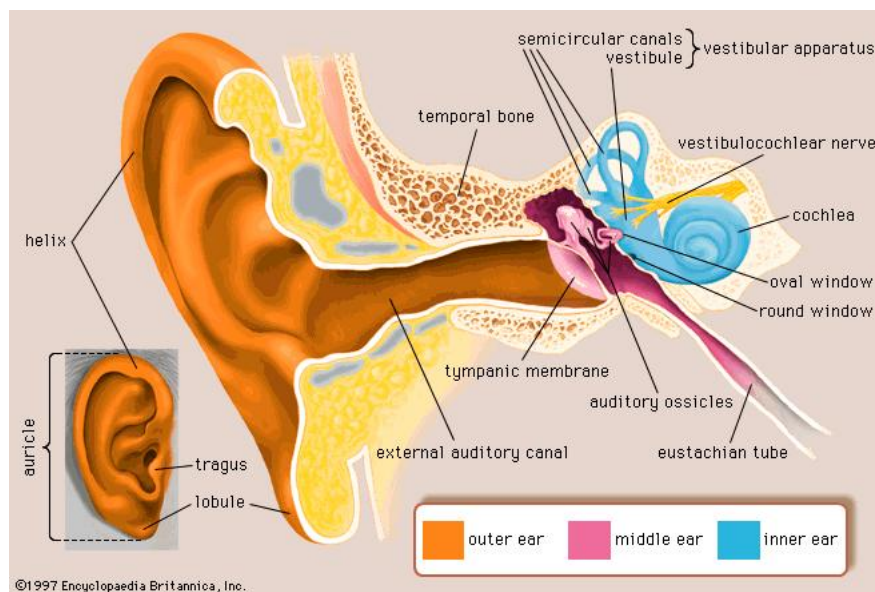


FIGURE 2.2: Inner ear [17]

2.2.2.3 The base of support : the foot

The foot is an important organ for the postural stability process, which is also the contact area between the human body and the ground. It informs the postural system on the geometry of the body support zone on the ground and also on the characteristics of the reaction force acting on that zone. The foot is equipped with multiple sensory receptors at different levels : cutaneous, joint, tendon and muscle. The proprioception of the foot is about four times higher than that of the leg. By transmitting the ground reaction force to the body, the foot accurately adjusts the posture of the human body. Indeed, plantar soles continuously indicate the differential pressure between the two plantar vaults. In consequence, the feet generates its own internal forces and adapts its compliance [16].

Each foot consists of three support points which constitute three arches : The internal arch is normally the most hollow goes from the first metatarsal head to the support center of the calcaneus (Figure 2.3). The external arch is much less hollow and goes from the fifth metatarsal head to the support center of the calcaneus. The anterior arch is relatively flat and goes from the head of the first metatarsal head of the fifth metatarsal.

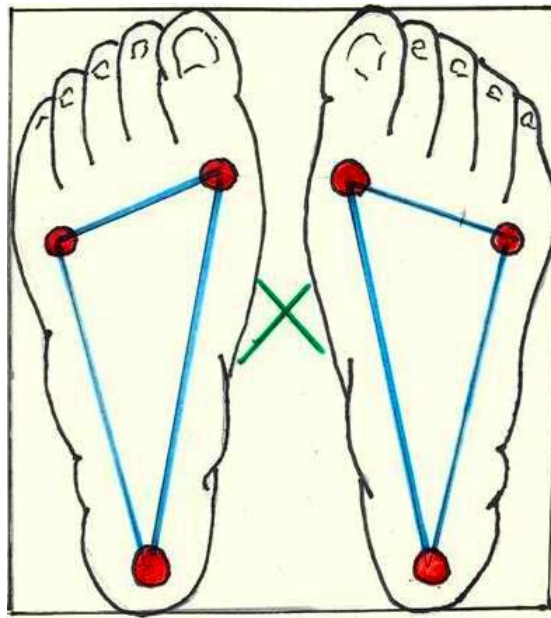


FIGURE 2.3: Feet polygon

The feet position on the ground and their symmetrical arches determine the support polygon. This polygon is constituted by the surface of the foot on the ground. Normally, the projection of the body center of gravity passes through the center of the polygon in the static posture. In contrast, a projection appearing outside the polygon, induces a balance problem.

2.2.2.4 Central regulation system

Central regulation is based on the actions of superior centers. The nerve impulses lead to cortical and subcortical structures. Their integrative action allows control of all components of the tonic postural system through intermediary reflexes. The control of stabilizing look is possible thanks to vestibulo-ocular and visual-oculomotor reflexes. The vestibulo-spinal and vestibular-ocular-cervical reflexes allow the overall control and the maintenance of posture by their action on the myotatic reflex [18].

2.2.2.5 Motor response

The whole skeleton-Musculature provides a chain of articulated segments. The form of these segments, the functional distribution of muscles, and the degrees of freedom of the various joints especially in the lower limbs for the standing posture cause effective movements to maintain their position and thus body stability [19]. The muscles are the main effectors of corporal movement. The adaptation of postural disturbances involves the following muscles : At the level of the posterior compartment of the leg innervated by the tibial nerve, the soleus is a primary agonist in standing position. The muscles of the anterior compartment innervated by the deep peroneal nerve are involved in the dorsal flexion of the ankle with the main agonist anterior tibialis. Among the muscles acting on the knee flexion, there is the semitendinosus, which has as primary antagonist, the right thigh and the vast quadriceps (medial and lateral).

According to the directions in which postural adjustments are required, the osteoarticular biomechanics and muscular system use specific strategies such as, ankle strategy, hip strategy and stepping strategy.

2.2.3 The primary strategies to maintain stability

Generally, the postural control system uses three types of movement strategies (Figure 2.4) [18]. The first strategy considers the whole body to be an inverted pendulum that moves around the ankle to maintain the equilibrium during quiet stance (ankle strategy). This strategy is used for small disturbances to maintain the body center of mass (COM) within the feet polygon.

The second strategy uses fast movements when the body exerts torque at the hip in order to generate an appropriate center of mass position to avoid falling (hips strategy). This strategy is used for rapid external disturbances and for small support surfaces.

The third strategy consists of moving the feet (stepping) to bring back the human body to a stable position (stepping strategy) [20-22]. It is used when the person has a high risk of falling.

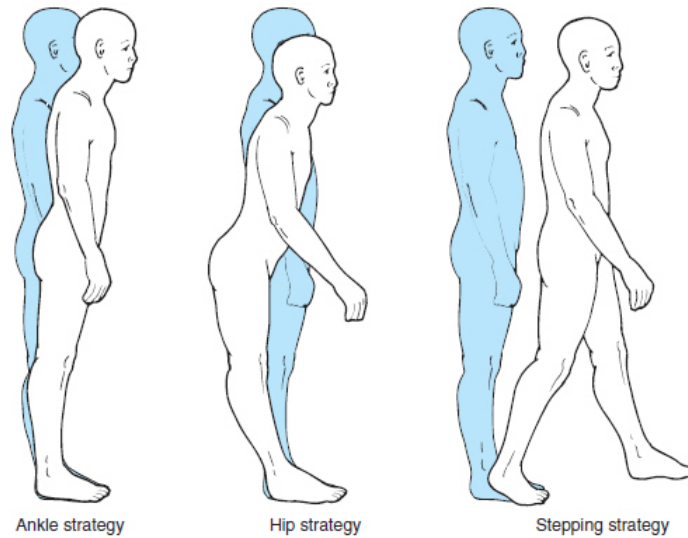


FIGURE 2.4: Movements strategies [23]

2.3 Tools for evaluating postural stability

2.3.1 Postural recording systems

In fact, any person is not able to remain perfectly standing without movements of low amplitudes. To assess the performance of the human postural system, it is necessary to assess the movements of the center of mass of human body in static and/or in dynamic situations. Consequently, in almost static situations, precise systems are necessary to detect these weak oscillations of the human body. The first stabilometric measurements were recorded by Karl Vierordt in 1960 (Figure 2.5) [24]. The equipment used by Vierordt to record the postural sway was rudimentary : a feather attached to the top of a helmet scratching a sheet coated by black carbon, and attached to the ceiling. Only the envelope of the drawing made through this feather worn by the person for each of the following conditions : (a) with eyes open, (a') with eyes closed ; (b) the right leg being the support ; (c) sitting with eyes open, (c') sitting with eyes closed ; and (d) standing on the only right foot.

In the literature, there are several methods to measure the human body displacements in quiet standing. Three categories of methods can be identified :

1. Video-based methods [25, 26],
3. Inertial sensors-based methods [27].



FIGURE 2.5: First stabilometric recordings [24]

2. Force platform-based methods [28–30],

The first category includes video-based methods allowing to model the human body as one or several articulated segments; this modeling refers to segmental postural stability. [31–33]. These methods are not easy to use because they require specific environment with video cameras and sensors that must be placed on the human body. The second category uses accelerometers for the human postural assessment. The third category, based on the use of force platforms, includes three methods that are detailed below.

2.3.1.1 Video-based methods

The motion analysis video-based system was used by Collins et al. to analyze the influence of added noise under feet of subjects (Fig. 2.6) [34]. This system consists of cameras and a reflective marker placed on the shoulder of the subject. The camera records the human body displacements through the marker displacements [34].

Another system, called active markers system, uses powered markers sending an infrared signal which is captured by sensor units. This technology requires small powered boxes that should be attached to the subject.

The video-based methods can provide qualitative and quantitative information about postural stability, using markers or sensors placed on the subject body (Fig. 2.7), and can also provide high level of accuracy and reliability during the recording of the postural sway in a quiet stance [25, 26].

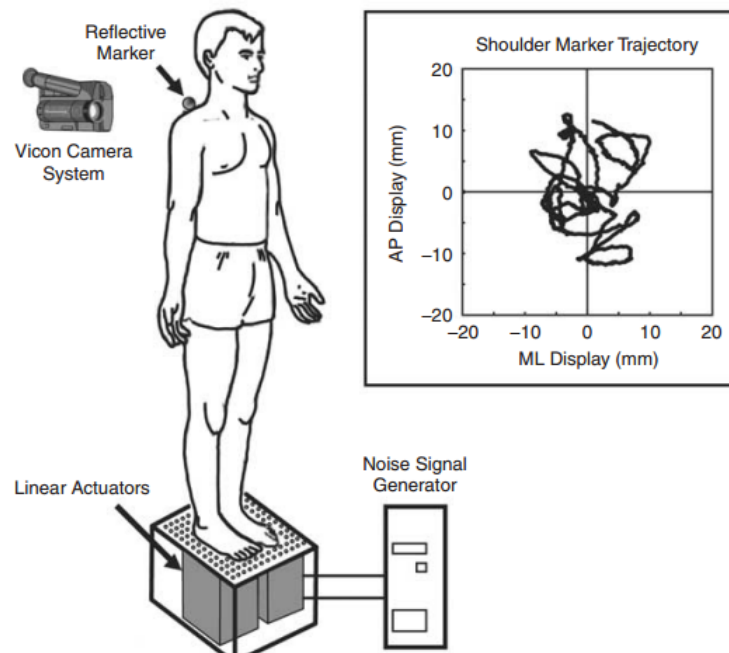


FIGURE 2.6: Vicon camera system [34]

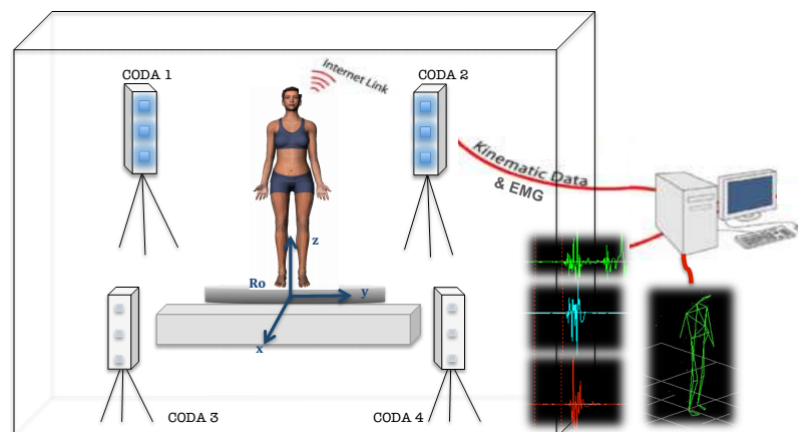


FIGURE 2.7: Multicamera system (According to Maeva Le Goic)

2.3.1.2 Body-worn inertial sensors-based methods

Accelerometers are used as an alternative technique to assess the posture stability in both static and dynamic conditions. This technology is widely used due to the low-cost of items compared to other systems such as videos systems [27]. Accelerometers can be placed on the posterior trunk to estimate the center of mass (COM) displacements or on specific positions to assess joint movements. There are other techniques to estimate the human body movements such as Electrogoniometers that have been mainly used to analyze changes in segmental postural position by measuring the joint angular displacements.

2.3.1.3 Force platform-based methods : the stabilometer

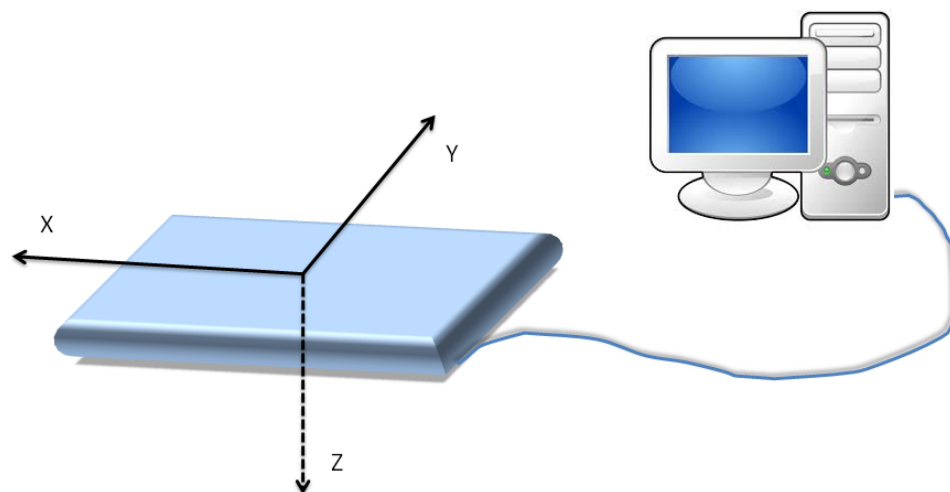


FIGURE 2.8: Force platform connected to a PC. The three axes (x, y, z) represent, respectively, the anteroposterior (AP), mediolateral (ML) and the vertical axes.

Three different graph types can be used to visualize the center of pressure displacements :

The first method used in the force platform-based techniques consists of integrating twice the acceleration of the COM to estimate its displacements [35, 36]. The second method is based on the modeling of the human body as an inverted pendulum [32, 37, 38]. The third method is the frequency method [39–42]. Its principle is that the center of pressure is interpreted as a noisy signal of the center of mass. It uses the low-frequency filter, defined by the relationship between the center of pressure and the center of mass in the frequency domain, to calculate the center of mass displacements. This method has some problems with inertia moments to define the filter parameters. The COP position can be easily estimated using a force platform and it is widely used to characterize the human balance in quiet standing [28–30]. Therefore, to determine the position of the center of pressure in static posture and to analyze its fluctuations versus time, stabilometry is widely used as a measurement technique for postural assessment.

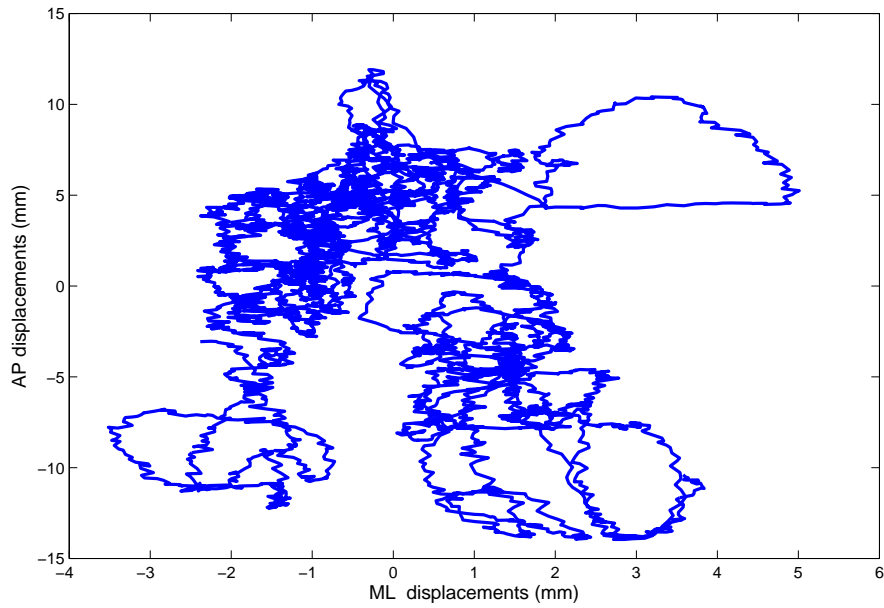


FIGURE 2.9: Planar illustration of COP displacements (Mondor stabilometric data)

Stabilometry is a specialized clinical assessment technique used to quantify the center of pressure displacements of human body in standing position under a variety of conditions such as : open eyes, closed eyes, stable or unstable support, feet apart, and feet together. This quantification is performed using a force platform for determining the coordinates of the center of pressure exerted by the person on the surface of this platform (Figure 2.8).

The center of pressure is the application point of the reaction forces generated by the person on the surface of the force platform. This platform allows to measure six components : three reaction forces F_x , F_y and F_z and three moments M_x , M_y and M_z from which the anteroposterior (AP) and mediolateral (ML) displacements of the center of pressure will be calculated. The coordinates of the center of pressure can be calculated from the following equations :

$$\begin{aligned} X = AP &= -\frac{M_y}{F_z} \\ Y = ML &= -\frac{M_x}{F_z} \end{aligned} \quad (2.1)$$

Figure 2.9 shows the COP position trajectory according to AP axis (x) and ML axis (y).

Indeed, it is possible to extract from this trajectory spatial and temporal parameters to characterize the balance, such as the mean position, the mean velocity, etc.

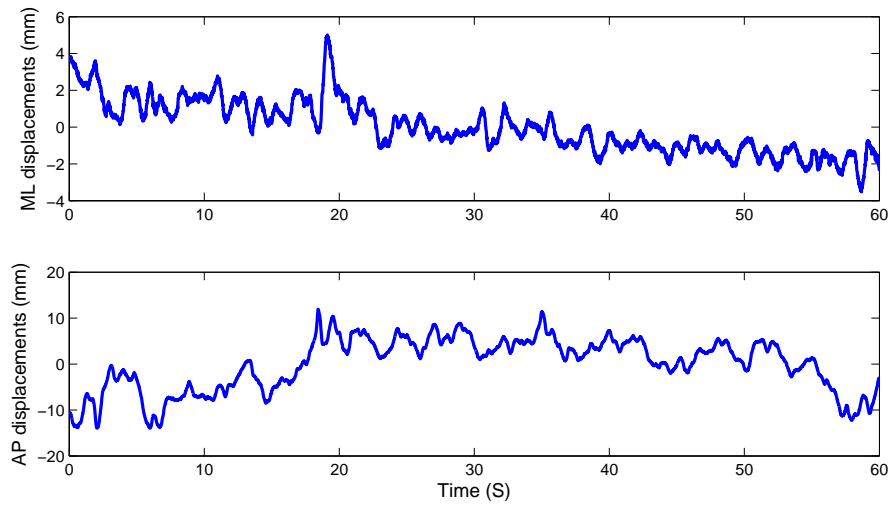


FIGURE 2.10: Temporal representation of ML and AP displacements

The stabilogram shown in figure 2.10 represents a linear illustration of the anteroposterior and mediolateral displacements of center of pressure versus time. From this representation, the linear, non-linear parameters and those related to the temporal aspects of the trajectory of the center of pressure can be extracted, such as Lyapunov exponent, the Hurst exponent and entropy.

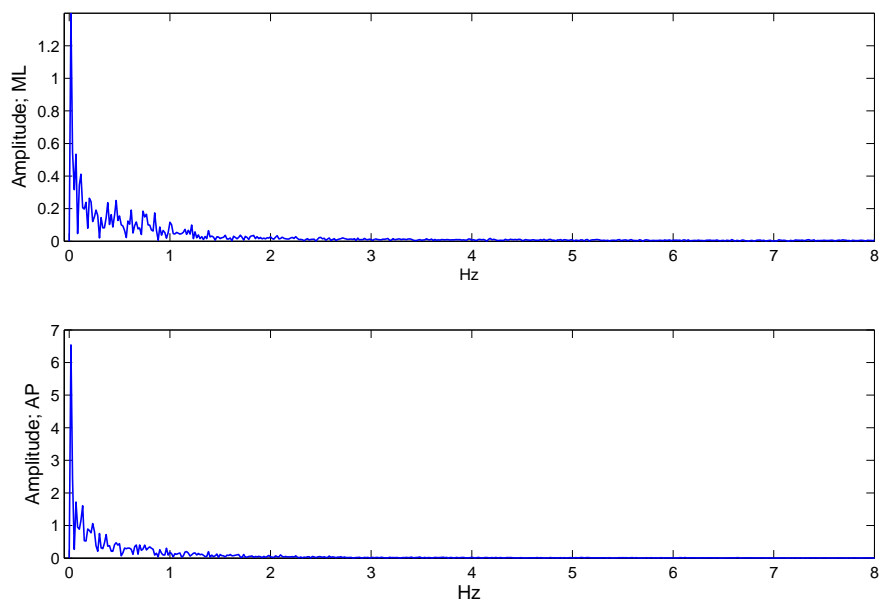


FIGURE 2.11: Spectral representation of ML and AP displacements

In figure 2.11, a spectral representation of the center of pressure in both AP and ML directions is illustrated. In static position, the frequency band of the center of pressure in both directions is between 0 and 5 Hz. From this representation, the frequency parameters can be extracted such as mean and median frequencies, etc.

2.3.2 Protocols for COP displacements recordings

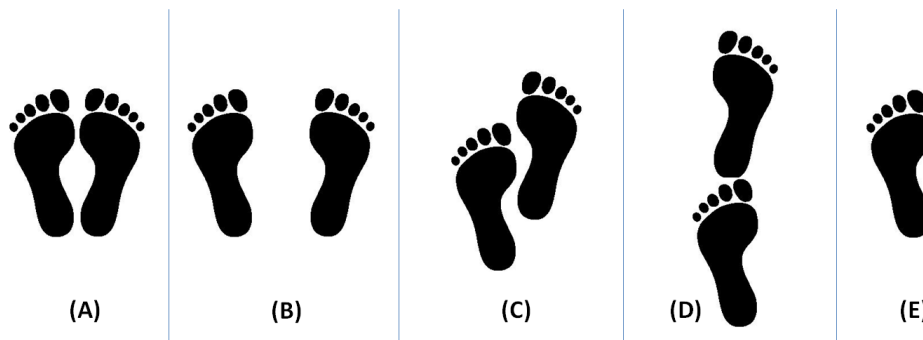


FIGURE 2.12: Feet positions : (A) feet together, (B) feet apart, (C) semi tandem, (D) full tandem, (E) single foot

Various protocols and postural conditions have been used in the literature to record the center of pressure (CoP) displacements. Usually, the main controlled variables are : feet position, visual input (eyes closed, eyes open), test duration, and sampling frequency.

For feet position, postural tests are recorded either in a bipedal stance (see figure 2.12 (a), (b), (c), and (d)) or in a monopedal stance (see figure 2.12 (e)). In both stances, there are many types of feet displacements such as : feet together, feet apart, quiet stance using one foot, semi tandem, full tandem, etc. (Figure 2.12). The feet either form an angle of 15 to 30 degrees or they are positioned in parallel. The inter-feet distance is usually between 5 to 15 cm with an angle of 15 to 30 degrees.

For visual input, the postural tests are recorded with or/and without visual information. The suppression of visual input occurs by closing the eyes to compare the human stability with and without these information.

On the other hand, most of time, the postural tests are recorded in static or/and in dynamic conditions. This is accomplished to analyze and compare the postural stability under perturbations such as arm, leg and platform perturbations [43–47]. In addition, the postural tests are measured under different test durations. The test duration commonly used varies between 20 and 60 s.

2.3.3 Clinical stabilometry standardization

As mentioned in the previous section, there are a lot of experimental protocols used in different postural conditions. In [48], Scoppa et al. propose a clinical stabilometry standardization technique for test duration and sampling frequency.

As shown in figure 2.13, standard parameters (Sway Path, Sway Area and Confidence Ellipse Area) are steady and a sampling rate of 50 Hz seems to be acceptable to get reliable values of these parameters. Both oscillations and sway density parameters instead requires a higher sampling frequency. The 100 Hz sampling rate is recommended to use for postural stability analysis [48].

To analyze the effect of test duration, 25 time series of 40 s sampled at 100 Hz, were analyzed and processed to calculate the standard parameters at different test times (5, 10, 15, 20, 30, 35 and 40 s). For duration times less than 25 sec, the sway parameters are not steady, and therefore these testing times are not acceptable for static postural analysis (Figure 2.14).

This study shows that 30 s of recording time sampled at 100 Hz is acceptable for static human postural stability analysis.

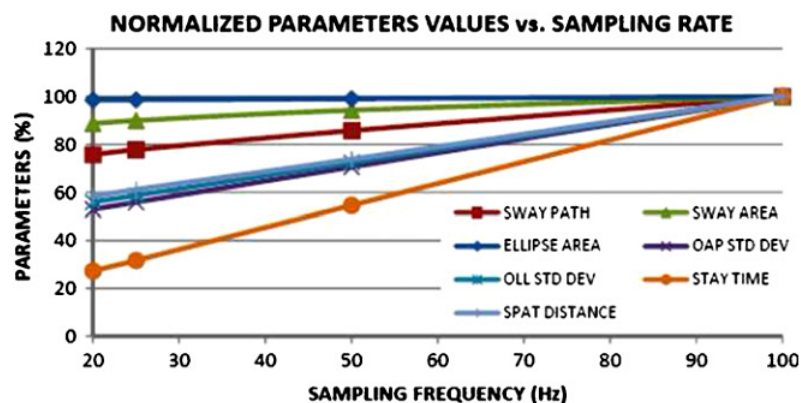


FIGURE 2.13: Normalized parameters values vs. sampling frequency [48]

In [49], the authors studied the preferred feet position of 262 subjects in order to establish a standardized stance position for static standing analysis. All subjects were asked to stand quietly with a comfortable and preferred feet position. The width and angle of orientation between feet are calculated and recorded for each subject. As shown in figure 2.15, there is a high degree of variability in preferred stand width and foot angle. The authors identify the standard width and angle by computing the averages of

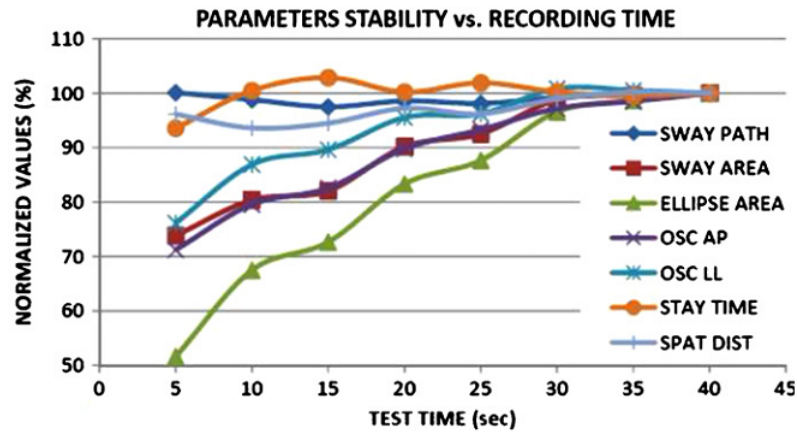


FIGURE 2.14: Normalized parameters values vs. testing time [48]

width and angle parameters for all subjects. These standard values are 0.17 m and 14 degrees for width and angle respectively.

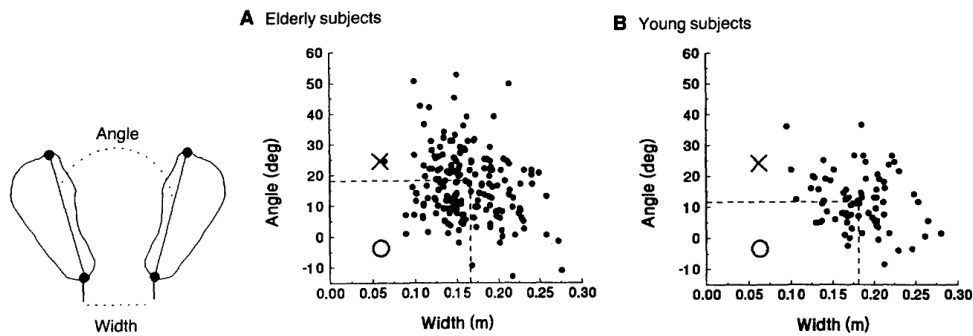


FIGURE 2.15: Preferred feet position for young and elderly subjects [49]

2.4 Postural stability analysis techniques

Over the last decade, human balance control strategies have received increasing interest from the research community. This is mainly due to the necessity of understanding the complex mechanisms of the human postural system, which will contribute to the development of efficient solutions for unstable postures in terms of orientation and equilibrium [18], and will help decrease the high rate of falls among elderly and patients [50–53].

The human postural system maintains the stability of the body both in the static posture (quiet standing) and during locomotion by considering external disturbances. It successfully keeps the human body in the upright position through the interactions among

the central nervous system, the musculoskeletal system, and three sensory systems : vestibular, visual and proprioception systems [54–56].

One effective way to assess human stability is to analyze the postural sway during upright standing. This can be performed by quantifying the center of pressure (CoP) displacements of the human body in quiet standing. The CoP displacements are recorded in the medio-lateral and antero-posterior directions over time, and the resulting signals are called stabilometric signals.

Many classical parameters can be extracted from the stabilometric signals (for each direction alone ML/AP and also for planar representation) to characterize the human static stability. These parameters can be grouped into two categories [34, 57–59].

The first category includes parameters taking into account the geometric and temporal characteristics of the center of pressure such as :

1. The mean position : It is given by the following formula :

$$MP = \frac{1}{n} \sum_{i=1}^n x_i \quad (2.2)$$

where x is the stabilometric signal and n is the samples number. This parameter was used in studies [60–63]

2. The standard deviation which is expressed as follows :

$$SD = \sqrt{\frac{1}{n} \sum_{i=1}^n (x_i - \bar{x})^2} \quad (2.3)$$

3. The root mean square (RMS) of CoP displacements can be expressed as follows :

$$RMS = \sqrt{\frac{1}{n} \sum_{i=1}^n x_i^2} \quad (2.4)$$

4. The covered distance (total excursions TOTEX) is the length of the path. It is given by :

$$TOTEX = \sqrt{(x_{i+1}^{AP} - x_i^{AP})^2 + (x_{i+1}^{ML} - x_i^{ML})^2} \quad (2.5)$$

where x^{AP} and x^{ML} represent the CoP displacements respectively in AP and ML directions.

5. The covered distance in ML or AP directions ($TOTEX_{AP}$ or $TOTEX_{ML}$) : It is equal to the sum of the distance between two consecutive points in the AP or ML signals :

$$TOTEX_{AP} = \sum |x_{i+1}^{AP} - x_i^{AP}| \quad (2.6)$$

$$TOTEX_{ML} = \sum |x_{i+1}^{ML} - x_i^{ML}| \quad (2.7)$$

6. The mean velocities in ML/AP, AP and ML directions. Their expressions are as follows :

$$MVELO = \frac{TOTEX}{T} \quad (2.8)$$

$$MVELO_{AP} = \frac{TOTEX_{AP}}{T} \quad (2.9)$$

$$MVELO_{ML} = \frac{TOTEX_{ML}}{T} \quad (2.10)$$

where T represents the time interval of CoP displacements.

7. The range : It represents the maximum distance between any two points of CoP. It can be calculated for AP, ML directions and for planar (AP, ML).

$$Range = \max[x] - \min[x]; \quad (2.11)$$

8. The 95% confidence circle area AREA-CC : It represents the area of the circle of planar displacements. It contains, in the case of normal distribution, 95% of the CoP points. It is given by the following formula :

$$AREA - CC = \pi \times (MDIST + 1.645 \times STD_P) \quad (2.12)$$

Where $STD_P = \sqrt{RDIST^2 - MDIST^2}$ is the standard deviation for planar CoP.

9. The 95% confidence ellipse area AREA-CE : It is computed based on ML and AP stabilometric signals, by considering the main axes of the ellipse, which contains 95% of data points.
10. The total sway area : It represents the time integral of the COP trajectory.

Moreover, numerous spectral parameters extracted from the stabilometric signals are used to characterize the postural stability, such as, total power frequency, mean frequency, centroid frequency, median frequency, the frequency which includes 95% of the total power, etc.

In addition, based on the nonlinear structure of the stabilometric signals, many nonlinear methods of signal processing and models have been used to better analyze human stability, such as inverted pendulum model, auto-regressive model, Fourier transformations, Wavelet analysis and Empirical mode decomposition [64, 65, 70].

In [66–68], the authors have shown that the postural sway in quiet standing can be modeled as a correlated random walk. This is achieved by calculating the mean square displacements of the postural sway over many time intervals. The plot of the mean square CoP displacements versus time intervals is called the stabilogram-diffusion plot. It shows two regions corresponding to positive and negative correlated random walks. In addition, it illustrates that the postural control system adopts both open-loop and closed-loop control mechanisms. The open-loop mechanism is generally related to the short-term intervals when the postural system shows a positive correlation between past and future increments. Conversely, the closed-loop mechanism is related to the long-term intervals when the postural system shows a negative correlation between past and future increments.

In [69], the authors have analyzed the postural system using a 3D electromagnetic system. The tests were conducted with open/closed eyes and stable/unstable surfaces. The results proved significant differences between stable and unstable surfaces. However, no significant differences were observed between open and closed eyes on the stable surface.

In [70], Tanaka et al. proposed a new methodology to assess the postural stability through the center-of-pressure (COP) trajectories during quiet standing. New sensitive parameters were extracted and then utilized to investigate changes in postural stability with respect to visual input. The experimental data consists of stabilometric signals of eleven healthy subjects (20-27 years). These signals were recorded under eyes open and eyes closed conditions using a force platform during quiet standing. The proposed approach was applied separately for medio-lateral and antero-posterior stabilometric signals.

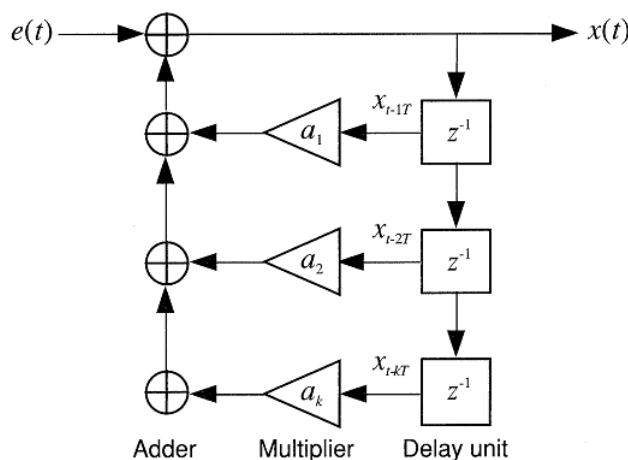


FIGURE 2.16: A schematic diagram of the auto-regressive model [70].

For each subject and for each condition, the stabilometric signals were modeled as an auto-regressive (AR) model (Figure 2.16). This is achieved for each direction (ML and AP) separately, and the order of the AR models was practically fixed at $M=20$. The new measures (The percentage contributions and geometrical moment of AR coefficients) were obtained from the estimation of the AR models parameters. They showed statistically significant differences between open eyes and closed eyes conditions [70]. The quiet standing under eyes-open condition showed higher correlation between present and past COP displacements compared to the eyes-closed condition. In contrast, no significant differences between vision conditions were found for conventional classical parameters (the total length of the COP path, mean velocity). The results showed that the AR parameters are useful to assess postural stability during static posture for visual conditions.

Recently, in [71], the authors have tried to assess human postural stability away from the standard COP characteristics used in the literature. A large dataset consisting of 168 subjects has been used. These subjects were divided into three groups : young, elderly and PD subjects. They were asked to perform quiet standing under eyes open and eyes closed conditions. To assess the postural stability under visual input, age, and pathology factors, three new sensitive parameters were extracted from the stabilometric signals including the sway directional index (DI), the sway ratio (SR), and the sway vector (SV). These measures were computed using the COP path length and its directional components in ML and AP directions. These new parameters are very sensitive with visual input, age, and PD disease. They showed significant differences between young

and elderly groups, young and PD groups, elderly and PD groups and between eyes open and eyes closed conditions. Specifically, the SV may be recommended as a useful parameter to assess postural control in quiet standing.

Some authors [72, 73] studied the positive impact of an added-noise under the feet using a vibrating insoles, on the balance control in elderly people. This noise stimulates and enhances the functions of the somatosensory system. This technique was also applied on subjects with specific diseases such as : diabetes and stroke. The results showed significant reductions in eight sway parameters, leading to improve the overall balance control.

Other studies explored the risk of fall in elderly population using CoP displacements measured during quiet standing [74–76]. Other studies tried to isolate each physiological system (visual, vestibular, and proprioceptive systems) to describe their specific role on balance control. Several modalities are classically tested to explore human balance : with and without visual input [77], with mechanic perturbations, such as arm movement [78–80], leg movement [43, 44], or platform perturbations [45–47].

PD is one of the incurable diseases that strongly affects human balance control. Tremors, muscle rigidity, and postural and balance problems often occur with PD and inevitably lead to falls and injuries [81]. Many researchers have investigated the postural stability of PD subjects in static (quiet standing) and dynamic (gait) postures [81–84] [85–89]. Several data mining techniques were used to extract information from PD data and provide better discrimination between control and PD subjects [90, 91].

In [90], Palmerini et al. used accelerometer-based data recorded from control and PD subjects to analyze posture in a quiet stance. First, 175 temporal and spectral features were computed, and feature selection with classification techniques were then used to select the best parameters that discriminate between control and PD subjects. Two parameters were selected to clearly separate the control subjects from the PD subjects.

2.5 Conclusion

In this chapter, we presented various techniques and methods for recording, evaluating, and analyzing postural stability in quiet standing. The standard parameters commonly

used are not able to characterize efficiently the COP displacements due to the complex structure of the stabilometric signals. In this study, we propose a new strategy to analyze the postural stability using the Empirical Mode Decomposition (EMD) method. This method is a specialized approach to analyze nonlinear and non-stationary signals as stabilometric signals. It is capable to explore the signal and provide an effective time-frequency analysis. The next chapter describes the proposed methodology for human postural analysis based on EMD method.

Chapitre 3

EMD-BASED APPROACH FOR POSTURE ANALYSIS

3.1 Introduction

In this chapter, we propose a new approach for the assessment of the human balance control. One effective way to assess the human stability is to analyze the postural sway during upright standing. This can be performed by quantifying the center of pressure (CoP) displacements of the human body during quiet standing. The proposed approach is based on the decomposition of the CoP displacements signal using the Empirical Mode Decomposition method (EMD). This approach is motivated by the fact that the EMD provides an effective time-frequency analysis of non-stationary signals.

Stabilogram-diffusion analysis technique is applied to analyze the mean square displacement versus time interval (diffusion curve) of each Intrinsic Mode Function (IMF) signal. Each diffusion curve is modeled as a second order system and provides representative features, such as, the gain parameter. Then, the proposed method compares favorably to conventional stabilometric analysis based on CoP excursion calculation.

The chapter is organized as follows : Section 3.2 describes the protocol used for measuring the stabilometric signals. Section 3.3 presents the EMD method and its extension Ensemble EMD (EEMD). Section 3.4 describes the principal of the Stabilogram-diffusion analysis technique. Section 3.5 describes the EMD-based proposed approach to extract new sensitive parameters for a better analysis and assessment of the human posture. In section 3.6, the performances of the proposed approach are presented and discussed.

3.2 Stabilometric data acquisition protocol

The experiments were conducted at the Mondor Hospital (Créteil-France). The resulting dataset is composed of stabilometric signals of 28 healthy subjects : 14 subjects are young (24 ± 4 years), and 14 subjects are elderly (65 ± 10 years) (Table : 1). The 28 subjects correspond to 14 women and 14 men. All subjects were asked to perform quiet standing during measuring of their stabilometric signals in the AP and ML directions. ML trajectories correspond to the CoP displacements in the left/right direction of the human body, while AP trajectories correspond to the CoP displacements in the forward/backward direction (Fig 3.1).

The stabilometric signal were measured in four conditions :

TABLE 3.1: Subjects information are expressed in mean±standard deviation [min-max] values.

	Young		Elderly	
	Women	Men	Women	Men
Number of subjects	7	7	7	7
Age	24±2 [20-27]	24±3 [20-27]	61±5 [55-70]	66±7 [55-75]
Height (cm)	166±2 [164-170]	182±6 [175-193]	163±9 [150-173]	171± 6 [163-182]
Weight (kg)	56±6 [45-63]	78±12 [54-92]	65±10 [52-85]	77±9 [61-86]

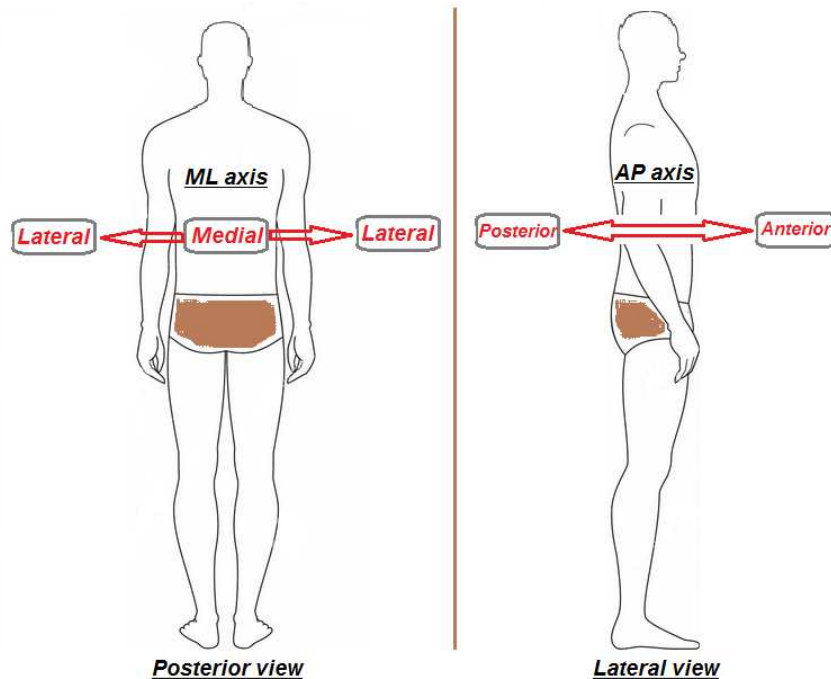


FIGURE 3.1: ML and AP directions of human body

- FAEC : Feet are Apart with Eyes Closed.
- FAEO : Feet are Apart with Eyes Open.
- FTEC : Feet are placed closed Together with Eyes Closed.
- FTEO : Feet are placed closed Together with Eyes Open.

For each condition, three trials were performed to measure the stabilometric signals in ML and AP directions. The duration of each trial is 60 seconds. Fig. 3.2, 3.3 and 3.4 show the recorded signals of one subject in AP, ML and planar directions.

Data were collected from a 6-components force plate (60 x 40 cm, strain gauge based device, Bertec Corporation, Columbus, OH, USA) at a sampling rate of 1000 Hz by means of an AD-converter (National Instruments, Austin, TX, USA) and a data acquisition

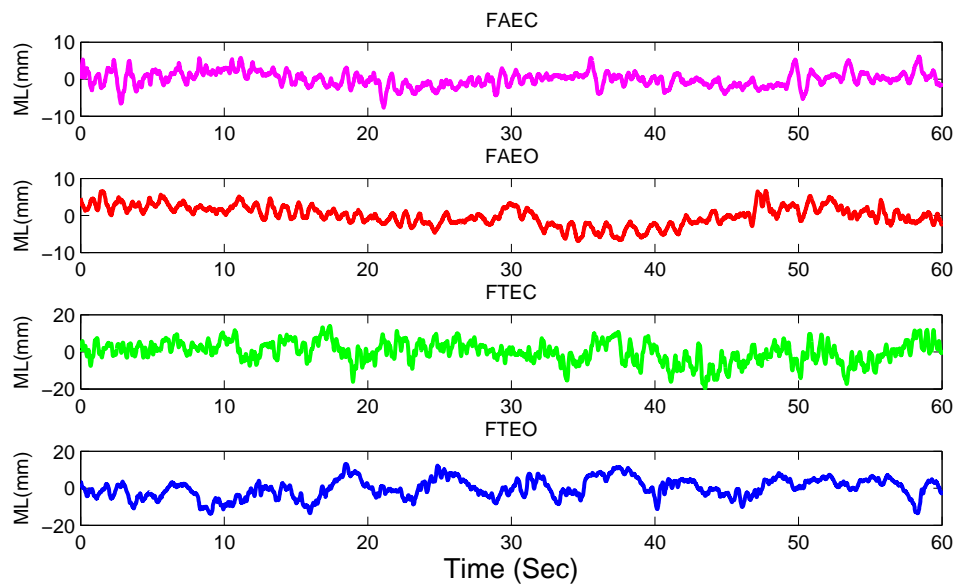


FIGURE 3.2: Stabilometric signals in ML direction for FAEC, FAEO, FTEC and FTEO conditions.

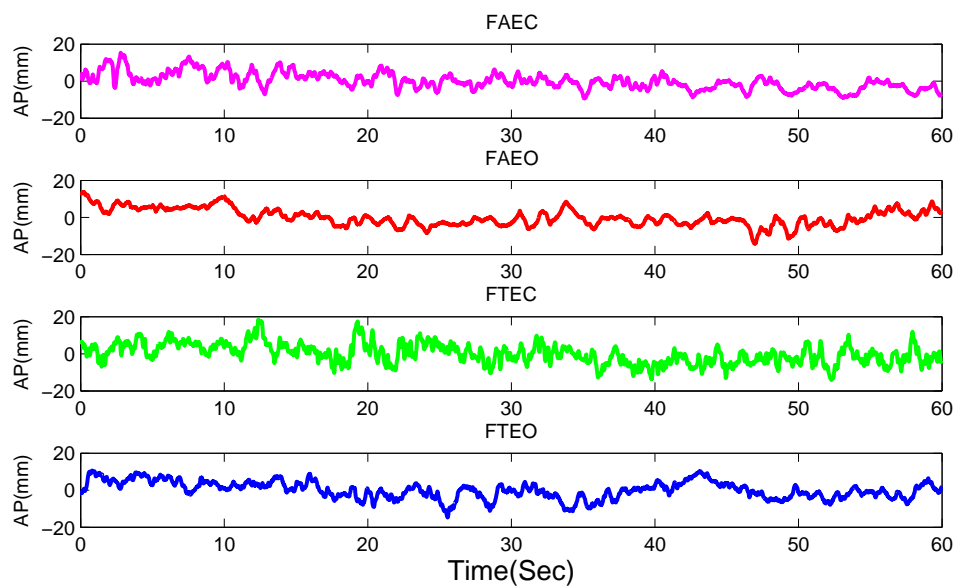


FIGURE 3.3: Stabilometric signals in AP direction for FAEC, FAEO, FTEC and FTEO conditions.

system (Cortex, Motion Analysis, Motion Analysis Corporation, Santa Rosa, CA, USA). The COP trajectories were determined in antero-posterior (AP) and mediolateral (ML) directions. The investigator traced the outline of the feet of each subject in the two tested foot positions (see details below) on an A3-sheet, which was laid centrally and fixed on the force plate in order to standardize foot positions throughout the experiment.

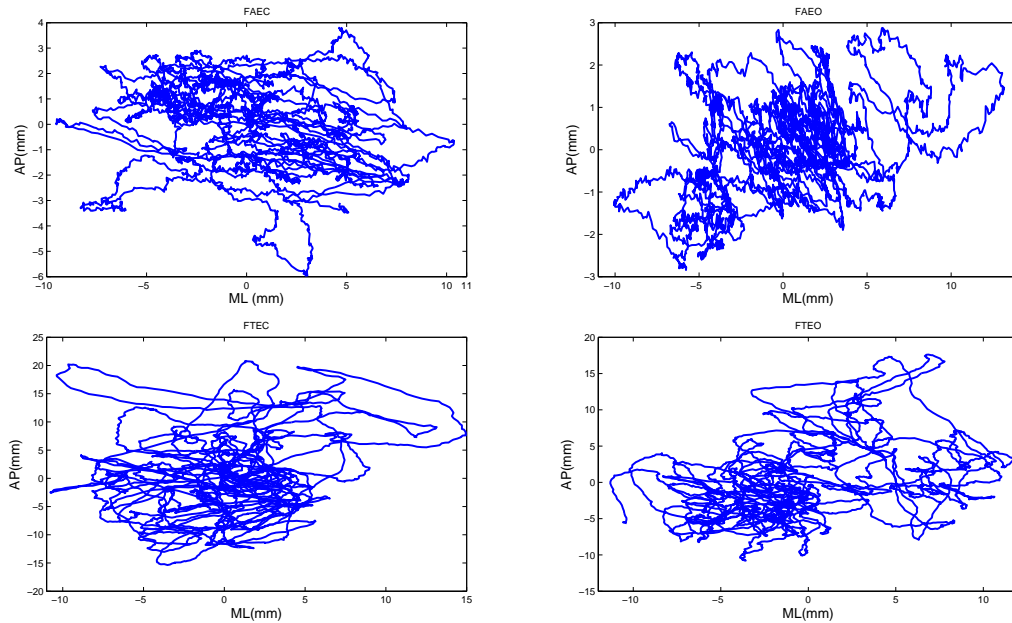


FIGURE 3.4: Planar representation of ML and AP signals for FAEC, FAEO, FTEC and FTFO conditions.

Participants stood upright with feet apart or feet together, with eyes open or eyes closed. For each subject, the order of the experimental conditions was randomized. For each condition, subjects were asked to stand as steady as possible with the arms hanging alongside the body [92]. With feet apart, subject feet were placed with an inter-calcaneus distance of 16 cm and a foot angle of 17 degrees [93]. With feet together, heels and big toes were in contact. With eyes open, subjects were asked to focus on a point at eye height on a wall at a distance of 3 meters across. With eyes closed, they were blindfolded, starting in the same head position as with eyes open. Each condition began with a 5 to 10 seconds period of familiarization. Each data collection started when subjects stood quietly and trials of 60 seconds were then recorded [94]. 60 seconds rest periods were provided to subjects, between two consecutive trials. Data were analyzed off-line with the Matlab software (The MathWork R, Inc., Natick, MA, USA).

3.3 Empirical Mode Decomposition and its variant Ensemble Empirical Mode decomposition

Empirical mode decomposition (EMD) was introduced in order to offer a flexible employment method to facilitate reading, exploring, and then extracting information from

TABLE 3.2: Characteristics comparison between Fourier, wavelet and EMD methods

	Fourier	Wavelet	EMD
Basics	a priori	a priori	adaptive
Frequency	Global	Regional	Local
Presentation	Energy-frequency	Energy-time-frequency	Energy-time-frequency
Non-stationary	No	Yes	Yes
Nonlinear	No	No	Yes

the data, usually for a given application. In the following, we describe the basics of this method, the sifting process, the stopping criteria and various applications domains.

3.3.1 EMD basics

EMD technique is a nonlinear method for analyzing nonlinear and non-stationary signals that was introduced by Norden Huang, a NASA engineer, in 1998 [95] [96] [97]. It is similar to Fourier and wavelet transforms in the sense that any signal is composed of many elementary signals. Table 3.2 provides a comparison between Fourier, wavelet and EMD methods.

Unlike classical methods, the advantages of EMD lie in the fact that it decomposes any given signal into a finite number (K) of oscillating components extracted directly without any a priori condition. These components are called intrinsic mode functions (IMFs) : they are interpreted as non-stationary waveforms. Ideally, these IMFs are oscillating functions with zero mean, and reflect the frequencies present locally in the signal from the highest frequencies to the lowest ones. The residue is a low frequency term that gives the overall trend of the signal (Figures 3.9, 3.10). Any signal x of length n can be modeled as follows :

$$x = \sum_{k=1}^K IMF_k + r_K \quad (3.1)$$

where K is the number of IMFs, IMF_k the k^{th} mode and r_K the residual signal.

An IMF (Intrinsic Mode Function) is an amplitude and frequency modulated signal that has the following characteristics :

1. The number of local minima and the number of local maxima are equal or differ at most by one.

2. The mean of the upper envelope and the lower envelope is approximately null everywhere.

EMD is an iterative method in which the first component (IMF) is extracted from the original signal, the second component from the residual signal, and so on.

3.3.2 Sifting process

The sifting process allows extracting, from the original signal, elementary signals (IMFs) starting from the highest frequency to the lowest one. The final component represents the residual of the signal [98]. Mathematically, the interpolation of maxima points and the minima points of a signal gives the upper envelope e^+ and the lower envelope e^- respectively using cubic-spline interpolation (Figure 3.5). The mean of these envelopes $l_{k,j}$ is subtracted from the local signal $h_{k,j}$. These steps are repeated with the proto-mode function $h_{k,j+1}$ until the generation of an IMF (Algorithm 1) [98]. Once the first IMF (Mode) is computed, it is subtracted from the original signal and the sifting process is repeated again with the residual signal r_{k+1} to extract the other IMFs.

Algorithm 1 Sifting process to extract the k^{th} IMF

- 1: **set** $j \leftarrow 0, h_{k,j+1} \leftarrow r_k$ Initialization
 - 2: **repeat** (Loop)
 - 3: **set** $j \leftarrow j + 1$
 - 4: **find** extrema of $h_{k,j}$ (minima and maxima)
 - 5: **compute** upper envelope e^+ by interpolation between maxima
 - 6: **compute** lower envelope e^- by interpolation between minima
 - 7: **compute** proto-local mean $l_{k,j} \leftarrow (e^+ + e^-)/2$
 - 8: **update** proto-local function $h_{k,j+1} \leftarrow h_{k,j} - l_{k,j}$
 - 9: **until** $h_{k,j+1}$ is an IMF. (End Loop)
 - 10: **set** $IMF_{k+1} \leftarrow h_{k,j+1}$, and $r_{k+1} \leftarrow r_k - IMF_{k+1}$ (Result)
-

3.3.3 Stopping criteria

Different approaches have been proposed to determine when the sifting process should be stopped. In general, in all these approaches, two objectives are considered :

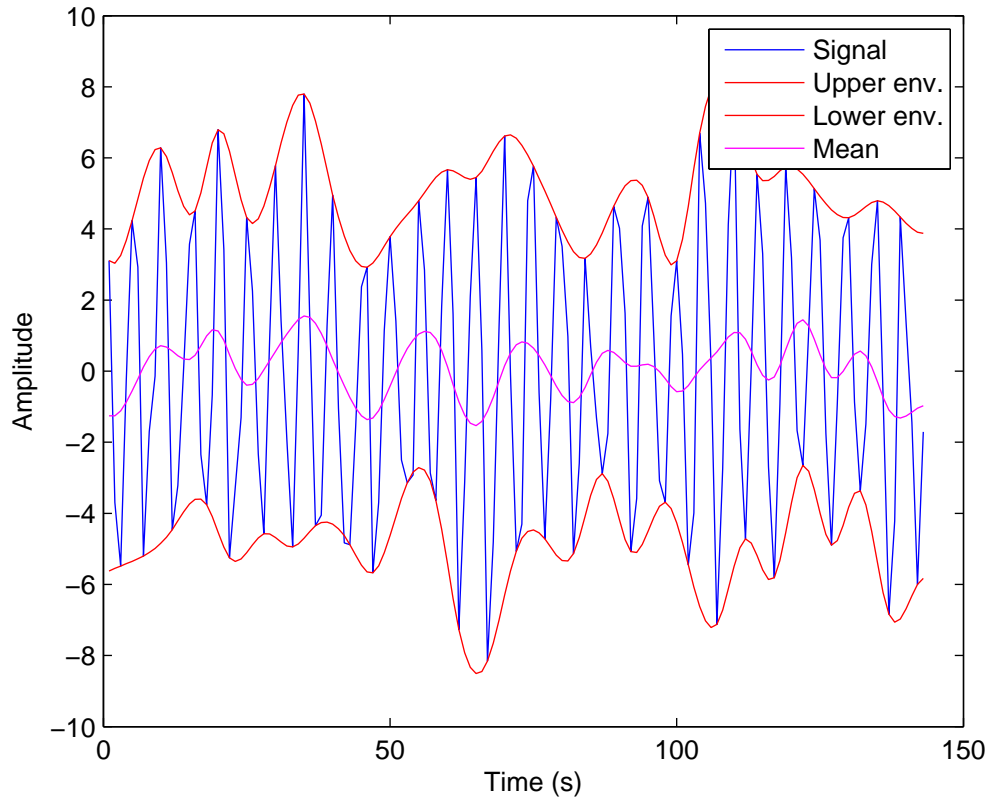


FIGURE 3.5: Upper, lower and mean envelopes of a signal

1. The signal being processed should verify the definition of an IMF.
2. The sifting process should not be iterated too many times to avoid denaturing the information within an IMF.

Mainly focused on the first objective, the approach proposed in [95] consists of stopping the sifting process when :

- All maxima are strictly positive and all minima are strictly negative.
- The SC criterion must be less than a threshold ϵ , in the range of 0.2-0.3 for a signal of 1024 points. The SC criterion can be expressed as follows :

$$SC = \sum_{i=1}^n \left(\frac{h_{k,j+1}(i) - h_{k,j}(i)}{h_{k,j}(i)} \right)^2 < \epsilon \quad (3.2)$$

where n is the number of sample in the signal $h_{k,j+1}$;

A new formulation of the SC criterion was proposed in [99, 100] :

$$SC = \frac{\sum_{i=1}^n (h_{k,j+1}(i) - h_{k,j}(i))^2}{\sum_{i=1}^n (h_{k,j}(i))^2} < \epsilon \quad (3.3)$$

Figure 3.6 summarizes the basic steps of EMD in a block diagram.

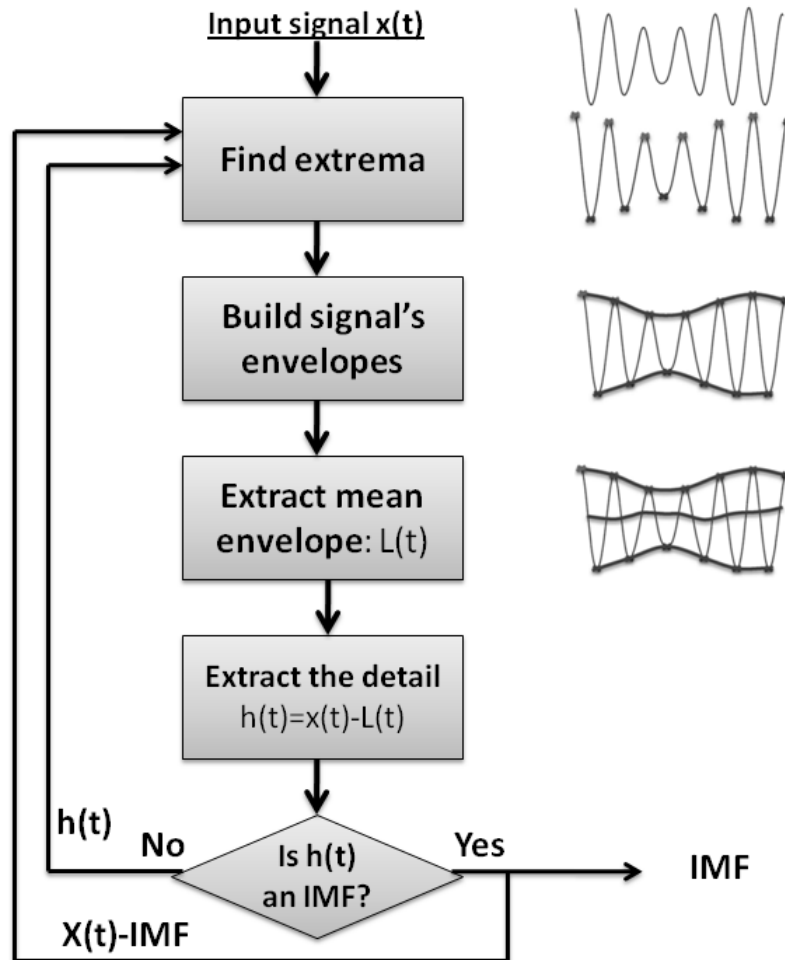


FIGURE 3.6: Block diagram of EMD

The EMD method has been widely used in signal and image processing [101], [102], [103], biomedical applications [104], and mechanical system identification [105]. It is well adapted for processing non-linear and non-stationary signals such as stabilometric signals. Moreover, it describes the signals locally, and separates the different oscillation components, which facilitate the analysis of each component apart.

The EMD method has various extensions such as Bivariate EMD (BEMD) for images analysis and bivariate signals, and Multiple EMD (MEMD) for multivariate analysis. The MEMD method allows to decompose several signals together at the same time.

Moreover, the Ensemble EMD (EEMD) method was proposed to improve the signal decomposition used in the classical EMD method.

3.3.4 Ensemble Empirical Model Decomposition

An extension of the EMD method, called Ensemble Empirical Mode Decomposition (EEMD) method [106] was introduced by Huang to enhance the performances obtained with the classical EMD method, which suffers from the mode-mixing problem that appears in some IMFs. The mode-mixing appears when an IMF consists of two different elementary signals, or when an elementary signal appears in two different IMFs.

The underlying idea in the EEMD method is to generate a finite number of white noise signals that have small standard deviation. Classical EMD should be applied to a set of signals; each trial consists of the original signal plus a white noise signal. Finally, the intrinsic mode functions are computed by averaging the IMFs resulting from all trials (Algorithm 2). This methodology avoids the mixing-mode problems and provides a good separation between modes that ensures isolation of each component having specific scales. This method allows obtaining a better decomposition of the stabilometric signals that ensures sensitive separation of frequencies in intrinsic mode functions. Consequently, this separation provides a better analysis of the diffusion curves than the standard EMD method.

Algorithm 2 EEMD algorithm

- 1: **Set** L : The number of the white noise signals and x : the initial signal
 - 2: **Loop** $l = 1$ to L
 - 3: **Generate** $w^{(l)}$: a white Gaussian noise signal of length n
 - 4: **Set** $X^{(l)} = x + w^{(l)}$ (the initial signal + a white noise signal)
 - 5: **Decompose** $X^{(l)}$ using classical EMD
 - 6: $X^{(l)} = \sum_{k=1}^K IMF_k^{(l)} + r_K^{(l)}$
 - 7: **End Loop**
 - 8: **Set** $\widetilde{IMF}_k = \frac{1}{L} \sum_{l=1}^L IMF_k^{(l)}$ where $k = 1, \dots, K$
 - 9: **Result** $x = \sum_{k=1}^K \widetilde{IMF}_k + \widetilde{r}_K$
-

3.4 Stabilogram-diffusion analysis

3.4.1 Brownian motion

Brownian motion is a special case from the family of Fractional Brownian Motion (FBM) that was introduced by Mandelbrot [107] [108]. FBM is a non-stationary Gaussian process characterized by the Hurst parameter H . This parameter has a real value between 0 and 1 that specifies the nature of correlations in a given process (positive or negative correlations). Note that the classical Brownian motion has a Hurst parameter (H) equal to 0.5, which means that past and future increments are not correlated. For $H < 0.5$, past and future increments of a stochastic process are negatively correlated. On the other hand, for $H > 0.5$, past and future increments are positively correlated, and consequently, the stochastic process is positively correlated.

3.4.2 Mean square displacement

The Hurst parameter can be calculated using the Mandelbrot equation (eq. 3.4) that is generalized from the relation given in equation (eq. 3.5). This is achieved by computing the mean square displacement of the stochastic process over a time interval (eq. 3.6) :

$$\langle \delta x^2 \rangle_{\tau} = \tau^{2H} \quad (3.4)$$

$$\langle \delta x^2 \rangle_{\tau} = 2 * D * \tau \quad (3.5)$$

$$\langle \delta x^2 \rangle_{\tau} = \frac{1}{n} \sum_{i=1}^n (x_{i+\tau} - x_i)^2 \quad (3.6)$$

Where $\langle \delta x^2 \rangle_{\tau}$ represents the mean square displacement for a signal x of n samples over a time interval τ ; D is the diffusion coefficient, and H , the Hurst parameter.

In [66, 67], Collins et al. study the center of pressure displacement of human body as a stochastic process. The random walk theory and the diffusion equation are applied on stabilometric signals to calculate the mean square displacement for each direction

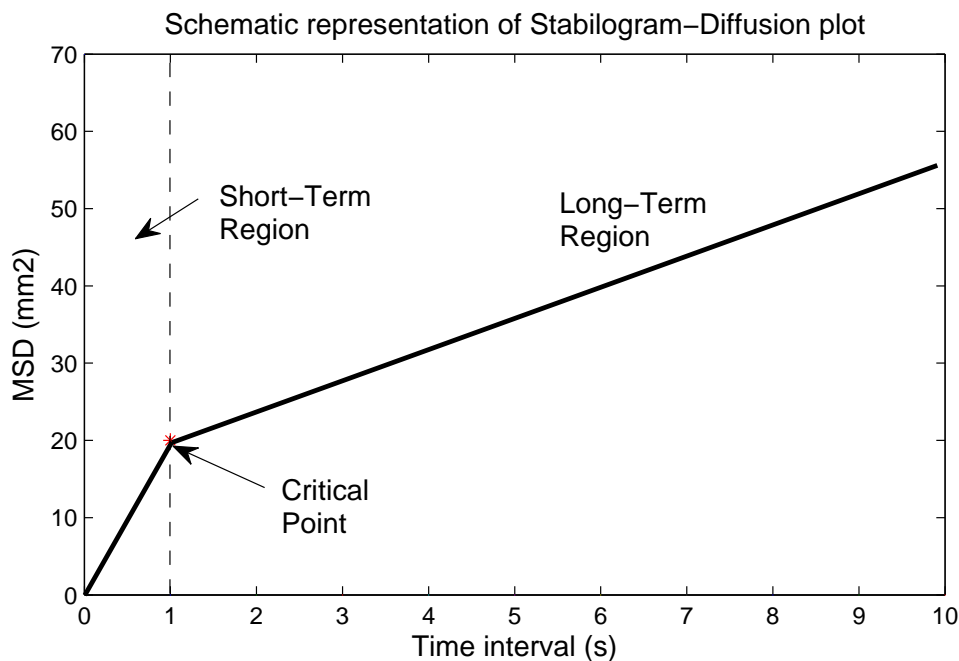


FIGURE 3.7: Diffusion curve of a stabilometric signal

ML/AP apart and for the planar (ML Vs. AP), as one and two-dimensional random walk. This study is called Stabilogram-diffusion analysis. The mean square displacement versus time interval values ($0.1 < \tau < 10$ sec) is called the diffusion curve (Figure 3.7). This diffusion curve shows two different regions. The first region corresponds to a relatively small time interval where the Hurst parameter is greater than 0.5 [66, 67]. The second region corresponds to the remaining time interval where the Hurst parameter is less than 0.5. Consequently, the postural control system consists of two processes, a positive correlated process (the past and future increments are positively correlated in the quiet standing), and a negative correlated process, where the past and future increments are negatively correlated for long time interval values.

3.5 EMD-based approach for posture analysis

The block diagram presented in figure 3.8 shows the global methodology proposed to extract parameters including the gain and the critical point. First, the stabilometric signals in ML and AP directions are decomposed using the EMD method to generate several IMFs components (Figures 3.9 and 3.10). Second, the stabilogram-diffusion technique is applied over five IMFs starting from IMF3 to generate their diffusion curves. These

curves are then modeled as a system of second order response to extract sensitive parameters for control postural analysis. The first IMFs (IMFs 1 and 2) are ignored because they mostly represent noises. Repeated measures analysis of variance (ANOVA) is used to perform a statistical analysis of these parameters under feet and visual conditions, as well as for young/elderly and for women/man groups.

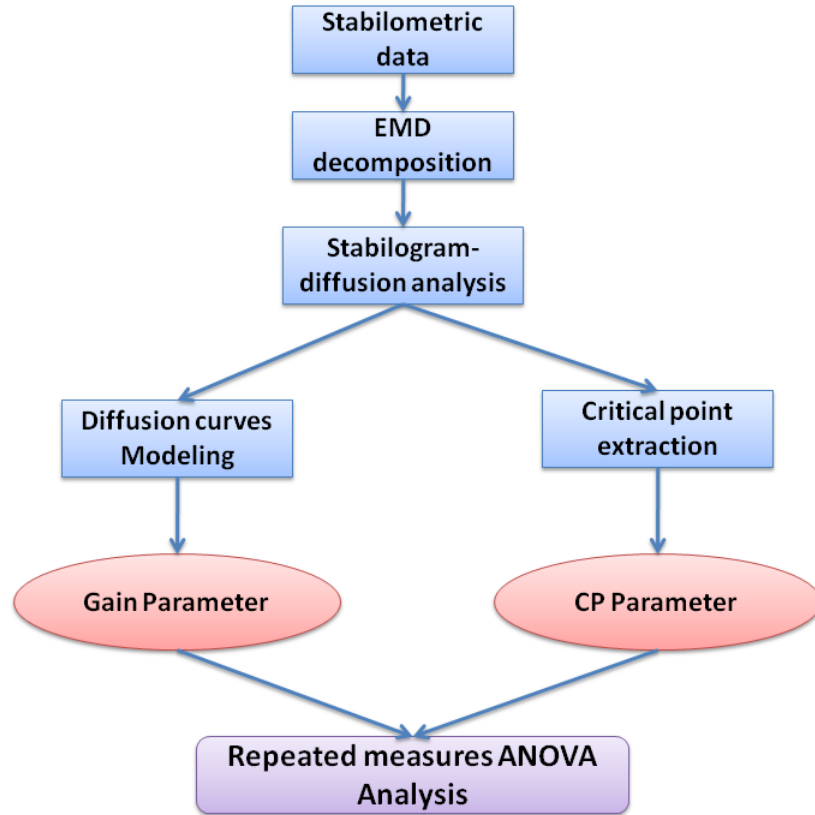


FIGURE 3.8: The proposed methodology

3.5.1 Diffusion curves modeling

The diffusion curves of the obtained IMFs correspond to different forms of the classical diffusion curve proposed by Collins (Figure 3.7). These curves can be modeled as a system of second order response. First, the values of the mean square displacement increase and then converge to a specific value (Figure 3.12). For this purpose, a second order response equation is used to model these curves, such as :

$$\langle \delta x^2 \rangle_t = G * \left(1 - \frac{e^{-z \cdot w_n \cdot t}}{\sqrt{1 - z^2}} \cdot \sin(w_n \cdot \sqrt{1 - z^2} \cdot t + \arcsin(\sqrt{1 - z^2})) \right) \quad (3.7)$$

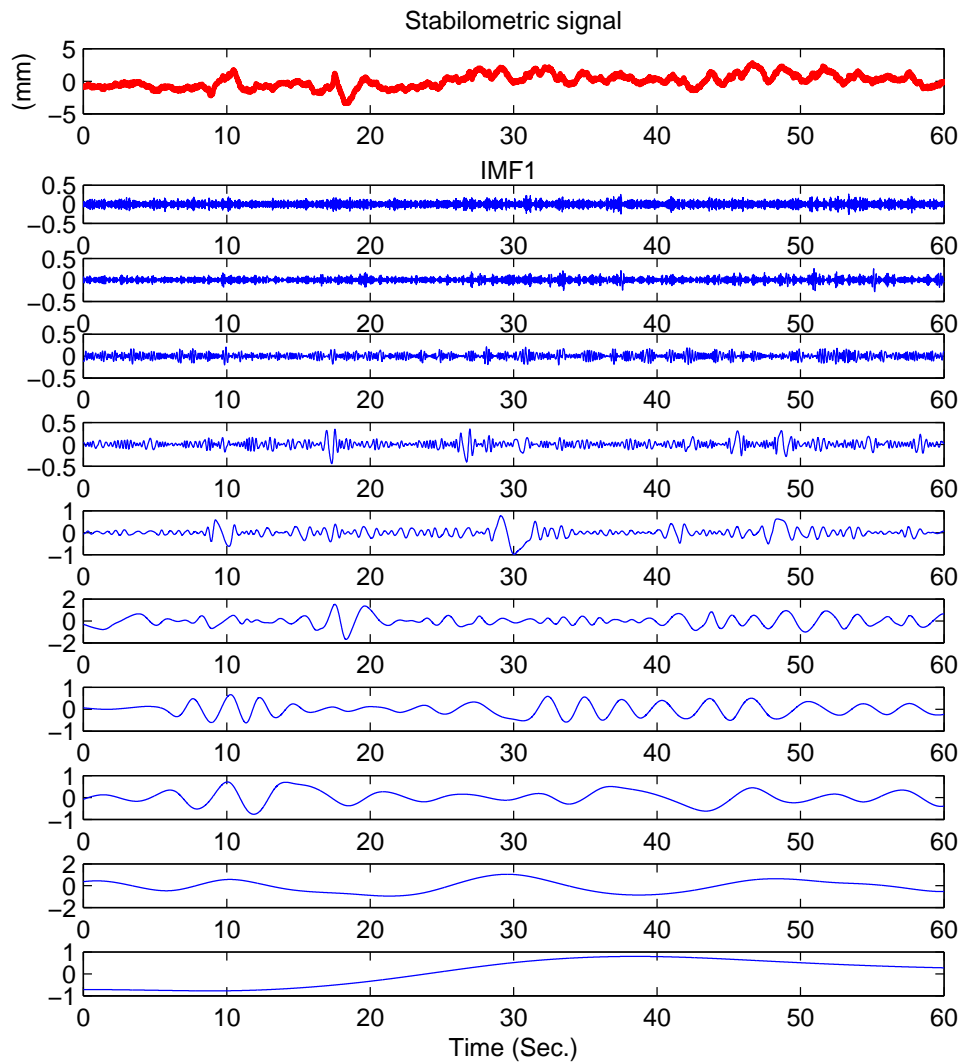


FIGURE 3.9: ML stabilometric signal and its EMD decomposition for FAEO condition

where G represents the gain, z the damping ratio and w_n the natural frequency.

A least square optimization strategy is used to identify the parameters G , z , and w_n for each mode. The adopted least squares strategy minimizes the square errors between the real values and the estimated values of parameters for each diffusion curve. The first IMFs (IMFs 1 and 2) are ignored because they mostly represent noises.

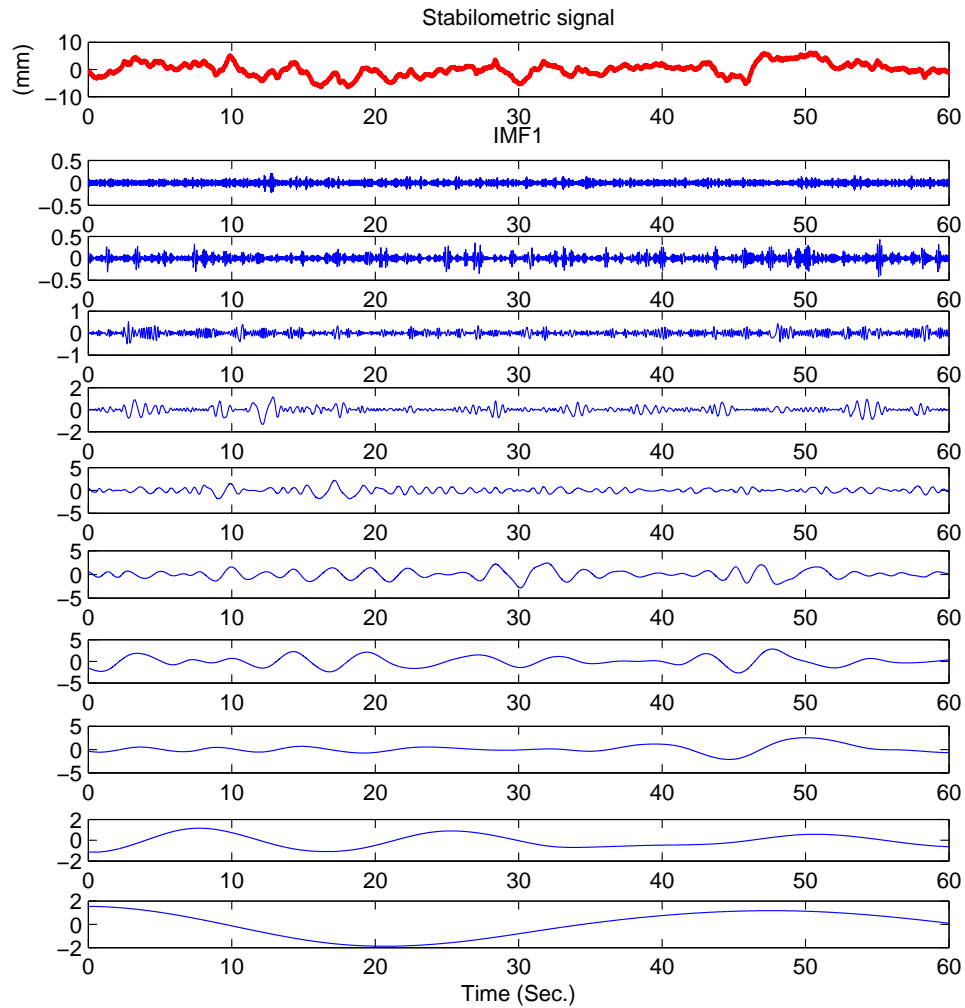


FIGURE 3.10: AP stabilometric signal and its EMD decomposition for FAEO condition

3.6 Results and discussions

3.6.1 Balance analysis : classical approach

All obtained results are presented in Tables 3.3 and 3.4. "ns" means no significant differences was founded. One can observe that CoP excursion for women is lower along AP and ML directions than for men, while CoP planar velocity is similar. Feet together condition induces an increase in CoP excursions (AP and ML) and mean velocity. Similarly, an increase in ML CoP excursion and mean velocity can be observed under the eyes closed condition. These results show an interaction between feet condition and each gender. No effect of age on CoP excursion and mean velocity was found.

TABLE 3.3: Stabilometric results

	Range of CoP		Mean velocity
	AP (mm)	ML (mm)	(mm/s)
Young			
Women (=7)			
Feet apart			
Eyes open	19 ± 5	9 ± 3	7 ± 3
Eyes closed	21 ± 5	9 ± 2	8 ± 5
Feet Together			
Eyes open	25 ± 5	27 ± 4	10 ± 4
Eyes closed	25 ± 5	29 ± 4	12 ± 6
Men (n=7)			
Feet apart			
Eyes open	26 ± 7	12 ± 7	7 ± 2
Eyes closed	30 ± 10	10 ± 1	8 ± 2
Feet together			
Eyes open	32 ± 6	34 ± 6	12 ± 5
Eyes closed	29 ± 5	35 ± 4	15 ± 7
Elderly			
Women (n=7)			
Feet apart			
Eyes open	24 ± 10	8 ± 3	8 ± 2
Eyes closed	24 ± 8	8 ± 3	8 ± 3
Feet together			
Eyes open	25 ± 9	29 ± 4	12 ± 6
Eyes closed	27 ± 9	30 ± 7	15 ± 7
Men (n=7)			
Feet apart			
Eyes open	26 ± 4	10 ± 2	11 ± 7
Eyes closed	31 ± 8	11 ± 2	14 ± 8
Feet together			
Eyes open	32 ± 8	35 ± 7	15 ± 7
Eyes closed	40 ± 8	45 ± 8	25 ± 16

3.6.2 Balance analysis using EMD

The parameters G , z and w_n defined in the previous section, are calculated and compared with respect to the five diffusion curves. These diffusion curves correspond to IMF3, IMF4, IMF5, IMF6 and IMF7 of the EMD decomposition of the original stabilometric signals. By analyzing the relationship between the gain parameter G and the natural frequency w_n , it can be observed that the gain values related to IMF3 and IMF4 are relatively small while their natural frequencies are relatively high, as shown on the right part of figure 3.11. Also, as shown in the left part of figure 3.11, the IMF5, IMF6 and IMF7 show relatively high gain values and low w_n values.

TABLE 3.4: Effect of age, gender, feet position and vision for the COP excursion and the mean velocity parameters

	Range AP	Range ML	MPV
Age	ns	ns	ns
Gender	0.007	0.0002	ns
Age*Gender	ns	ns	ns
Feet	<0.0001	<0.0001	<0.0001
Feet*Age	ns	ns	ns
Feet*Gender	ns	0.002	ns
Feet*Age*Gender	0.01	ns	ns
Vision	ns	0.003	<0.0001
Vision*Age	ns	ns	ns
Vision*Gender	ns	ns	ns
Vision*Age*Gender	ns	0.049	ns
Feet*Vision	ns	0.0007	0.0005
Feet*Vision*Age	ns	ns	ns
Feet*Vision*Gender	ns	ns	ns
Feet*Vision*Age*Gender	ns	ns	ns

p-value based on 4-way repeated measures ANOVA.

3.6.2.1 Gain analysis

The mean and standard deviation of the gain G as a function of w_n is shown in Figure 3.11 with respect to the four conditions FAEC, FAEO, FTEC and FTEO. It is clearly observed that the gain parameter related to feet together condition (FTEC and FTEO) shows higher values with respect to those under apart condition (FAEC and FAEO). The gain parameter can be seen as a stability indicator of the human body. Indeed, the gain parameter gives a significant and fair image of the fluctuation of the center of pressure. When the the gain value is small, the stability of the human body is high, and when the value of the gain is relatively high, the stability is weak.

Table 3.5 provides a representation of the gain parameters (Gain3, Gain4, Gain5, Gain6 and Gain7) related to the diffusion curves of the IMF3, IMF4, IMF5, IMF6 and IMF7. The gain values for all subjects who participated in this study are shown in terms of means and standard deviations. To facilitate the analysis, the results are analyzed using four groups : young-women, young-men, elderly-women and elderly-men. For each group, the results are expressed in AP and ML directions based on feet and eyes conditions.

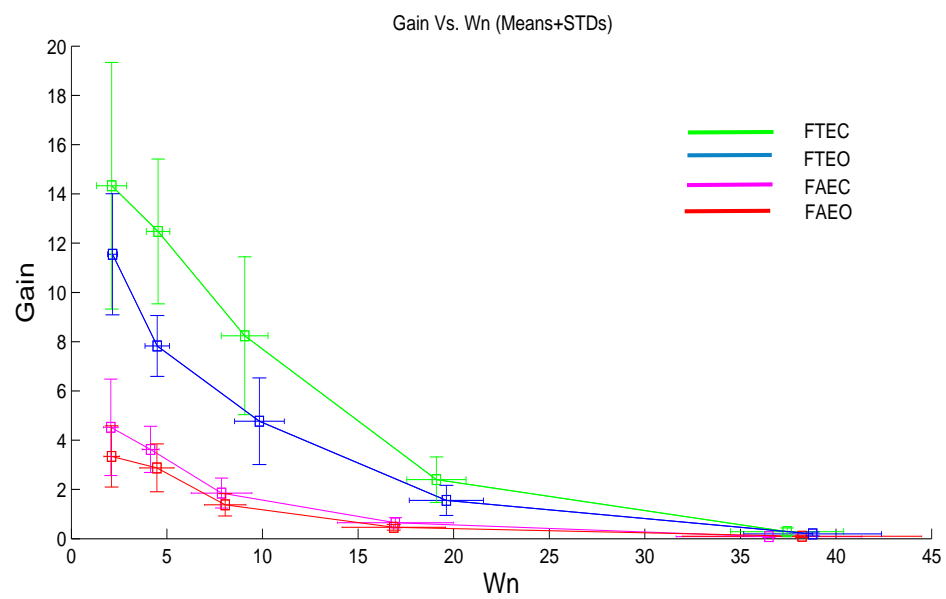
FIGURE 3.11: Natural frequencies (ω_n) Vs Gain (G) : means + STDs

TABLE 3.5: Mean (STD) of gain parameters

	Gain 3		Gain 4		Gain 5		Gain 6		Gain 7	
	AP (mm)	ML (mm)								
Young										
<i>Women</i>										
Feet apart										
Eyes open	0.15 ± 0.13	0.01 ± 0.01	0.10 ± 0.07	0.04 ± 0.04	0.22 ± 0.1	0.2 ± 0.16	0.66 ± 0.3	0.30 ± 0.12	1.69 ± 0.91	0.22 ± 0.14
Eyes closed	0.17 ± 0.09	0.02 ± 0.01	0.12 ± 0.05	0.05 ± 0.05	0.33 ± 0.16	0.39 ± 0.48	1.13 ± 0.77	0.35 ± 0.17	2.75 ± 1.90	0.21 ± 0.09
Feet together										
Eyes open	0.37 ± 0.4	0.22 ± 0.15	0.22 ± 0.18	0.17 ± 0.06	0.39 ± 0.16	0.8 ± 0.3	1.01 ± 0.29	1.98 ± 0.74	2.38 ± 0.9	4.44 ± 1.76
Eyes closed	0.50 ± 0.76	0.23 ± 0.12	0.32 ± 0.38	0.23 ± 0.07	0.68 ± 0.3	1.45 ± 1.05	1.77 ± 0.54	3.83 ± 1.61	3.72 ± 2.66	7.31 ± 2.2
<i>Men</i>										
Feet apart										
Eyes open	0.73 ± 0.8	0.09 ± 0.21	0.43 ± 0.41	0.09 ± 0.11	0.47 ± 0.2	0.23 ± 0.06	1.13 ± 0.37	0.65 ± 0.47	2.08 ± 1.02	0.51 ± 0.43
Eyes closed	0.75 ± 0.09	0.10 ± 0.01	0.44 ± 0.5	0.05 ± 0.04	0.59 ± 0.31	0.25 ± 0.12	1.52 ± 0.65	0.77 ± 0.41	3.97 ± 0.74	0.38 ± 0.21
Feet together										
Eyes open	1.09 ± 1.35	0.74 ± 0.61	0.65 ± 0.64	0.47 ± 0.40	0.83 ± 0.33	1.17 ± 0.36	1.82 ± 0.74	2.41 ± 0.64	2.74 ± 1.2	4.33 ± 1.47
Eyes closed	0.87 ± 0.23	0.57 ± 0.39	0.39 ± 0.31	0.49 ± 0.41	1.01 ± 0.61	1.77 ± 1.17	3.5 ± 0.96	4.97 ± 2.66	4.48 ± 1.57	11.01 ± 4.93
Elderly										
<i>Women</i>										
Feet apart										
Eyes open	0.58 ± 0.71	0.01 ± 0.01	0.33 ± 0.51	0.02 ± 0.01	0.52 ± 0.39	0.18 ± 0.11	1.02 ± 0.48	0.31 ± 0.14	2.42 ± 1.57	0.18 ± 0.12
Eyes closed	0.65 ± 0.31	0.02 ± 0.01	0.25 ± 0.19	0.03 ± 0.03	0.53 ± 0.31	0.24 ± 0.12	1.07 ± 0.41	0.36 ± 0.25	2.58 ± 0.94	0.21 ± 0.10
Feet together										
Eyes open	0.30 ± 0.29	0.25 ± 0.13	0.21 ± 0.18	0.23 ± 0.06	0.54 ± 0.17	1.57 ± 0.35	1.97 ± 0.96	3.03 ± 0.83	2.62 ± 1.45	5.27 ± 2.06
Eyes closed	0.27 ± 0.29	0.30 ± 0.25	0.24 ± 0.19	0.34 ± 0.18	1.04 ± 0.29	2.09 ± 0.79	2.78 ± 1.26	4.66 ± 2.40	3.54 ± 1.80	6.34 ± 2.65
<i>Men</i>										
Feet apart										
Eyes open	0.36 ± 0.41	0.02 ± 0.01	0.33 ± 0.23	0.05 ± 0.04	0.82 ± 0.51	0.31 ± 0.26	2.07 ± 1.01	0.54 ± 0.27	3.64 ± 1.22	0.31 ± 0.20
Eyes closed	0.37 ± 0.29	0.05 ± 0.01	0.54 ± 0.53	0.07 ± 0.06	1.56 ± 1.07	0.43 ± 0.39	3.59 ± 2.01	0.66 ± 0.24	5.77 ± 1.77	0.36 ± 0.16
Feet together										
Eyes open	1.37 ± 2.21	0.54 ± 0.35	0.93 ± 1.36	0.54 ± 0.24	1.11 ± 0.58	2.56 ± 1.58	2.52 ± 0.44	4.80 ± 1.61	3.76 ± 1.33	8.16 ± 3.44
Eyes closed	1.08 ± 0.68	1.15 ± 0.89	1.52 ± 1.37	1.45 ± 1.05	3.14 ± 3.07	5.75 ± 3.75	7.78 ± 6.21	8.74 ± 4.17	6.45 ± 3.01	12.6 ± 5.52

TABLE 3.6: Effect of age, gender, feet position and vision on EMD results.

p-value	Gain3		Gain4		Gain5		Gain6		Gain7	
	AP	ML	AP	ML	AP	ML	AP	ML	AP	ML
Age	ns	ns	ns	ns	ns	0.005	0.007	0.006	ns	ns
Gender	ns	0.003	0.008	0.001	0.008	ns	0.001	0.003	0.008	0.005
Age*Gender	ns	ns	ns	ns	ns	ns	ns	ns	ns	ns
Feet	ns	<0.0001	0.006	<0.0001	0.001	<0.0001	0.003	<0.0001	0.002	<0.0001
Feet*Age	ns	ns	ns	0.015	ns	0.004	ns	ns	ns	ns
Feet*Gender	ns	0.0018	ns	0.0009	ns	0.02	ns	ns	ns	0.01
Feet*Age*Gender	0.002	ns	0.008	ns	ns	ns	ns	ns	ns	ns
Vision	ns	ns	ns	ns	0.01	0.0002	0.001	<0.0001	<0.0001	<0.0001
Vision*Age	ns	ns	ns	ns	ns	ns	ns	ns	ns	ns
Vision*Gender	ns	ns	ns	ns	ns	ns	ns	ns	ns	0.009
Vision*Age*Gender	ns	ns	ns	ns	ns	ns	ns	ns	ns	ns
Feet*Vision	ns	ns	ns	0.009	ns	0.0003	<0.0001	<0.0001	ns	<0.0001
Feet*Vision*Age	ns	ns	ns	ns	ns	ns	ns	0.006	ns	ns
Feet*Vision*Gender	ns	ns	ns	ns	ns	ns	ns	ns	ns	0.007
Feet*Vision*Age*Gender	ns	ns	ns	ns	ns	ns	ns	ns	ns	ns

It is clearly observed that the gain values with eyes open condition are often smaller than those with eyes closed condition for all groups : young/elderly or women/men, in both ML and AP directions. For example, the mean value of Gain4 for young-women under feet together is equal to 0.22 for eyes-open condition and 0.32 for eyes-closed condition, in the AP direction. It is equal to 0.17 and 0.23 respectively in the ML direction.

Furthermore, the gain values under feet apart condition are smaller than those under feet together condition. For example, the mean value of Gain5 for elderly-men with eyes open in AP direction is equal to 0.82 and 1.11 for feet apart and feet together conditions respectively, while it is equal to 0.31 and 2.56 for the same conditions in the ML direction. It can be noted that the feet position affects more the stability in ML direction rather than in AP direction as the variability of the gain values between feet apart and feet together condition is more important in ML than in AP direction. These results show clearly that, the human body during quiet standing is more stable with eyes-open rather than eyes-closed condition, and is more stable under feet apart condition rather than under feet together condition. Moreover, the highest differences between gain values is shown between young subjects under feet apart and elderly subjects under feet together and particularly with regards to the gains of the fifth, sixth and seventh IMFs. These relatively high differences are mainly related to two conditions that affect the stability of the human body, that are the age and the feet position. For example, the mean value of Gain6 for young-men under feet apart and eyes closed is equal to 0.77 whereas it is equal to 8.74 for elderly-men under feet together and closed eyes, both in AP direction (Table 3.5).

Table 3.6 shows a statistical analysis using repeated measures ANOVA by taking into account the different conditions for each gain in both ML and AP directions. These conditions are : age (young versus women), gender (women versus men), feet position (feet apart versus together) and eyes condition (eyes open versus together). Anova Statistical analysis is done for each condition first, and then, for combinations of different conditions, such as Age with gender, feet with age, and feet with age and gender, etc. In total, 15 statistical tests in different combinations are conducted for all conditions. In the following, we consider a p -value with a value less than 0.05 equivalent to significant differences between groups based on the related conditions. In the other cases, "ns" means no significant differences was founded.

It can be noted from Table 3.6 that the number of p -values less than 0.05 in the ML direction is greater than in the AP direction. For example, Gain3 has only one p -value less than 0.05 in AP direction and three in ML direction . For Gain4, there are four p -values less than 0.05 in the AP direction and five p -values less than 0.05 in the ML direction. Also, Table 3.6 shows significant differences for Gain6 between the different conditions in the ML direction. As a result, Gain4 and Gain5 have the highest sensitivity and many small p -values, especially in the ML direction.

By analyzing the rows of Table 3.6, it can be noted that the feet position is ranked first as an essential condition since all parameters are affected and show p -values less than 0.05. These parameters have significant differences between feet apart and feet together conditions. Also, all parameters have high sensitivities and show significant differences between women and men (gender) in AP and ML direction. Furthermore, vision, feet*vision, age, and feet*gender have an important number of p -values that reflect significant differences between groups.

Compared to the statistical parameters calculated in section 3.6.1, the gain parameter extracted using the proposed approach for the different IMFs, shows significant differences as a function of visual conditions, feet position, age and gender (p -values less than 0.05). The gain parameter shows better sensitivity with respect to the different conditions including subjects who have small influence on the stability, while the statistical parameters are limited to detect the differences between feet apart and feet together conditions and do not show significant differences based on the feet placements, age and

gender (p -values > 0.05).

3.6.2.2 CP analysis

The critical point CP is identified as the first maximum of the diffusion curve that separates the two regions (Figure 3.12).

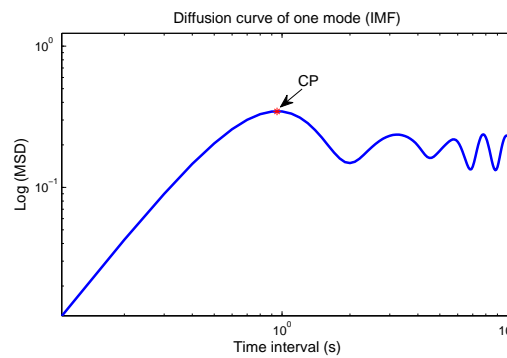


FIGURE 3.12: Diffusion curve of an IMF (mode)

Indeed, there are also two regions in each new diffusion curve; the MSD values increase linearly in the first region and then oscillate around a specific value in the second one. In this study, CP_i corresponds to the critical point of IMF_i .

TABLE 3.7: Mean (STD) of CP parameters

	CP 3		CP 4		CP 5		CP 6		CP 7	
	AP (mm)	ML (mm)	AP (mm)	ML (mm)	AP (mm)	ML (mm)	AP (mm)	ML (mm)	AP (mm)	ML (mm)
Young: Women										
Feet apart										
Eyes open	0.03 ± 0.01	0.006 ± 0.004	0.05 ± 0.02	0.06 ± 0.05	0.33 ± 0.15	0.31 ± 0.23	1.04 ± 0.48	0.51 ± 0.19	2.66 ± 1.4	0.33 ± 0.19
Eyes closed	0.02 ± 0.01	0.007 ± 0.006	0.06 ± 0.04	0.07 ± 0.06	0.50 ± 0.24	0.63 ± 0.76	1.68 ± 1.12	0.56 ± 0.26	4.48 ± 3.03	0.34 ± 0.14
Feet together										
Eyes open	0.04 ± 0.03	0.031 ± 0.014	0.09 ± 0.03	0.12 ± 0.03	0.50 ± 0.21	1.26 ± 0.50	1.58 ± 0.51	3.14 ± 1.15	3.83 ± 1.33	6.99 ± 2.29
Eyes closed	0.07 ± 0.07	0.034 ± 0.012	0.14 ± 0.06	0.17 ± 0.07	0.92 ± 0.45	2.27 ± 1.47	2.75 ± 0.82	6.16 ± 2.34	6.13 ± 4.06	11.67 ± 3.08
Young: Men										
Feet apart										
Eyes open	0.08 ± 0.07	0.019 ± 0.025	0.11 ± 0.05	0.07 ± 0.03	0.49 ± 0.19	0.32 ± 0.1	1.65 ± 0.54	1.02 ± 0.7	3.46 ± 1.56	0.77 ± 0.58
Eyes closed	0.09 ± 0.09	0.014 ± 0.017	0.13 ± 0.08	0.077 ± 0.072	0.65 ± 0.20	0.34 ± 0.18	2.28 ± 1.10	1.16 ± 0.62	6.66 ± 1.09	0.61 ± 0.27
Feet together										
Eyes open	0.14 ± 0.13	0.091 ± 0.079	0.21 ± 0.12	0.19 ± 0.12	0.98 ± 0.43	1.7 ± 0.69	2.75 ± 1.19	3.87 ± 1.14	4.36 ± 1.77	6.79 ± 2.21
Eyes closed	0.10 ± 0.10	0.095 ± 0.081	0.33 ± 0.41	0.32 ± 0.36	1.49 ± 0.88	2.82 ± 1.82	5.50 ± 0.93	8.03 ± 4.04	7.93 ± 2.23	17.62 ± 7.45
Elderly: Women										
Feet apart										
Eyes open	0.07 ± 0.10	0.07 ± 0.005	0.12 ± 0.08	0.02 ± 0.02	0.63 ± 0.49	0.28 ± 0.17	1.49 ± 0.55	0.51 ± 0.23	3.79 ± 2.23	0.29 ± 0.18
Eyes closed	0.05 ± 0.04	0.09 ± 0.007	0.13 ± 0.082	0.03 ± 0.03	0.77 ± 0.51	0.32 ± 0.19	1.69 ± 0.62	0.57 ± 0.41	4.16 ± 1.45	0.27 ± 0.15
Feet together										
Eyes open	0.04 ± 0.04	0.102 ± 0.039	0.10 ± 0.03	0.45 ± 0.25	0.77 ± 0.16	4.03 ± 2.51	3.84 ± 1.22	7.75 ± 2.28	4.22 ± 2.17	13.21 ± 5.09
Eyes closed	0.04 ± 0.03	0.348 ± 0.267	0.18 ± 0.10	1.38 ± 1.20	1.59 ± 0.39	9.21 ± 5.64	4.70 ± 2.05	13.9 ± 6.26	5.81 ± 2.74	20.77 ± 8.36
Elderly: Men										
Feet apart										
Eyes open	0.07 ± 0.05	0.011 ± 0.009	0.24 ± 0.18	0.06 ± 0.07	1.24 ± 0.86	0.46 ± 0.54	3.24 ± 1.42	0.92 ± 0.44	5.82 ± 1.77	0.50 ± 0.29
Eyes closed	0.13 ± 0.12	0.017 ± 0.016	0.65 ± 0.60	0.09 ± 0.09	2.44 ± 1.58	0.74 ± 0.71	5.60 ± 3.06	1.09 ± 0.37	9.71 ± 2.85	0.57 ± 0.23
Feet together										
Eyes open	0.71 ± 0.26	1.42 ± 0.012	0.41 ± 0.34	0.16 ± 0.04	1.37 ± 0.66	2.54 ± 0.56	3.97 ± 0.77	4.86 ± 1.2	6.06 ± 2.03	15.55 ± 3.37
Eyes closed	0.91 ± 0.41	1.57 ± 0.028	1.53 ± 0.34	0.31 ± 0.19	4.69 ± 4.44	3.41 ± 1.20	7.19 ± 9.72	13.39 ± 3.71	10.44 ± 4.56	22.63 ± 4.20

TABLE 3.8: Repeated measures ANOVA analysis of CP parameters

p-values	CP3		CP4		CP5		CP6		CP7	
	AP	ML	AP	ML	AP	ML	AP	ML	AP	ML
Age	ns	ns	ns	0.04	0.016	0.005	0.003	0.008	Ns	ns
Gender	0.01	0.002	0.04	0.02	0.02	0.027	0.003	0.003	0.008	0.005
Age*Gender	ns	ns	ns	ns	ns	ns	ns	ns	Ns	ns
Feet	0.006	<0.0001	0.02	0.0001	0.004	<0.0001	<0.0001	<0.0001	0.001	<0.0001
Feet*Age	ns	0.02	ns	0.011	ns	0.004	0.02	0.008	Ns	ns
Feet*Gender	0.02	0.001	ns	0.016	ns	0.03	ns	0.035	Ns	0.01
Feet*Age*Gender	0.02	ns	ns	ns	ns	ns	ns	ns	Ns	ns
Vision	ns	0.026	ns	0.008	0.008	0.0001	0.002	<0.0001	<0.0001	<0.0001
Vision*Age	ns	0.027	ns	ns	ns	ns	ns	ns	Ns	ns
Vision*Gender	ns	ns	ns	ns	ns	0.03	0.03	ns	0.01	0.01
Vision*Age*Gender	ns	0.046	ns	ns	ns	0.02	ns	ns	Ns	ns
Feet*Vision	ns	0.017	ns	0.007	0.003	0.0002	0.006	<0.0001	Ns	<0.0001
Feet*Vision*Age	ns	0.026	ns	0.05	0.049	0.03	ns	ns	Ns	ns
Feet*Vision*Gender	ns	0.032	ns	ns	ns	0.02	0.03	ns	Ns	0.009
Feet*Vision*Age*Gender	ns	0.041	ns	ns	ns	0.05	ns	ns	Ns	ns

Table 3.7 gives the mean and the standard deviation values of the CP parameters. These results are related to four groups : young-women, young-men, elderly-women and elderly-men. For each group, the results are shown in both AP and ML directions based on feet and eyes conditions. The CP parameter can be seen as a stability indicator of the human body ; it gives information about the fluctuation of the center of pressure. When the values of the CP are high, the stability is weak. It is clearly noticed that the CP5 values with eyes open condition are often smaller than those with eyes closed. Furthermore, the CP values under feet apart condition are smaller than those under feet together condition. We can notice here that the evolution of CP values between feet apart and feet together conditions is more remarkable in the ML direction than in AP direction, and hence, the feet position affects more the stability in the ML direction than in the AP direction. Moreover, one can notice the high differences between CP values due to the influence of both age and feet position conditions. For example, the mean value of CP5 for elderly-men group under feet together condition is higher than that for young-men group under feet apart condition.

Table 3.8 shows the p-values of the statistical tests repeated measures ANOVA for all combinations : age (young vs women), gender (women vs men), feet position (feet apart vs together) and vision (eyes open vs together). This analysis is achieved for all CP parameters in the the ML and AP directions. This statistical test allows to analyze each condition separately and also all combinations between conditions such as Age with gender, feet with age, feet with age with gender. In Table 3.8, one can observe that the CP parameters in ML direction have p-values less than 0.05 more than those in AP direction. For CP3, there are four p-values less than 0.05 in AP direction but there are

eleven p-values less than 0.05 in the ML direction. Also, CP5 shows significant differences for almost all conditions combinations in the ML direction. For CP6, several p-values less than 0.05 were found for the following conditions and combinations : age, gender, feet position, feet*age, feet*gender, vision, and feet*vision in the ML direction. In addition, feet position is ranked first as an essential condition since all CP are affected and have significant differences between feet apart and feet together conditions. All parameters have high sensitivities with respect to women and men (gender) in both AP and ML directions. Furthermore, vision, feet*vision, age, feet*gender, and feet*age combinations have a lot of relatively small p-values that reflect the high sensitivity of the CP.

3.7 Conclusion

We presented in this chapter a new approach based on the EEMD method to analyze the human stability during quiet standing. The obtained results show that the gain and CP parameters, extracted from the diffusion curves, are more sensitive than conventional stabilometric parameters in the postural stability analysis.

The analysis of the gain and CP parameters shows how the visual condition and feet position can improve the equilibrium in the quiet standing, especially, the feet position affects the human stability more than the visual conditions.

By using the gain and CP parameters extracted from the diffusion curves, it can be noticed that the human body is more stable under feet apart condition than under feet together condition. It is also more stable with open eyes condition than with closed eyes condition. The extracted parameters reveal also that the feet position affects more the stability in the ML direction than in AP direction. It is also shown that young population shows better stability in the static posture with significant differences compared to the elderly population. Women present also better stability in terms of IMFs gain values with respect to men in the same conditions. The present findings could help clinicians to better understand the motor strategies used by the patients during their static postures and may guide the rehabilitation process.

Chapitre 4

EMD-BASED FEATURE EXTRACTION AND SELECTION FOR SUBJECTS CLASSIFICATION

4.1 Introduction

Parkinson's disease (PD) is one from the most common degenerative movement disorders which is characterized by the progressive loss of specific neurons in the substantia nigra, called dopaminergic neurons. It has a strong effect on postural stability during quiet standing situations, and during locomotion.

Many researchers have investigated the postural stability of PD subjects in static (quiet standing) and dynamic (gait) postures [81–89]. Several data mining techniques were used to extract information from PD data for differentiating between healthy and PD subjects [90, 91]. Most of the commonly analyzed COP output measures are not sensitive enough. Thus, the standard spatio-temporal analysis of the COP provides only descriptive information which is not sufficiently relevant to analyze the postural system behaviors of PD disease.

In [90], accelerometer-based data recorded from healthy and PD subjects were used to analyze posture in a quiet stance. First, 175 temporal and spectral features were computed, and then, feature selection with classification techniques were used to select the best parameters that discriminate between healthy and PD subjects. Two parameters were selected to clearly differentiate the healthy subjects from the PD subjects.

In this chapter, we propose a novel methodology for discriminating between healthy and PD subjects through EMD-based temporal and spectral features extraction from stabilometric signals. The data used in this study are those collected from twenty eight healthy subjects that were described in chapter III, in addition to data collected from thirty two PD subjects that are also measured in Mondor hospital with the same equipment and data collection protocols.

The proposed methodology consists of four steps. In the first step, the EMD is applied to decompose each stabilometric signal into several elementary signals called Intrinsic Mode Functions (IMFs). This decomposition provides an effective time-frequency analysis of the stabilometric signals. The first eight IMFs are selected for further processing. The second step consists of a feature extraction which is performed by calculating the temporal and spectral characteristics from raw stabilometric data and their corresponding IMFs. In the third step, a feature selection method is applied to retain the first five

relevant characteristics. In the fourth step, four well-known classification methods including KNN, CART, RF and support vector machine (SVM) are used for the classification task.

The rest of this chapter is organized as follows : The supervised classification methods used in this study are described in Section 4.2. Section 4.3 presents the proposed framework for discriminating between healthy and PD subjects using stabilometric data. Finally, section 4.4 presents the experimental results and discussions of this study.

4.2 Classification techniques

In this section, we describe briefly the supervised classification techniques that are used in the study.

4.2.1 K Nearest Neighbors

K-Nearest Neighbors (KNN) [109] is a supervised classification method widely used for its simplicity and performance. This method is one of the non-parametric approaches that do not need any information about the distribution of different classes or type of separating surfaces. KNN does not need any modeling or explicit training phase before the classification process. The classification of new individual includes two main steps :

- (1) Calculating the distance between this individual with all the individuals in the training data set. The Euclidean distance is used in this study.
- (2) Selecting the K nearest neighbors to assign as output label, the majority class of these k nearest individuals (Figure 4.1).

The performance of this approach depends on the value of K ; this value is in general determined by a cross validation.

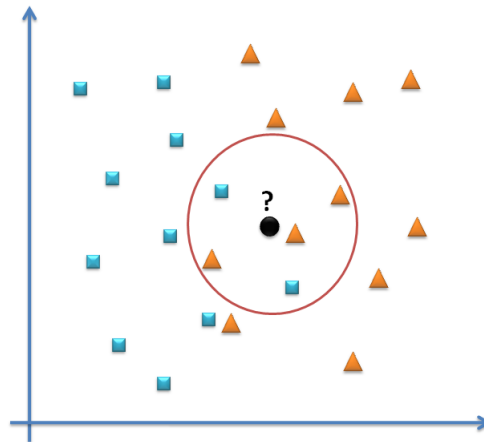


FIGURE 4.1: Classification of new individual using KNN with $K=5$

4.2.2 Classification and regression tree (CART)

A decision tree is a decision support model commonly used in machine learning [110]. The wide use of this model is essentially based on several factors : simplicity, efficiency, easily interpretable. It has also an ability to capture nonlinear relationships between inputs and outputs of system. A decision tree is a recursive partitioning classifier of variables. It consists of nodes and branches. Nodes of a decision tree are composed of one root node, many internal nodes and leaves (a leaf node does not has outgoing branches). In fact, many algorithms are used for the construction of a decision tree including : ID3 (Iterative Dichotomiser 3), C4.5, CART (Classification And Regression Tree), CHAID (CHi-squared Automatic Interaction Detector), etc.

In this study, we use the CART algorithm, which solves both classification and regression problems. The CART algorithm allows to build only binary trees. A binary tree has exactly two outgoing branches for each internal node. The nodes division criterion used by this algorithm is the Gini criterion. The leaves give the final decision about the labels of new observations.

4.2.3 Random Forest

The random forests (RF) are a family of methods for classification, regression and other tasks, that operate by constructing multitude decision trees [111]. The main idea of the

RF method is to create a set of decision trees using the bootstrap aggregating technique [112]. This technique leads to decrease the effects of the noisy data and therefore gives high classification performances. In [111], Breiman combines the bagging technique and the random selection of variables in the construction of each tree. This combination is known as the random forest method that improves the classification performances of a single tree. The assignment of a new observation vector to a class is based on a majority vote of the different decisions provided by each tree constituting the forest. However, RF needs huge amount of labeled data to achieve good performances.

4.2.4 Support Vector Machine

The Support Vector Machine (SVM) represents in the last years a widely recognized approach in the community of the supervised classification for its excellent overall performance [113]. Basically, the SVM is a supervised classification method essentially used for solving binary classification problems. In the case of linearly separable data, the main idea of SVM is to find the hyperplane (separator) $f(x) = w^T x + b$ that separates positive observations ($y_i = +1$) from negative ones ($y_i = -1$), and maximizes the distance between the closest observations (support vectors) and the hyper-plane as much as possible (left part of Figure 4.2); where w^T and b are the parameters of the hyperplane equation. The margin is twice the distance between the hyperplane and the support vectors.

In the case of separable data, we can find an infinite number of separators between positives and negatives points, but the performances of these separators are different. There is a unique optimal separator that maximizes the margin between itself and the support vectors. For the nearest points (support vectors), the output values of the hyperplane equation should be equal to one, i.e. $|w^T x_{sv} + b| = 1$ for all support vectors x_{sv} .

The distance between a point x_i and the hyperplane can be expressed as follows :

$$distance_i = \frac{|w^T x_i + b|}{\|w^T\|} \quad (4.1)$$

In particular, for the support vectors (x_{sv}), this distance becomes :

$$distance_{sv} = \frac{|w^T x_{sv} + b|}{\|w^T\|} = \frac{1}{\|w^T\|} \quad (4.2)$$

Therefore, the margin can be formulated as follows :

$$\text{Margin} = \frac{2}{\|w^T\|} \quad (4.3)$$

Finally, the problem is therefore to maximize the term $\frac{2}{\|w^T\|}$. This problem is equivalent to the problem of minimizing a function $F(w^T)$ with some constraints.

$$\min_{w^T, b} F(w^T) = \frac{\|w^T\|^2}{2} \quad (4.4)$$

subject to $l_i(w^T x_i + b) \geq 1$ for all x_i , where $l_i \in \{-1, +1\}$ is the label of point x_i .

This is a Lagrangian optimization problem that can be solved using Lagrange multipliers to obtain the weight vector w^T and the bias b of the optimal hyperplane, where the Lagrangian is given by :

$$L(w^T, b, \alpha) = \frac{1}{2}\|w\|^2 - \sum_i \alpha_i (l_i(w^T x_i + b) - 1) \quad (4.5)$$

This Lagrangian must be minimized with respect to w^T and b , and maximized with respect to α ; where α is the Lagrange multiplier.

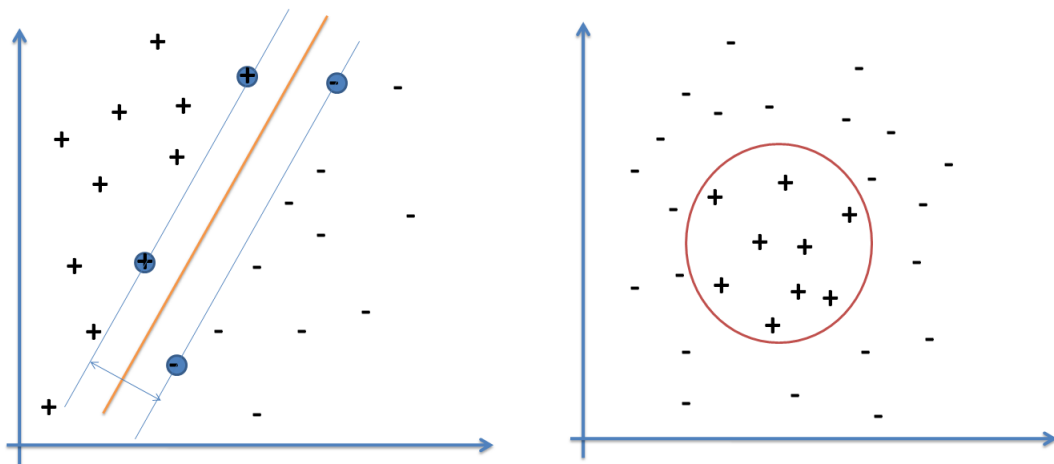


FIGURE 4.2: Linear and non-linear hyperplanes of SVM classifier

Moreover, if no linear separator is found between data, (right part of Figure 4.2), the idea of SVM is to reconsider the classification problem in a space of higher dimension, possibly of infinite dimension. In this new space, it is likely to find a linear separator between data.

More formally, it should apply to the input data, a non-linear transformation ϕ ; for all x_i . In this new space, we can search the linear hyperplane that discriminates between data :

$$f(x) = w^T \phi(x) + b \quad (4.6)$$

which verifies $l_i(w^T \phi(x_i) + b) \geq 1$ for all x_i

The kernel trick is used to do this transformation. It consists of using a kernel function that verifies the following equation :

$$K(x_i, x_j) = \phi(x_i)^T \cdot \phi(x_j) \quad (4.7)$$

The interest of the kernel function is that the calculation is made in the original space. This is much less expensive than a scalar product in large dimension. The transformation ϕ does not need to be explicitly known, only the kernel function is used in the calculations.

The simplest example of the kernel function is the linear one :

$$K(x_i, x_j) = x_i \cdot x_j \quad (4.8)$$

There is also, the Gaussian kernel function expressed in the following equation :

$$K(x_i, x_j) = \exp\left(-\frac{\|x_i - x_j\|^2}{2\sigma^2}\right) \quad (4.9)$$

4.3 Feature extraction and selection for subjects classification

In this section, we describe the proposed approach for discriminating between healthy and PD subjects through EMD-based temporal and spectral features extraction from stabilometric signals. This approach includes four steps.

1. EMD decomposition of the stabilometric signal, to generate a set of IMFs. The first eight IMFs are selected for further processing and feature extraction (Figures 4.4, 4.5, 4.6, 4.7).
2. Feature extraction : three time-domain features, namely, standard deviation (σ), Skewness (β) and Kurtosis ($Kurt$), and three frequency-domain features, namely, spectral centroid (C_{spec}), spectral Skewness (β_{spec}) and spectral Kurtosis ($Kurt_{spec}$) are extracted from raw stabilometric data and their IMFs in ML and AP directions.
3. Feature selection : the five most relevant features characterizing the postural sway of healthy and PD subjects are selected using random forest-based selection method.
4. Classification, four well-known classification methods including KNN, CART, RF and support vector machine (SVM) are used for the classification of healthy and PD subjects using 10-fold cross validation.

Figure 4.3 shows the block diagram of the proposed approach for the classification of healthy and PD subjects.

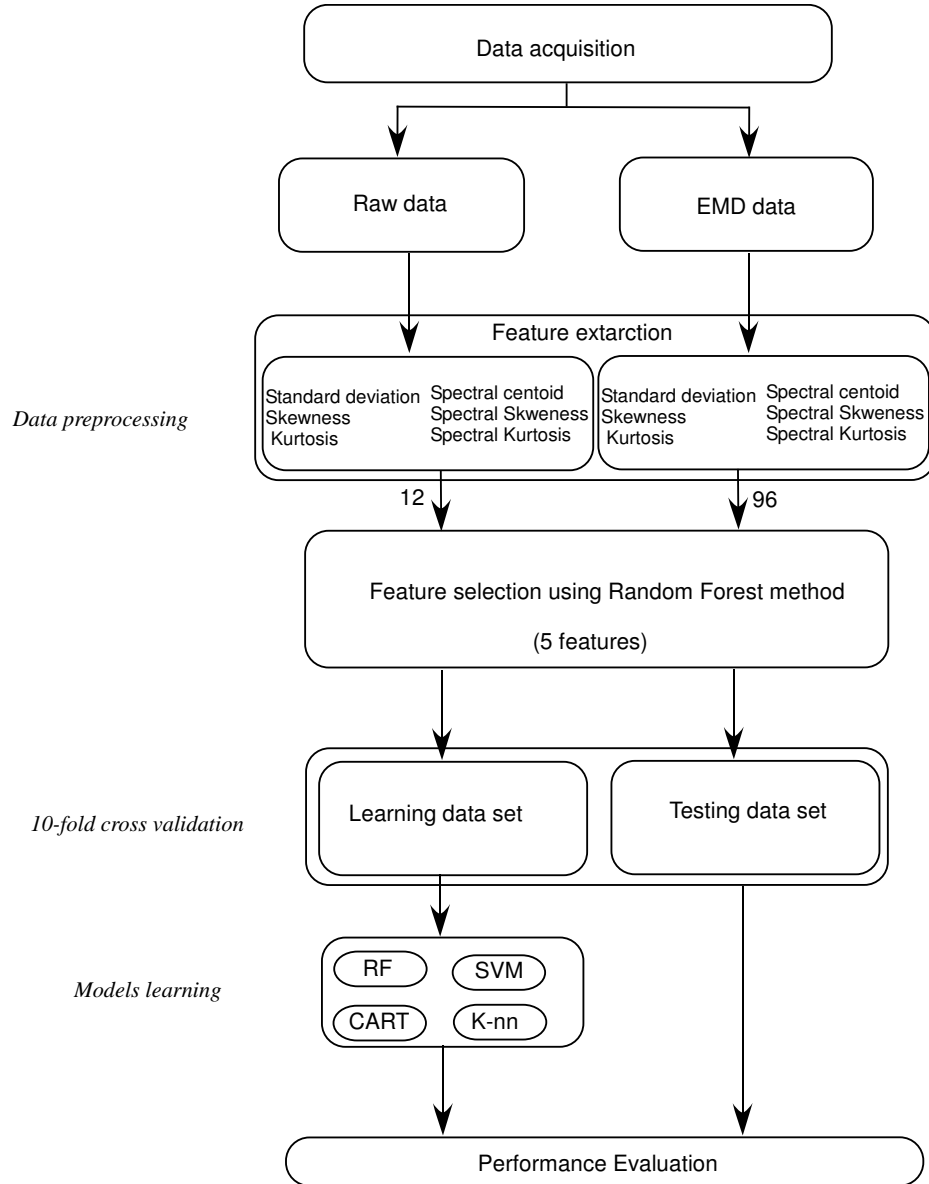


FIGURE 4.3: Healthy and PD subjects classification process

4.3.1 Feature extraction

Three temporal features are used in this study :

1. The standard deviation σ is the mean square root of the variance of the signal. It can be expressed as follows :

$$\sigma = \sqrt{\frac{1}{n} \sum_{i=1}^n (x_i - \mu)^2} \quad (4.10)$$

where n is the number of samples in a given signal x , and μ is the mean value.

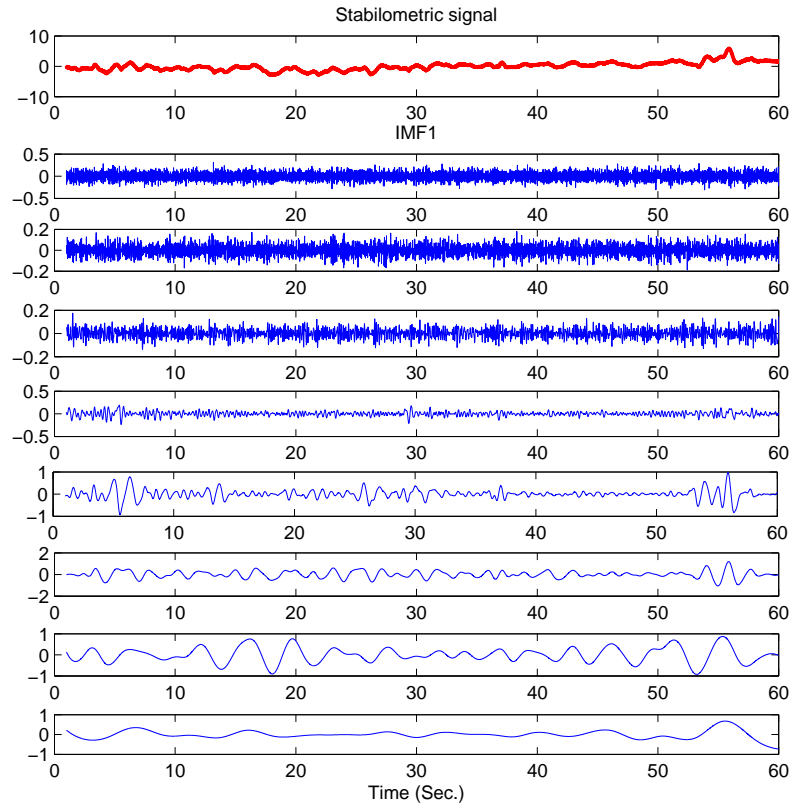


FIGURE 4.4: AP stabilometric signal and its first eight IMFs for a healthy subject in FAEO condition

2. Skewness β is a parameter that evaluate the asymmetry of the probability distribution of data ; it is calculated from the third order moment of a given signal x as follows :

$$\beta = \frac{1}{n} \sum_{i=1}^n \left(\frac{x_i - \mu}{\sigma} \right)^3 \quad (4.11)$$

3. Kurtosis $Kurt$ measures the tailedness of the probability distribution ; it is calculated from the fourth order moment as follows :

$$Kurt = \frac{1}{n} \sum_{i=1}^n \left(\frac{x_i - \mu}{\sigma} \right)^4 \quad (4.12)$$

Moreover, three spectral features are calculated and extracted from the stabilometric signal itself and from the extracted IMFs. These features are characteristics of the spectral energy distribution of data. The spectral centroid C_{spec} is the balance point or the center of mass of the spectrum. It is widely used for the brightness of sound and for the

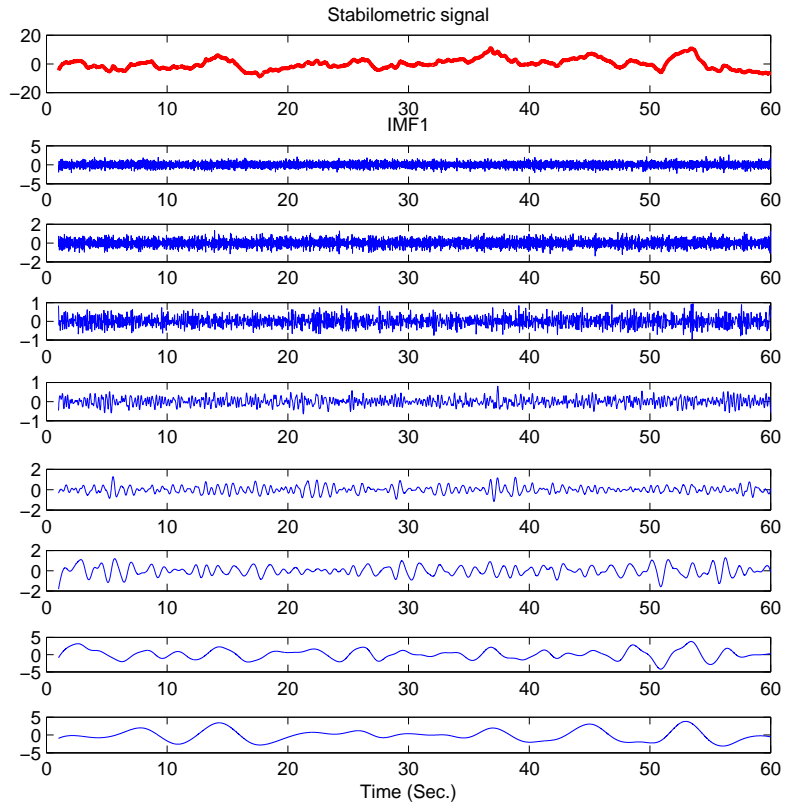


FIGURE 4.5: ML stabilometric signal and its first eight IMFs for a healthy subject in FAEO condition

musical timbre analysis. It can be expressed as follows :

$$C_{spec} = \frac{\sum_w w P(w)}{\sum_w P(w)} \quad (4.13)$$

where $P(w)$ is the amplitude of the frequency w in the spectrum.

The spectral Skewness β_{spec} and the spectral Kurtosis $Kurt_{spec}$ measure, respectively, the asymmetry and the tailedness of the spectral energy distribution (eq. 4.14 and 4.15).

These parameters can be expressed as follows :

$$\beta_{spec} = \frac{\sum_w \left(\frac{w - C_{spec}}{\sigma_{spec}} \right)^3 P(w)}{\sum_w P(w)} \quad (4.14)$$

where σ_{spec} is the mean square root of the spectral variation.

$$Kurt_{spec} = \frac{\sum_w \left(\frac{w - C_{spec}}{\sigma_{spec}} \right)^4 P(w)}{\sum_w P(w)} \quad (4.15)$$

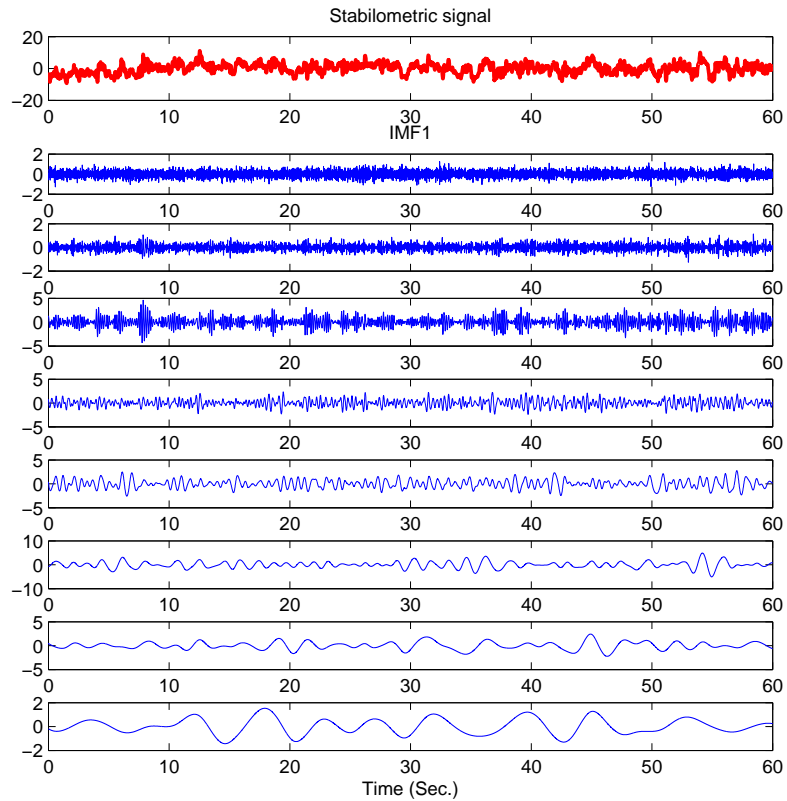


FIGURE 4.6: AP stabilometric signal and its first eight IMF's for a PD subject in FAEO condition

4.4 Experimental results

4.4.1 Performance evaluation

In order to evaluate the performances of the proposed methodology for classification of health and PD subjects, the accuracy, the F-measure, the recall, and the precision metrics are used.

$$Accuracy = \frac{T_p + T_n}{T_p + T_n + F_p + F_n}, \quad (4.16)$$

$$recall = \frac{T_p}{T_p + F_p}, \quad (4.17)$$

$$precision = \frac{T_p}{T_p + F_n}, \quad (4.18)$$

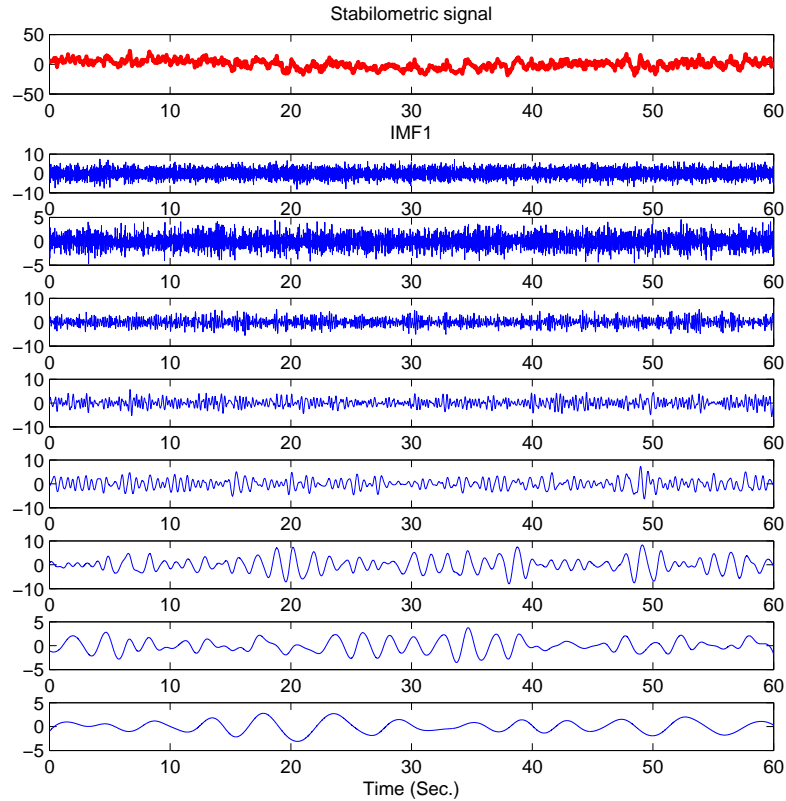


FIGURE 4.7: ML stabilometric signal and its first eight IMF's for a PD subject in FAEO condition

where :

- T_p represents the number of true positive examples ;
- T_n represents the number of true negative examples ;
- F_p represents the number of false positive examples ;
- F_n represents the number of false negative examples.

The F-measure criterion is given by the following equation :

$$F_{\beta} - measure = \frac{(1 + \beta^2).recall.precision}{\beta^2 recall + precision}, \quad (4.19)$$

where β represents a weighting factor that characterizes the degree of importance with respect to recall and precision metrics. In order to give the same importance to these two metrics, β is set to 1.

The classification of healthy and PD subjects is achieved within a supervised learning framework using their stabilometric data. In this context, the data labels are used to

train and test the classification methods. In this study, the training dataset and the testing dataset are estimated using a 10-fold cross-validation method.

4.4.2 Results and discussions

In this study, for each condition, a total of 12 and 96 characteristics are calculated, respectively, from raw stabilometric data and their corresponding IMFs. In order to select the subset of the most relevant features, a feature selection process is carried out. This process consists of finding a minimal subset of features that are necessary and sufficient to adequately differentiate between the healthy and PD subjects. For this purpose, a random forest feature selection method is used to select the most relevant features from the extracted ones. This method belongs to the family of wrapper methods, in which the prediction performance is included in the score calculation phase. The Random forest feature selection method consists of reordering the features according to their scores. In this study, a set of 5 relevant features representing the best scores are selected as the classifiers inputs in both cases : raw data and IMFs data.

4.4.2.1 Obtained results using data collected from all conditions

In this paragraph, we present the obtained results using the features extracted/selected from raw stabilometric data, IMFs data and both IMFs & Raw data together from all conditions. In this case, a total of 48 ($12*4$), 384 ($96*4$) and 432 ($12*4 + 96*4$) features are used, respectively, for raw data, IMFs data and IMFs & Raw data under the four conditions : FAEO, FAEC, FTEO and FTEC.

The obtained results using data collected from all conditions are given in tables 4.1, 4.2 and 4.3. Table 4.1 summarizes the results obtained using features extracted/selected from IMFs data. It can be observed that the obtained recognition rate is higher than 78%. It can be also noticed that the SVM method gives the best performance in terms of Accuracy, F-measure, precision, and recall, followed by RF, then KNN, and at the last, CART approach gives the worst performances.

Table 4.2 summarizes the results obtained using features extracted/selected from Raw data. It can be observed that the obtained recognition rate is higher than 73%. It can be noticed that RF method gives the best performance in terms of Accuracy, F-measure,

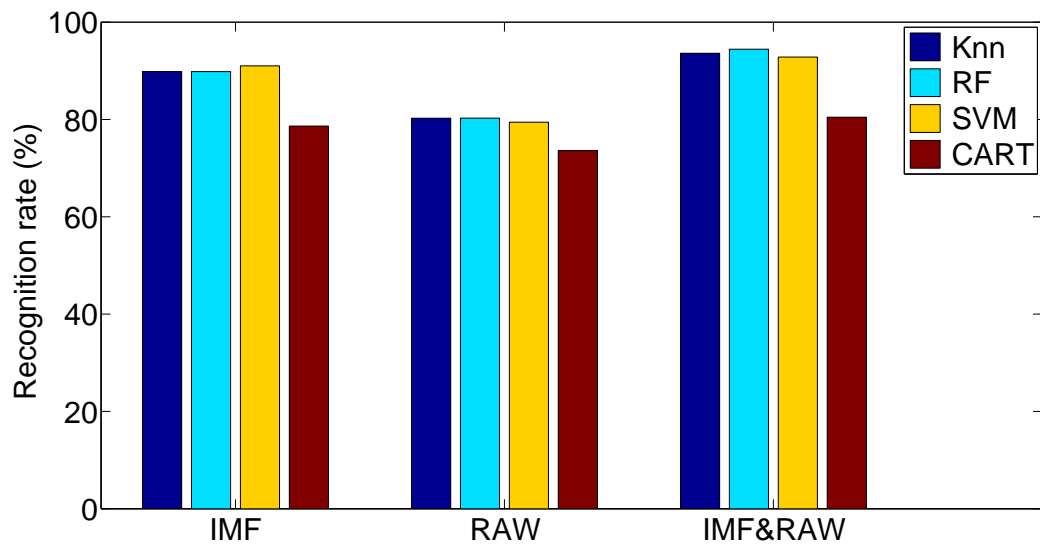


FIGURE 4.8: Obtained results in terms of recognition rate for each classifier using extracted/selected features from EMD, Raw and EMD& Raw data.

TABLE 4.1: F_1 -measure per class, F_1 -measure, precision, recall, and average of accuracy rates (R) and its standard deviation (std) using IMFs data

	F_1 measure per class		F_1 measure	Precision	Recall	Accuracy (R) \pm (std)
	Healthy	PD				
KNN (%)	89.85	89.82	89.83	90.26	90.25	89.83 \pm 4.94
SVM (%)	90.69	91.6	91.14	91.1	91.23	91.17 \pm 4.01
RF (%)	89.62	90.35	89.99	89.98	90.16	90 \pm 3.16
CART (%)	75.67	81.01	78.34	79.01	78.19	78.67 \pm 3.78

precision, and recall, followed by KNN, then SVM, and at the last Cart approach gives the worst performances. It can be also noticed that RF and KNN approaches give almost the same performances.

TABLE 4.2: F_1 -measure per class, F_1 -measure, precision, recall, and average of accuracy rates (R) and its standard deviation (std) using Raw data

	F_1 measure per class		F_1 measure	Precision	Recall	Accuracy (R) \pm (std)
	Healthy	PD				
KNN (%)	79.23	81.33	80.28	80.25	80.33	80.33 \pm 4.96
SVM (%)	77.13	81.97	79.55	80.14	79.4	79.83 \pm 5.59
RF (%)	79.29	81.57	80.43	80.41	80.47	80.5 \pm 6.33
CART (%)	71.81	75.58	73.7	73.72	73.68	73.83 \pm 7.13

Table 4.3 summarizes the results obtained using features extracted/selected from EMD&raw

data. It can be observed that the obtained recognition rate is higher than 80%. As in the previous case, RF method also gives the best performance in terms of Accuracy, F-measure, precision, and recall, followed by KNN, then SVM, and at the last CART approach gives the worst performances.

TABLE 4.3: F_1 -measure per class, F_1 -measure, precision, recall, and average of accuracy rates (R) and its standard deviation (std) using EMD and Raw data

	F_1 measure per class		F_1 measure	Precision	Recall	Accuracy (R) \pm (std)
	Healthy	PD				
KNN (%)	93.15	93.51	93.33	93.39	93.57	93.33 \pm 2.41
SVM (%)	92.25	92.73	92.49	92.51	92.7	92.5 \pm 2.04
RF (%)	93.81	94.49	94.15	94.11	94.2	94.17 \pm 2.82
CART (%)	79.37	81.21	80.29	80.27	80.38	80.33 \pm 4.74

By comparing the results obtained using the extracted/selected features from IMFs data, raw data and EMD& raw data, it can be noticed that the best results are obtained using the EMD and EMD& raw data. It can also be noticed that the worst results are obtained features extracted/selected from raw data.

4.4.2.2 Obtained results using data collected from each condition (IMFs data)

As presented above, the best results are obtained using features extracted/selected from IMFs data. These features are used to analyze the effect of each condition on the classification performances. Figure 4.9 shows the obtained results using SVM, RF, Cart and KNN on data collected from each condition (FAEC, FAEO, FTEC and FTEO) in terms of accuracy and standard deviation.

The obtained results using data collected from each condition are given in tables 4.4, 4.5, 4.6 and 4.7. Table 4.4 summarizes the results obtained using features extracted/selected from IMFs data in the case of data collected under FAEC condition. It can be observed that the obtained recognition rate is higher than 77%. It can be also noticed that SVM method gives the best performance in terms of Accuracy, F-measure, precision, and recall, followed by CART, then RF, and at the last KNN method gives the worst performances.

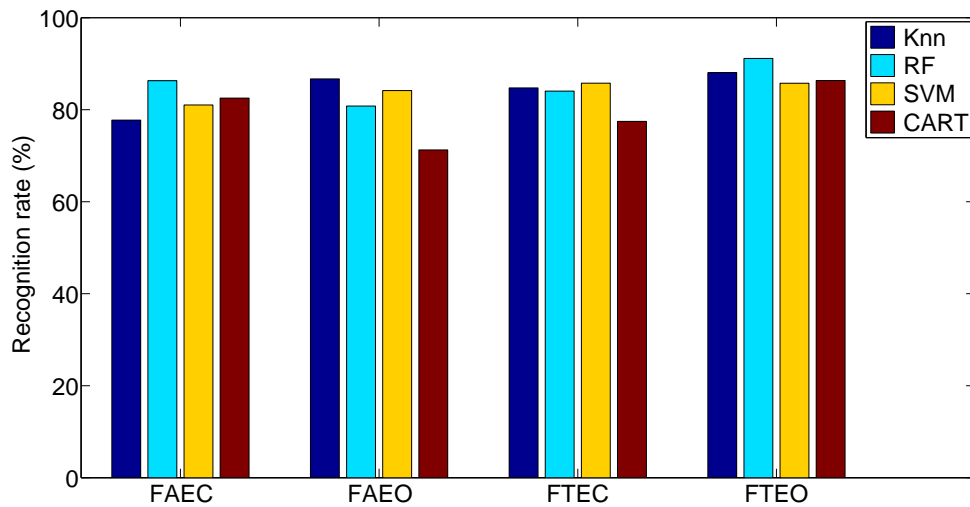


FIGURE 4.9: Obtained results in terms of recognition rate for each classifier using extracted/selected features from IMFs data for each condition.

TABLE 4.4: F_1 -measure per class, F_1 -measure, precision, recall, and average of accuracy rates (R) and its standard deviation (std) for FAEC condition

	F_1 measure per class		F_1 measure	Precision	Recall	Accuracy (R) \pm (std)
	Healthy	PD				
KNN (%)	75.81	79.26	77.53	77.58	77.5	77.67 \pm 4.43
SVM (%)	79.11	82.85	80.98	81.26	80.87	81.17 \pm 5.8
RF (%)	85.14	87.35	86.25	86.34	86.18	86.33 \pm 4.94
CART (%)	82.05	82.93	82.49	82.56	82.7	82.5 \pm 6.02

Table 4.5 summarizes the results obtained using features extracted/selected from IMFs data in the case of data collected under FAEO condition. It can be observed that the obtained recognition rate is higher than 71%. It can be also noticed that the KNN method gives the best performance in terms of Accuracy, F-measure, precision, and recall, followed by SVM, then RF, and at the last CART method gives the worst performances.

TABLE 4.5: F_1 -measure per class, F_1 -measure, precision, recall, and average of accuracy rates (R) and its standard deviation (std) for FAEO condition

	F_1 measure per class		F_1 measure	Precision	Recall	Accuracy (R) \pm (std)
	Healthy	PD				
KNN (%)	85.61	86.98	86.3	86.26	86.38	86.33 \pm 3.16
SVM (%)	82.61	85.19	83.9	83.98	83.84	84 \pm 4.14
RF (%)	78.68	82.32	80.5	80.71	80.4	80.67 \pm 4.7
CART (%)	67.42	74.14	70.78	71.19	70.71	71.17 \pm 5.73

Table 4.6 summarizes the results obtained using features extracted/selected from IMFs data in the case of data collected under FTEC condition. It can be observed that the obtained recognition rate is higher than 77%. The RF, SVM, and KNN methods give almost similar performance in terms of Accuracy, F-measure, precision, and recall, with slight performance in favor of SVM. Finally, the CART method gives the worst performances.

TABLE 4.6: F_1 -measure per class, F_1 -measure, precision, recall, and average of accuracy rates (R) and its standard deviation (std) for FTEC condition

	F_1 measure per class		F_1 measure	Precision	Recall	Accuracy (R) \pm (std)
	Healthy	PD				
KNN (%)	83.51	85.67	84.59	84.61	84.58	84.67 \pm 4.68
SVM (%)	85.67	86	85.83	86.05	86.14	85.83 \pm 5.52
RF (%)	81.82	85.71	83.77	84.46	83.57	84 \pm 3.36
CART (%)	74.58	79.82	77.2	77.69	77.08	77.5 \pm 4.57

Table 4.7 summarizes the results obtained using features extracted/selected from IMFs data in the case of data collected under FTEO condition. It can be observed that the obtained recognition rate is higher than 85%. In this case, The RF method outperforms the other classification approaches. The KNN and CART methods give almost similar performances, while SVM method gives the worst performances.

TABLE 4.7: F_1 -measure per class, F_1 -measure, precision, recall, and average of accuracy rates (R) and its standard deviation (std) for FTEO condition

	F_1 measure per class		F_1 measure	Precision	Recall	Accuracy (R) \pm (std)
	Healthy	PD				
KNN (%)	87	88.85	87.93	88	87.88	88 \pm 3.67
SVM (%)	84.42	86.73	85.57	85.67	85.51	85.67 \pm 3.79
RF (%)	90.56	91.4	90.98	90.94	91.09	91 \pm 3.41
CART (%)	85.76	86.86	86.31	86.3	86.45	86.33 \pm 2.87

By comparing the results obtained using the different conditions, it can be observed that the best results are obtained when using features calculated in the case of FTEO condition. The remaining results obtained under FAEC, FAEO, and FTEC conditions are almost similar.

4.4.2.3 Obtained results using data collected from each condition (Raw data)

Figure 4.10 shows the obtained results in terms of accuracy using SVM, RF, Cart and KNN methods applied on raw stabilometric data. It is observed that the best results are obtained under FTEO condition using SVM classifier.

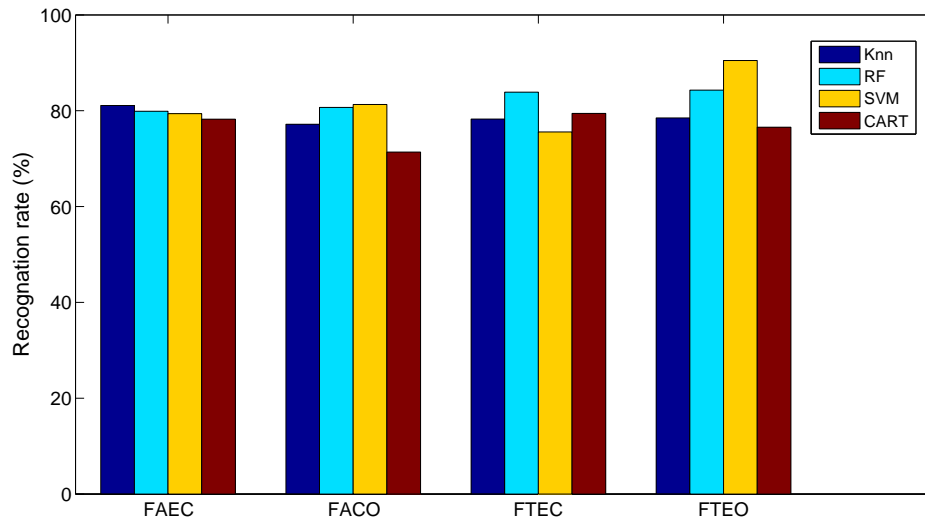


FIGURE 4.10: Obtained results in terms of recognition rate for each classifier using extracted/selected features from raw data for each condition.

The results obtained using raw data collected under each condition are given in tables 4.8, 4.9, 4.10, and 4.11.

Table 4.8 summarizes the results obtained using features extracted/selected from raw data collected under FAEO condition. It can be observed that the obtained recognition rate is higher than 71%. The SVM method gives the best performance in terms of accuracy, F-measure, precision, and recall, followed by RF, then KNN, and at the last CART method gives the worst performances.

Table 4.9 shows the results obtained using features extracted/selected from raw data collected under FAEC condition. It can be observed that the obtained recognition rate is higher than 78%. The KNN method gives the best performance in terms of Accuracy, F-measure, precision, and recall, followed by RF, then SVM, and finally, the CART method gives the worst performances.

TABLE 4.8: F_1 -measure per class, F_1 -measure, precision, recall, and average of accuracy rates (R) and its standard deviation (std) for FAEC condition

	F_1 measure per class		F_1 measure	Precision	Recall	Accuracy (R) \pm (std)
	Healthy	PD				
KNN (%)	80.56	81.74	81.21	78.52	82.58	81.1 \pm 5.65
SVM (%)	78.67	81.11	79.89	80.93	77.87	79.4 \pm 5.74
RF (%)	79.81	79.71	79.76	80.46	79.34	79.9 \pm 7.37
CART (%)	78.48	78.4	78.44	78.31	78.19	78.24 \pm 8.4

TABLE 4.9: F_1 -measure per class, F_1 -measure, precision, recall, and average of accuracy rates (R) and its standard deviation (std) for FAEO condition

	F_1 measure per class		F_1 measure	Precision	Recall	Accuracy (R) \pm (std)
	Healthy	PD				
KNN (%)	76.31	76.11	76.21	76.61	77.58	77.17 \pm 5.23
SVM (%)	80.67	80.11	80.39	81.53	81.07	81.30 \pm 7.12
RF (%)	79.82	81.71	80.76	80.46	80.94	80.7 \pm 8.27
CART (%)	71.58	71.82	71.70	72.69	70.08	71.37 \pm 7.04

Table 4.10 summarizes the results obtained using features extracted/selected from raw data collected under FTEO condition. The obtained recognition rate is higher than 76%. SVM method gives the best performance up to 90.48 % in term of accuracy, followed by RF 84%, then KNN 78.5%, and finally, the CART method gives the worst performances.

TABLE 4.10: F_1 -measure per class, F_1 -measure, precision, recall, and average of accuracy rates (R) and its standard deviation (std) for FTEC condition

	F_1 measure per class		F_1 measure	Precision	Recall	Accuracy (R) \pm (std)
	Healthy	PD				
KNN (%)	78.45	78.31	78.38	78.44	78.08	78.26 \pm 4.6
SVM (%)	76.56	75.04	75.80	75.86	75.28	75.57 \pm 5.11
RF (%)	85.17	83.64	84.41	84.41	83.39	83.89 \pm 4.63
CART (%)	78.65	77.32	77.48	79.99	79.89	79.44 \pm 6.07

Table 4.11 shows the results obtained using features extracted/selected from raw data collected under FTEC condition. It can be observed that the obtained recognition rate is higher than 75%. RF method gives the best performance up to 83 % in terms of Accuracy, followed by the CART method, then KNN. The SVM method gives the worst performances.

TABLE 4.11: F_1 -measure per class, F_1 -measure, precision, recall, and average of accuracy rates (R) and its standard deviation (std) for FTEO condition

	F_1 measure per class		F_1 measure	Precision	Recall	Accuracy (R) \pm (std)
	Healthy	PD				
KNN (%)	78.68	77.89	78.28	78.64	78.36	78.5 ± 3.6
SVM (%)	77.56	76.14	76.85	89.73	89.24	89.48 ± 3.12
RF (%)	85.02	83.64	84.33	83.76	84.85	84.30 ± 3.42
CART (%)	77.50	76.14	76.32	77.01	76.13	76.57 ± 5.34

4.5 Conclusion

In this study, we developed a methodology to discriminate PD subjects from healthy ones. This methodology consists of four main steps : stabilometric data decomposition using EMD, temporal and spectral features extraction, feature selection and classification using KNN, CAT, RF and SVM classifiers. The obtained results show that the proposed methodology is efficient for classifying PD subjects with classification rates up to 96%. The classifiers based on the IMFs data can classify subjects with better performances than those based on raw data. The best results are obtained under FTEO condition. This can be explained by the fact that under feet together condition, the stability of PD subjects becomes lower, and therefore, PD subjects become more distinguishable from healthy ones. It can be noticed also that the RF method outperforms the other classification approaches in terms of accuracy, F-measure, precision, and recall. Finally, this study shows that the proposed methodology is useful for differentiating between healthy and PD subjects.

Chapitre 5

HMM-BASED

CLASSIFICATION APPROACH

5.1 Introduction

In this chapter, we present a classification approach for discriminating healthy subjects from PD subjects using a Hidden Markov model (HMM). The raw data corresponding to stabilometric signals are used directly without any preprocessing task. The HMM model is constructed using ML, AP or both ML and AP signals. The 10-fold cross validation method is used to decompose data between training and testing dataset.

This chapter is organized into three main sections. Section 5.2 describes the hidden Markov models used in this study. The proposed approach for classifying healthy and PD subjects is detailed in section 5.3. Finally, the performances of this approach are presented and discussed in section 5.4.

5.2 Hidden Markov Models

5.2.1 Introduction

The Hidden Markov Model (HMM) was introduced by Baum et al. in years 1965-1970 [114]. A HMM is a statistical model defined by a structure composed of states and transitions between these states. This model is similar to the probabilistic automata with an essential difference that the generation of symbols is done on the states and not during transitions. Another difference could be noticed ; in the automata, each state is associated to one symbol from the alphabet, while in a HMM model, for each state, there are probability distributions of all symbols in the alphabet. HMM is an efficient tool for the analysis of temporal or sequential data. It is widely used in various domains and applications, such as, voice recognition, hand writing recognition, DNA and RNA sequencing, activity recognition, etc.

5.2.2 Markov Chain

Before describing the HMM model, it is important to present the probabilistic model of the observable sequences : the observable Markov model (Markov chain).

A Markov chain [115] is a stochastic process used for modeling various sequential and temporal phenomena in many applications areas. A Markov chain of an observable sequence is characterized by the initial distribution of states and by the transition probabilities between these states (Figure 5.1). In general, the elements of an observable sequence generated by a Markov chain should be dependent over time.

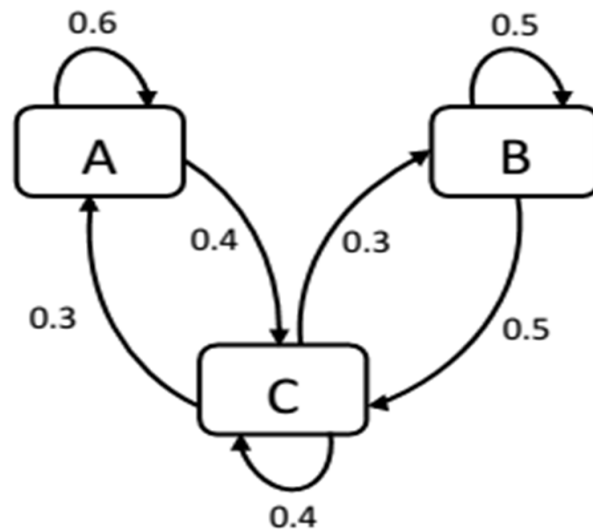


FIGURE 5.1: An example of a Markov Chain model

In the case of a Markov chain of first order, the transition probability of the current state, given the previous states sequence, is depend only from the previous state. Formally :

$$p(z_n | z_{n-1}, z_{n-2}, \dots, z_1) = p(z_n | z_{n-1}) \quad (5.1)$$

where, z_n is a sequence of random variables, for all $n > 0$.

Generally, a p -order Markov chain is a sequence of random variables that verifies the following equation :

$$p(z_n | z_{n-1}, z_{n-2}, \dots, z_1) = p(z_n | z_{n-1}, z_{n-2}, \dots, z_{n-p}) \quad (5.2)$$

where, z_n is a sequence of random variables, for all $n > 0$ and $n > p$.

Therefore, a typical Markov model can be characterized by :

- K : the state number of the model; it is similar to the number of characters in the used-alphabet.
- $A = \{a_{kl}\}$: the matrix of transition probabilities, where $a_{kl} = p(s_l|s_k)$ is the transition probability from the state s_k to the state s_l with $1 < k, l < K$ and $\sum_{l=1}^K a_{kl} = 1$
- π : the vector of the initial probabilities, where $\pi_k = p(s_k)$ is the initial probability of the state s_k , with $1 < k < K$

5.2.3 Discrete HMM

The Hidden Markov Model (HMM) is a statistical model that can be defined as a combination of two stochastic processes. The first process is a Markov chain that describes the hidden states sequence, while the second process is a sequence of random variables that describes the sequence of observations.

Unlike the observable Markov model, the states of a HMM model are not observable directly, but they emit observations which are weighted by their emission probabilities. Consider a first order HMM model, and let $S = \{s_1, s_2, \dots, s_K\}$ be the set of the states, and $O = \{o_1, o_2, \dots, o_M\}$ the set of the alphabet, where K is the number of states and M , the number of the characters in the observable alphabet. Let $X = \{x_1, x_2, \dots, x_n\}$ be the observations sequence generated from the HMM process using the hidden Markov chain sequence $Z = \{z_1, z_2, \dots, z_n\}$. It is important to note that an observation x_i takes its value from the set O and the hidden Markov chain z_i from the set S ; with $1 < i < n$.

A HMM model is defined by :

- K : the state number of the model ;
- M : the number of characters in the alphabet O ;
- $A = \{a_{kl}\}$: the matrix of transition probabilities, where $a_{kl} = p(z_i = s_l | z_{i-1} = s_k)$ is the transition probability from the state s_k to the state s_l with $1 < k, l < K$ and $\sum_{l=1}^K a_{kl} = 1$
- The emission probability of the character o_m by the state s_l , is defined by : $p(x_i = o_m | z_i = s_l)$. All emission probabilities are grouped in the emission probabilities matrix $B = \{b_{lm}\}$, where :
 $b_{lm} = p(x_i = o_m | z_i = s_l)$ for $1 < m < M$ and $1 < l < K$

- π : the vector of the initial probabilities, where $\pi_k = p(z_i = s_k)$ is the initial probability of the state k , with $1 < k < K$.

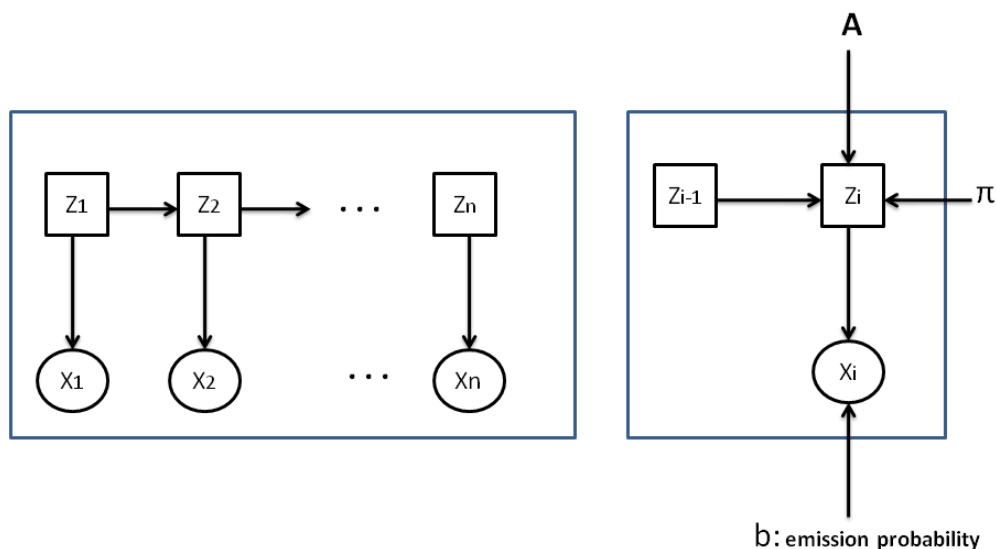


FIGURE 5.2: An example of a discrete hidden Markov model

Figure 5.2 shows an example of a graphical representation of a discrete HMM model. Each observable character x_i , associated to a hidden state z_i , is characterized by its emission probability.

When using a HMM to model time series, three main points should be considered :

- The evaluation problem : given the HMM model λ and the observations sequence, what is the probability that these observations are generated by the model?

The aim is to compute the probability $p(X|\lambda)$ to generate the observations sequence $X = \{x_1, x_2, \dots, x_n\}$ by the HMM model $\lambda = \{\pi, A, B\}$. This probability is equal to the sum of all probabilities that X can be generated using all possible states sequences. The analytical solution to this problem is time costly, and thus, the Forward-Backward algorithm is generally used for solving it [115].

- The decoding problem : given the HMM model λ and the observations sequence X , how to select the best state sequence (Hidden sequence) that generate the observations sequence? i.e., what is the most likely state sequence of the model λ that produce the observations sequence X . The Viterbi algorithm is generally used to solve this problem [116].
- The learning problem : how to adjust the parameters of the model $\lambda = \{\pi, A, B\}$ in order to maximize the probability of the observations sequence $p(X|\lambda)$? The Expectation-Maximization (EM) algorithm is commonly used to learn the HMM model.

Parameter estimation :

The distribution of the state sequence $Z = (z_1, z_2, \dots, z_n)$ in the case of a hidden Markov chain of first order can be written as follows :

$$p(Z; \pi, A) = p(z_1; \pi) \prod_{i=2}^n p(z_i | z_{i-1}; A) \quad (5.3)$$

The conditional distribution of the observations sequence Y given the state sequence Z can therefore be written as follows :

$$p(X|Z; \lambda) = \prod_{i=1}^n p(x_i | z_i; \lambda) \quad (5.4)$$

Finally, the joint distribution of X and Z (the complete-data likelihood) can be expressed as follows :

$$\begin{aligned} p(X, Z; \lambda) &= p(Z; \pi, A) p(X|Z; A) \\ &= p(z_1; \pi) p(x_1 | z_1; \lambda) \prod_{i=2}^n p(z_i | z_{i-1}; A) p(x_i | z_i; \lambda) \end{aligned} \quad (5.5)$$

For a HMM model $\lambda = \{\pi, A, B\}$, the parameters that should be estimated are : the initial distribution π , the transition probability matrix A and the emission probability matrix B . The maximum likelihood method is used in order to maximize the log-likelihood of the observation data. The log-likelihood can be expressed as follows

$$\begin{aligned}
\mathcal{L}(\lambda; X) &= \log p(X; \lambda) = \log \sum_Z p(X, Z; \lambda) \\
&= \log \sum_{z_1, \dots, z_n} p(z_1; A) p(x_1 | z_1, \lambda) \prod_{i=2}^n p(z_i | z_{i-1}; A) p(x_i | z_i; \lambda)
\end{aligned} \tag{5.6}$$

The maximization of this log-likelihood is very difficult analytically. The dedicated Expectation-Maximization (EM) algorithm for the HMMs (Baum-Welsh algorithm) is used for that propose [114].

The EM algorithm starts with initial parameters of the model $\lambda^{(0)} = \{\pi^{(0)}, A^{(0)}, B^{(0)}\}$, and then repeats two steps until convergence :

E-step : This step computes the expectation of the data log-likelihood :

$$\begin{aligned}
Q(\lambda, \lambda^{(q)}) &= \mathbb{E}[\mathcal{L}_c(\lambda; X, Z) | X, \lambda^{(q)}] \\
&= \sum_{k=1}^K \tau_{1k}^{(q)} \log \pi_k + \sum_{i=2}^n \sum_{k=1}^K \sum_{l=1}^K \xi_{ilk}^{(q)} \log A_{lk} + \sum_{i=1}^n \sum_{k=1}^K \tau_{ik}^{(q)} \log B_{ki}
\end{aligned} \tag{5.7}$$

where :

- $\mathcal{L}_c(\lambda; X, Z)$ is the complete-data log-likelihood.
- $\tau_{ik} = p(z_i = k | X; \lambda^{(q)})$ is the posterior probability of state k at time t , given the observations sequence X and the current model parameters $\lambda^{(q)}$.
- $\xi_{ilk} = p(z_i = k, z_{i-1} = l | X; \lambda^{(q)})$ is the joint posterior probability of state k at time i and state l at time $i-1$, given the observations sequence X and the current model parameters $\lambda^{(q)}$.

M-step : This step is used to maximize the expectation Q with respect to λ in order to update the model parameters $\lambda^{(q+1)}$. The model parameters are updated as follows :

$$\pi_k^{(q+1)} = \tau_{1k}^{(q)} \tag{5.8}$$

$$A_{lk}^{(q+1)} = \frac{\sum_{i=2}^n \xi_{ilk}^{(q)}}{\sum_{i=2}^n \tau_{ik}^{(q)}} \tag{5.9}$$

$$B_{km}^{(q+1)} = \frac{\sum_{i=1; x_i=o_m}^n \tau_{ik}^{(q)}}{\sum_{i=1}^n \tau_{ik}^{(q)}} \quad (5.10)$$

5.2.4 Gaussian HMM

In several applications, the observations are considered as continuous values. Thus, the emission probability of each state is given by a Gaussian density function. Therefore, the state conditional density (emission probability) can be written as follows :

$$p(x_i|z_k; \lambda) = \mathcal{N}(y_i; \mu_k, \Sigma_k), \quad (5.11)$$

where :

- \mathcal{N} : the Gaussian probability density function ;
- μ_k : the mean of the distribution of observations at state k , $\forall k=1, \dots, K$;
- Σ_k : the covariance matrix at state k , $\forall k=1, \dots, K$.

Figure 5.3 shows an example of a continuous HMM.

To estimate the parameters of a Gaussian HMM model, the equations used to update the initial probability π , and the transition probability of a discrete HMM model remain the same. For the emission probability, the Gaussian distribution parameters μ_k and Σ_k should be calculated for each state. This is achieved as follows :

$$\mu_k^{(q+1)} = \frac{1}{\sum_{i=1}^n \tau_{ik}^{(q)}} \sum_{i=1}^n \tau_{ik}^{(q)} x_i \quad (5.12)$$

$$\Sigma_k^{(q+1)} = \frac{1}{\sum_{i=1}^n \tau_{ik}^{(q)}} \sum_{i=1}^n \tau_{ik}^{(q)} (x_i - \mu_k^{(q+1)})(x_i - \mu_k^{(q+1)})^T \quad (5.13)$$

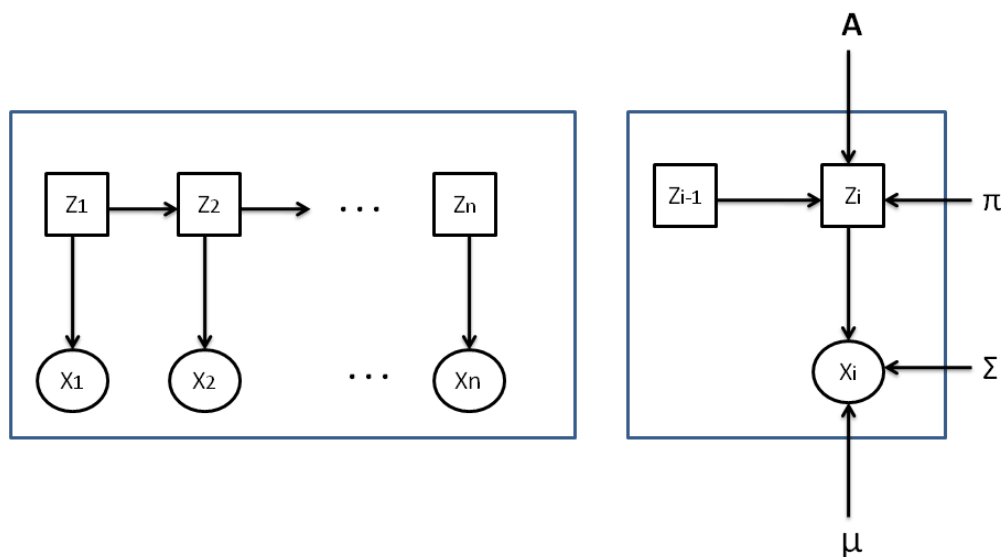


FIGURE 5.3: An example of a Gaussian hidden Markov model

5.3 HMM-based classification approach

In this section, we present the proposed HMM-based approach for differentiating between healthy and PD subjects using their COP displacements in quiet standing. The present study consists of constructing two HMM models : the HMM parameters are learned using the training dataset of healthy subjects in the first model (H-HMM), and the training dataset of PD subjects in the second model (PD-HMM). The construction of each HMM model is based on the sequential structure of the training signals. Healthy and PD subjects are classified first using either ML or AP stabilometric signals, and then using signals from both ML and AP directions.

The classification task of test subjects is carried out as follows : for each test subject, the processing described in fig. 5.4 is applied as follows : the observation probabilities of the test subject is computed for the H-HMM and PD-HMM models. The highest value between these two probabilities determines the class to which the test subject belongs. If the healthy HMM model gives the highest probability, the test subject is then considered as a healthy subject. In contrast, if the PD model gives the highest probability, the test subject is considered as a PD subject.

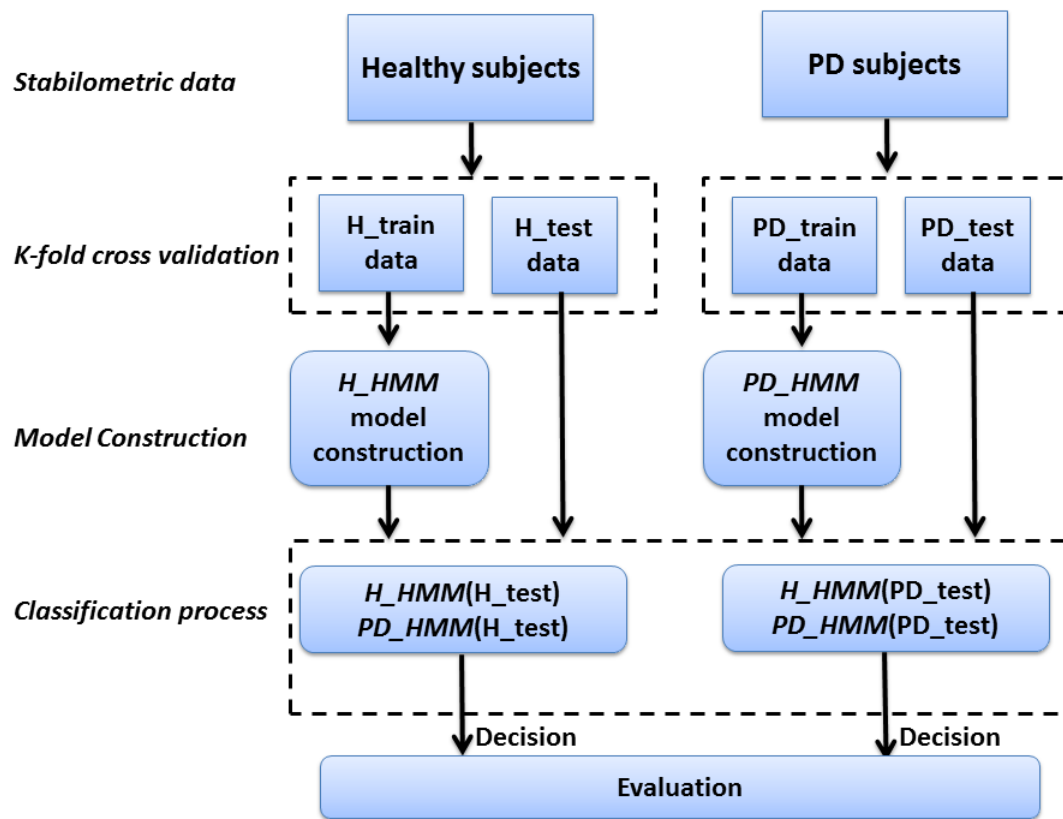


FIGURE 5.4: The block diagram of the proposed classification approach

5.4 Results and discussions

In this section, the classification performances obtained using the HMM models are presented and discussed. As previously mentioned, a HMM model is characterized by a set of parameters including, the initial probability, the transition probability matrix and the Gaussian model of each state. It is also characterized by the number of states and Gaussian mixtures that are considered. All of these parameters can affect the performances of the HMM model. Another parameter that should be taken into account is the number of iterations of the log-likelihood maximization process during the training of the model. A bad choice of the value of this parameter may decrease the model performances.

In this study, the K-means algorithm is used to estimate the initial values of Gaussian model parameters : the average μ_k and the covariance matrix Σ_k for each state s_k . Once,

the initial values of these parameters are estimated, the Baum-Welch algorithm is used to optimize these parameters by maximizing the log-likelihood of the training dataset. This maximization is characterized by the number of iterations of the process. Figure 5.5 shows the evolution of the log-likelihood probability during the maximization process for AP, ML and AP/ML signals. It can be observed that the log-likelihood value converges from the 15th iteration for the H-HMM and PD-HMM models. After fifteen iterations, the log-likelihood probability does not grow significantly and converges as shown in fig. 5.5. Therefore, the number of iterations of the log-likelihood maximization process is set to fifteen.

It is important to analyze the effect of the number of states on the HMM models performances to determine the number that gives the best results. Table 5.1 shows the correct classification rates of healthy and PD subjects using the two HMM models with different numbers of states.

TABLE 5.1: Classification rates with different numbers of states

Number of states	2	3	4	5	6	7	8
Classification rates	93.3	98.4	96.6	93.3	95	90	90

It can be noted that all obtained classification rates are higher than or equal to 90%, and that the best classification performances are obtained when the number of states is equal to three.

TABLE 5.2: Classification rates with different numbers of Gaussian mixtures

Number of Gaussian mixtures	2	3	4	5	6	7	8
Classification rates	98.4	97	97	95	95	90	91.6

The effect of the number of Gaussian mixtures on the HMM models' performances is also addressed in this study. Table 5.2 shows the correct classification rates of healthy and PD subjects using the two HMM models with different numbers of Gaussian mixtures. It can be noted that, all classification rates are higher than or equal to 90%. The best classification performance is obtained when the Gaussian mixtures number is equal to two. Finally, note that the best performances were obtained when the number of iterations used in the log-likelihood maximization process, the number of states, and the number of Gaussian mixtures are equal to 15, 3 and 2 respectively.

The 10-fold cross validation method was used to evaluate the performances of the HMM models. Three statistical parameters including sensitivity, specificity and the overall accuracy are calculated to evaluate the performances of the HMM models :

- Sensitivity : it represents the percentage of healthy subjects who are correctly classified ;
- Specificity : it is equal to the percentage of PD subjects who are correctly classified ;
- Accuracy : it represents the percentage of both healthy and PD subjects who are correctly classified.

TABLE 5.3: Performances of the proposed classification approach for differentiating between healthy and PD subjects using both ML and AP signals

	Subjects	Predicted H	Predicted PD	Sensitivity/Specificity	Overall Accuracy
Healthy	28	28	0	100%	98.4%
PD	32	1	31	96.8%	

Table 5.3 shows the classification performances of the HMM models using both ML and AP stabilometric signals. It can be observed that only one PD subject was classified incorrectly. The sensitivity and the specificity are 100% and 96.4% respectively. The overall accuracy of healthy and PD subjects classification is 98.4%.

TABLE 5.4: Performances of the proposed classification approach for differentiating between healthy and PD subjects using AP signals

	Subjects	Predicted H	Predicted PD	Sensitivity/Specificity	Overall Accuracy
Healthy	28	27	1	96.4%	96.6%
PD	32	1	31	96.8%	

TABLE 5.5: Performances of the proposed classification approach for differentiating between healthy and PD subjects using ML signals

	Subjects	Predicted H	Predicted PD	Sensitivity/Specificity	Overall Accuracy
Healthy	28	28	0	100%	98.4%
PD	32	1	31	96.8%	

Table 5.4 and table 5.5 give the performances of the proposed classification approach when using AP and ML signals respectively. The performances obtained using ML signals are similar to those obtained using both ML and AP signals, where the overall accuracy is 98.4%. Using AP signals, only one healthy subject and one PD subject were classified incorrectly. The overall accuracy is 96.6% (Table 5.4).

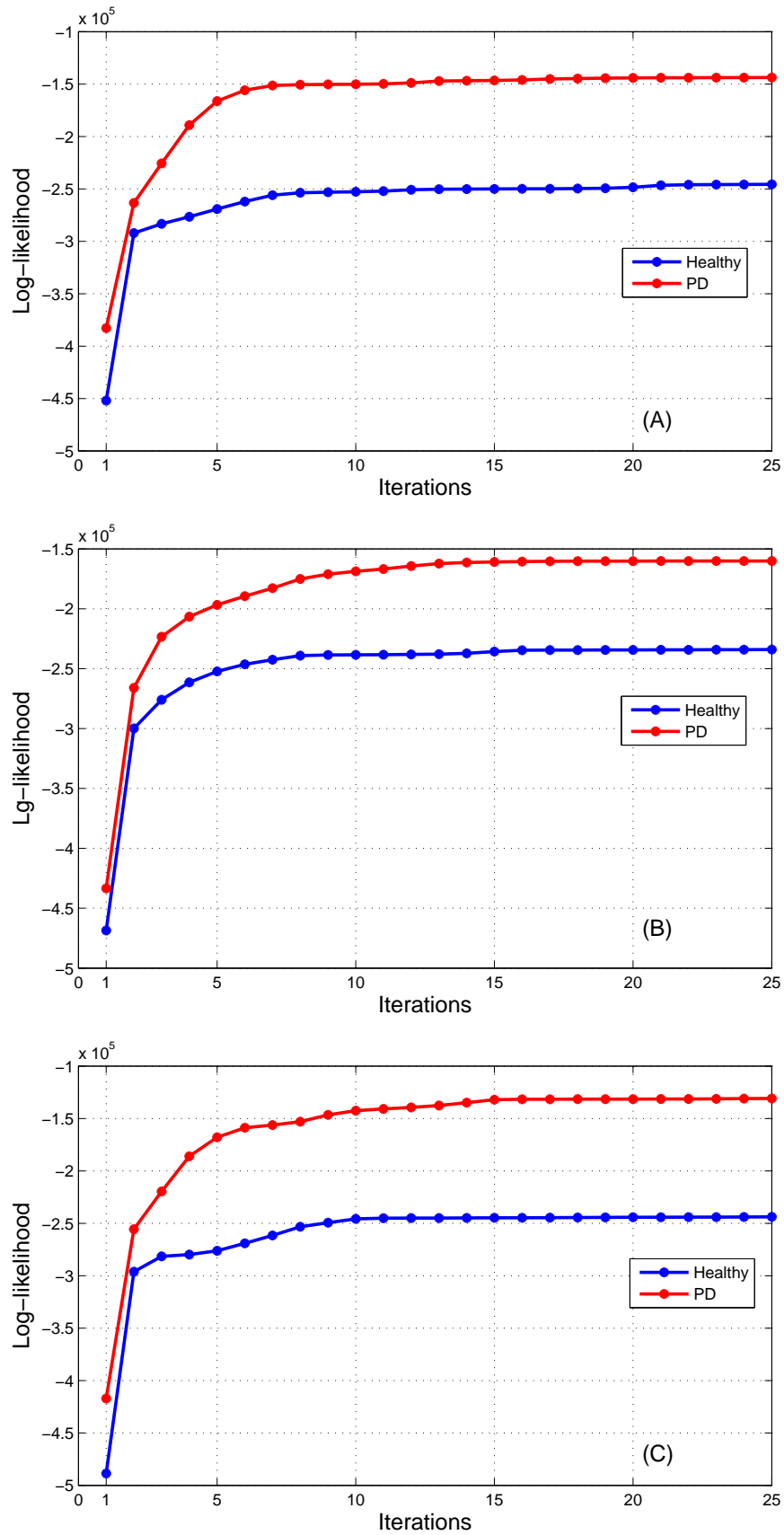


FIGURE 5.5: The log-likelihood maximization process of the HMM models for healthy and PD subjects (a) AP direction (b) ML direction (c) AP/ML directions.

5.5 Conclusion

In this chapter, we proposed a HMM-based classification approach to differentiate healthy from PD subjects using stabilometric signals measured in static posture. The classification performances obtained using this approach are better than those obtained in the previous chapter. We observed that by using both ML and AP signals, only one PD subject was classified incorrectly. The sensitivity and the specificity are 100% and 96.4% respectively, while the overall accuracy is equal to 98.4%. The proposed approach opens new perspectives in terms of posture analysis, for identifying the pathology degrees of patients and for fall prediction.

Chapitre 6

HMM REGRESSION-BASED APPROACH FOR AUTOMATIC SEGMENTATION OF STABILOMETRIC SIGNALS

6.1 Introduction

Posture analysis in quiet standing is an essential element in evaluating human balance control. Many conditions affect the human postural system's ability to maintain stability, such as the visual condition and base of support (feet) positions. In contrast, many neural pathologies, such as Parkinson's disease (PD) and cerebellar disorder, disturb human stability. This chapter addresses the problem of the automatic segmentation of stabilometric signals recorded under four different conditions related to vision and feet position. This is achieved for both healthy subjects and PD subjects. A Hidden Markov Model Regression (HMMR)-based approach is used to carry out the segmentation between the different conditions using simple and multiple regression processes. This approach allows to automatically detect the variation in structures of stabilometric signals between these conditions. The advantage of the used approach relies mainly in its capability to operate in an unsupervised context that avoids data labeling phase that is often time/computation efforts consuming, particularly in the case of massive databases.

This chapter is organized into three main sections. Section 6.2 describes the HMM regression used in this study. The HMMR-based approach proposed for segmentation of stabilometric signals is detailed in section 6.3. Finally, the performances of this approach are presented and discussed in section 6.4.

6.2 Hidden Markov Model Regression

The Hidden Markov Model Regression (HMMR) method is an extension of the classical HMM method for regression analysis [117]. It is useful for the segmentation of temporal sequences based on regression models governed by a hidden Markov chain. In fact, there are two types of regression models : i) the simple regression model that corresponds to the regression of one-dimensional observations sequence and ii) the multiple regression model that is commonly used for the regression of multidimensional time series.

6.2.1 Simple Hidden Markov Model Regression

Consider the simple regression model governed by a hidden Markov chain for time series. Let $X = (x_1, x_2, \dots, x_n)$ be a time series of n real observations $x_i \in \mathbb{R}$ observed at the time sequence $t = (t_1, t_2, \dots, t_n)$. The HMMR assumes that the observed sequence is generated using K states of a hidden process. The hidden state sequence $Z = z_1, z_2, \dots, z_n$ is obtained from the regression of the observed sequence X , where each z_i corresponds to a discrete value between 1 and K (number of classes). This means that each hidden value z_i is obtained from its related state. In this study, the observation sequence represents the whole stabilometric signal and the number of states in the Markov chain is equal to four because four conditions (classes) are considered : FTEO, FAEO, FTEC and FAEC.

Thus, the transition between states in the hidden Markov chain is done as a function of variation in the structure of the observation sequence. These variations are detected when the conditions change with respect to feet and eyes. The polynomial regression is used in the HMMR model in this study. Each observation x_i at time t_i corresponds to a regression model related to one state. The regression model can be written as follows :

$$x_i = \beta_{z_i}^T t_i + \sigma_{z_i} \epsilon_i; \text{ with } \epsilon_i \sim N(0, 1), \text{ and } 1 \leq i \leq n. \quad (6.1)$$

where z_i is a hidden variable corresponding to a discrete value between 1 and K . $\beta_{z_i} = (\beta_{z_{i0}}, \beta_{z_{i1}}, \dots, \beta_{z_{ip}})^T$ is a vector of dimension p . It represents the regression coefficients of the polynomial regression model z_i . $t_i = (1, t_i, t_i^2, \dots, t_i^p)$ is the $p+1$ covariate vector, and p is a finite integer that represents the order of the polynomial regression model.

6.2.1.1 Parameter estimation

In the case of a simple regression model, the HMMR model assumes that the hidden sequence $Z = (z_1, z_2, \dots, z_n)$ is a homogeneous Markov chain parameterized by the initial state probability distribution vector π and the transition probability matrix A . In this context, x_i has a Gaussian distribution, with a mean $\beta_k^T t_i$ and variance σ_k^2 . Thus, the HMMR model is parameterized by the parameters vector $\Phi =$

$(\pi, A, \beta_1, \dots, \beta_K, \sigma_1^2, \dots, \sigma_K^2)$. This vector is estimated by the maximum likelihood method. The log-likelihood can be written as follows :

$$L(\Phi; X) = \log \sum_{z_1} \dots \sum_{z_n} p(z_1; \pi) \prod_{i=2}^n p(z_i | z_{i-1}; A) \prod_{i=1}^n N(x_i; \beta_{z_i}^T t_i; \sigma_{z_i}^2) \quad (6.2)$$

Because this log-likelihood cannot be maximized analytically, the Expectation-Maximization (EM) iterative algorithm is used to provide efficient estimation of the parameters. The EM algorithm is described in the next section in the context of multiple regression model.

6.2.2 Multiple Hidden Markov Model Regression

In the case of multiple regressions, the observation data to be segmented should be a multidimensional time series. In this study, the multiple regression is achieved on the stabilometric signals in both the ML and AP directions. This is called joint segmentation of both ML and AP signals. Let $X = (x_1, x_2, \dots, x_n)$ be a multidimensional time series. Each observation $x_i = (x_i^{(1)}, x_i^{(2)}, \dots, x_i^{(d)}) \in \mathbb{R}^d$ is observed at time t_i ; d is the dimension of time series; in our case, $d=2$ for ML and AP signals. The multiple regression model with a hidden Markov chain can be written as follows :

$$\begin{aligned} x_i^{(1)} &= \beta_{z_i}^{(1)T} t_i + \sigma_{z_i}^{(1)} \epsilon_i \\ x_i^{(2)} &= \beta_{z_i}^{(2)T} t_i + \sigma_{z_i}^{(2)} \epsilon_i \\ &\dots \\ &\dots \\ &\dots \\ x_i^{(d)} &= \beta_{z_i}^{(d)T} t_i + \sigma_{z_i}^{(d)} \epsilon_i \end{aligned} \quad (6.3)$$

However, the multiple regression model performs the regression of all univariate sequences, which provides better model efficiency and provides better results based on the

joint segmentation. Model (6.3) can be rewritten as follows :

$$x_i = B_{z_i}^T t_i + \delta_i; \delta_i \sim N(0, \Sigma_{z_i}) \text{ with } 1 \leq i \leq n. \quad (6.4)$$

where $x_i = (x_i^{(1)}, x_i^{(2)}, \dots, x_i^{(d)}) \in \mathbb{R}^d$, B_{z_i} is the regression coefficients matrix with dimension $(p+1) \times d$ and Σ_{z_i} represents its covariance matrix.

The multiple regression model is therefore parameterized by the following parameters vector : $\Phi = (\pi, A, B_1, B_2, \dots, B_K, \Sigma_1, \Sigma_2, \dots, \Sigma_K)$.

To provide the best regression and segmentation, the estimation of these parameters is achieved using the EM algorithm that maximizes the log-likelihood of data.

6.2.2.1 Parameter estimation

The parameters vector Φ is estimated using the iterative algorithm EM. The log-likelihood that has been maximized is written as follows :

$$L(\Phi; X) = \log p(x_1, x_2, \dots, x_n; \Phi) =$$

$$\log \sum_{z_1} \dots \sum_{z_n} p(z_1; \pi) \prod_{i=2}^n p(z_i | z_{i-1}; A) \prod_{i=1}^n N(x_i; B_{z_i}^T t_i; \Sigma_{z_i}) \quad (6.5)$$

The EM algorithm, also known as the Baum-Welch algorithm for HMM, includes two main steps. At each iteration, the model parameters are estimated until they converge. The algorithm starts with initial values of model parameters $\Phi^{(0)}$.

E-step : From the observation data, time, and current estimation $\Phi^{(q)}$, the log-likelihood of completed data is estimated as follows :

$$Q(\Phi, \Phi^{(q)}) = \mathbb{E}[\log p(X, z, t, \Phi) | X, t; \Phi^{(q)}]. \quad (6.6)$$

The calculation of this expectation requires calculating two parameters :

1. The posterior probabilities that x_i is generated from the k^{th} regression model, given the observation data and the current estimation $\phi^{(q)}$:

$$\tau_{ik}^{(q)} = p(z_i = k | X, t; \Phi^{(q)}) \text{ for all } i \text{ and } k. \quad (6.7)$$

2. The joint posterior probabilities of state k at time t and state l at time $t-1$, given the observation data and the current estimation $\Phi^{(q)}$:

$$\xi_{ilk}^{(q)} = p(z_i = k, z_{i-1} = l | X, t; \Phi^{(q)}) \text{ for all } i, k \text{ and } l. \quad (6.8)$$

These probabilities can be calculated by using the forward-backward procedure used for the standard HMM.

M-step : This step consists of updating the values of model parameters vector Φ . The new values $\Phi^{(q+1)}$ are calculated by maximizing the expectation. The updated values of the initial state probability distribution vector π and the transition probability matrix A are calculated as follows :

$$\pi_k^{(q+1)} = \tau_{1k}^{(q)} \quad (6.9)$$

$$A_{lk}^{(q+1)} = \frac{\sum_{i=2}^n \xi_{ilk}^{(q)}}{\sum_{i=2}^n \tau_{ik}^{(q)}} \quad (6.10)$$

The regression coefficients of the matrix B and its covariance matrix Σ can also be updated as follows :

$$B_k^{(q+1)} = \left[\sum_{i=1}^n \tau_{ik}^{(q)} t_i t_i^T \right]^{-1} \sum_{i=1}^n \tau_{ik}^{(q)} t_i x_i^T \quad (6.11)$$

$$\Sigma_k^{(q+1)} = \frac{1}{\sum_{i=1}^n \tau_{ik}^{(q)}} \sum_{i=1}^n \tau_{ik}^{(q)} (x_i - B_k^{T(q+1)} t_i)^T (x_i - B_k^{T(q+1)} t_i) \quad (6.12)$$

The pseudo-code in the algorithm 3 summarizes the EM algorithm of the HMMR method with multiple regression.

Algorithm 3 Pseudo-code for EM algorithm with multiple regression

Input : time series X , number of polynomial components K , polynomial degrees p .

- 1: **Initialization** $\Phi = (\pi^{(0)}, A^{(0)}, B_1^{(0)}, \dots, B_K^{(0)}, S_1^{(0)}, \dots, S_K^{(0)})$
- 2: fix a threshold $\epsilon > 0$
- 3: set $q \leftarrow 0$
- 4: **while** increment in log-likelihood $> \epsilon$ (do)
- 5: **E-step :**
- 6: **for** $k=1, \dots, K$ do
- 7: compute $\tau_{ik}^{(q)}$ using Eq.6.7 and $\xi_{ilk}^{(q)}$ using Eq.6.8 for $i=1, \dots, n$
- 8: **M-step :**
- 9: **for** $k=1, \dots, K$ do
- 10: compute $\pi_k^{(q+1)}$ using Eq.6.9
- 11: compute $A_{lk}^{(q+1)}$ using Eq.6.10
- 12: compute $B_k^{(q+1)}$ using Eq.6.11
- 13: compute $\Sigma_k^{(q+1)}$ using Eq.6.12
- 14: **end for**
- 15: $q \leftarrow q + 1$
- 16: **end while**
- 17: $\hat{\Phi} = \Phi^{(q)}$

Outputs : $\hat{\Phi} = (\hat{\pi}, \hat{A}, \hat{B}_1, \dots, \hat{B}_K, \hat{\Sigma}_1, \dots, \hat{\Sigma}_K)$

6.3 HMM Regression-based approach for automatic segmentation of stabilometric signals

The Hidden Markov Model Regression (HMMR) approach is proposed for the segmentation of the measured stabilometric signals.

The problem of condition recognition can therefore be reformulated as one of a joint segmentation of multidimensional time series, in which each segment is associated with one condition.

The proposed statistical approach is dedicated to temporal segmentation by including a hidden process in which the process probabilities change over time according to the most likely condition. The approach performs in an unsupervised context from CoP excursion stabilometric signal recordings.

The configuration of the hidden process at each time step corresponds to a condition described by a regression model. The hidden process configuration depends on time, and

the regression model parameters are time-varying according to the most likely condition. The resulting model is therefore a type of latent data model that is particularly suitable for performing unsupervised activity recognition. Let us recall that from a statistical perspective, latent data models aim to represent the distribution of the observed data, which in this case are stabilometric signal recordings. The unsupervised learning task for the proposed approach is achieved by maximizing the observed-data log-likelihood via a dedicated iterative algorithm known as the expectation-maximization (EM) algorithm.

The approach proposed here, i.e., performing temporal segmentation of multivariate time series, is based on an alternative to the Markov process in the HMM regression model ([117]). It also directly uses raw data, rather than performing feature extraction and feature selection. This is indeed one of the main advantages of the proposed unsupervised approach because it does not require preprocessing and because the model parameters are learned in an unsupervised way from the acquired unlabeled raw data. However, the feature extraction step may itself require implementing additional models or routines, well-established criteria or additional expertise to extract and select the optimal features. The feature extraction step may also require an additional computational cost, which can be penalizing.

HMMR method takes as input the entire stabilometric signal and takes also the number of classes (segments). The Viterbi path is considered as the output of the regression process Fig. 6.1.

6.4 Results and discussions

In this section, the segmentation performances obtained using the HMMR approach are presented and discussed. For the simple regression, the HMMR approach takes the whole stabilometric signal as input for both the ML and AP directions as well as the number of classes (segments). For the multiple regression, the HMMR approach takes two stabilometric signals as input, which correspond to the ML and AP directions for the same subject, as well as the number of classes (segments). The proposed approach learns the model using the EM iterative algorithm to perform the best regression (segmentation)

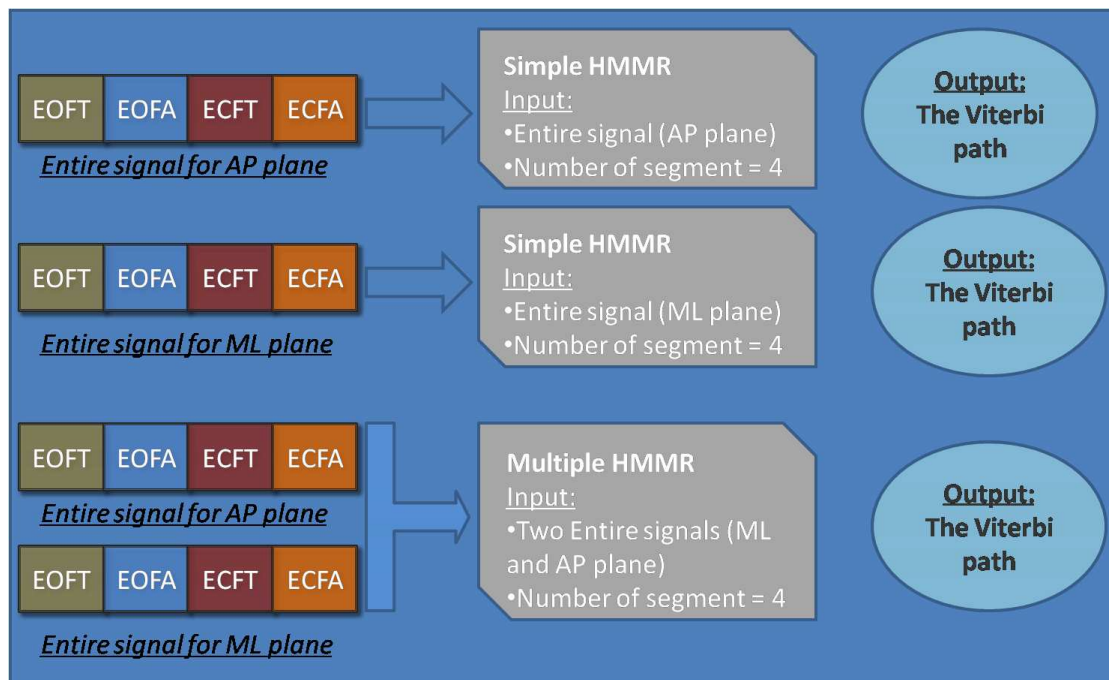


FIGURE 6.1: The input and the output of the HMMR model for the discrimination between visual and feet conditions

for the signals used. The Viterbi path is considered to be the output of the regression process (see Fig. 6.1). In fact, the Viterbi path is a signal that has the same dimension as the entire stabilometric signal, and each sample of the output signal (Viterbi) takes a value between one and four in case of discrimination between visual and feet conditions. To determine the performance of the proposed segmentation approach, the correct classification rate is calculated between the desired classes (Viterbi path) and the actual classes (Known classes) of our data.

6.4.1 Segmentation based on feet and visual conditions of healthy subjects

In this section, the segmentation results are shown for the healthy subjects. These results are compared to those obtained using standard well known classification methods to prove the efficiency of the segmentation strategy based on the HMMR method.

Fig. 6.2 shows the segmentation results obtained for both the HMM and HMMR methods in the AP direction. Fig. 6.2 (a) and (b) represent the entire stabilometric signal in the AP direction, and the separated lines between the truth segments can be observed. Fig. 6.2 (c) illustrates the posterior probabilities of the four conditions obtained with the

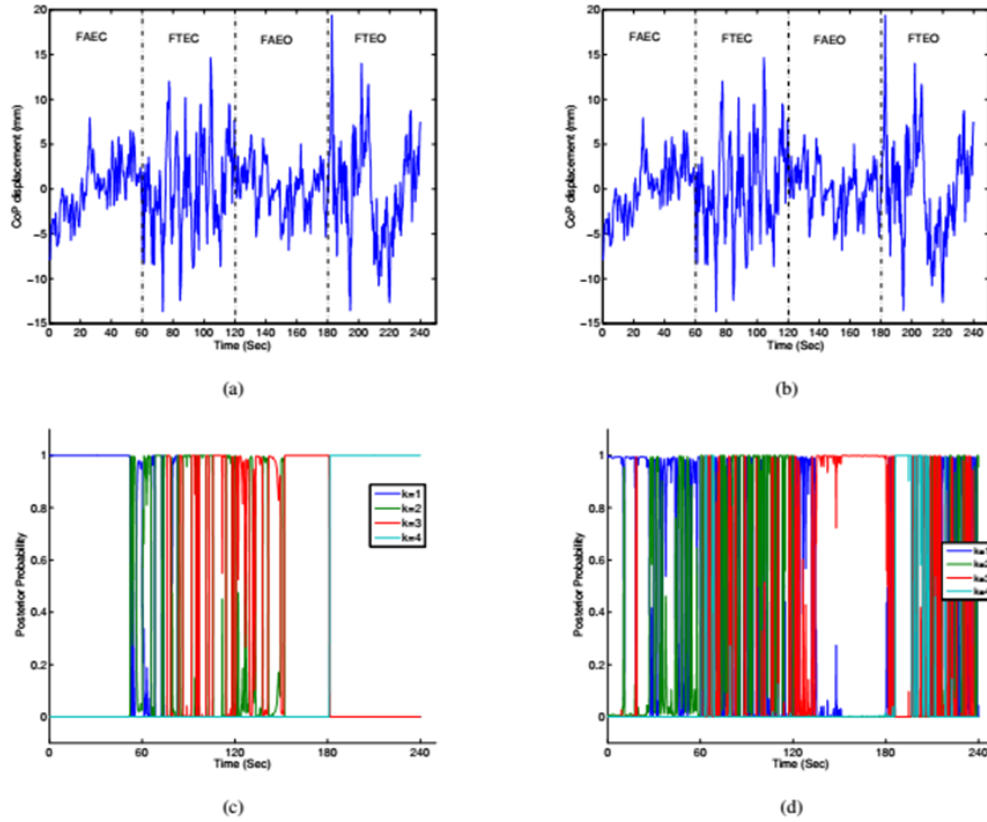


FIGURE 6.2: Results obtained in the case of HMMR (left) and HMM (right) for AP direction with $k=1$: FAEC, $k=2$: FTEC, $k=3$: FAEO, and $k=4$: FTEO.

HMMR model. The regression model k that has the highest posterior probability for a sample i is considered to be the model that generates this sample.

High rates of segmentation are obtained for $k=1$ (FAEC) and $k=4$ (FTEO), although there are some segmentation errors in segments $k=2$ (FAEO) and $k=3$ (FTEC). In contrast, Fig. 6.2 (d), which illustrates the posterior probabilities using the HMM method, shows segmentation errors in all parts of the signal.

In fig. 6.3, similar trends can be observed on the segmentation results obtained for both HMM and HMMR methods in the ML direction. Fig. 6.3 (a) and (b) represent the entire stabilometric signal in the ML direction. For HMMR segmentation, high rates of segmentation are obtained for $k=1$ (FAEC) and $k=2$ (FTEC), and some segmentation errors appear in the later segments : $k=3$ (FAEO) and $k=4$ (FTEO) in Fig. 6.3 (c). However, segmentation errors are observed in all parts of the signal. Fig. 6.3 (d) illustrates the posterior probabilities using the HMM method.

Fig. 6.4 shows the segmentation results using multiple inputs (stabilometric signals for

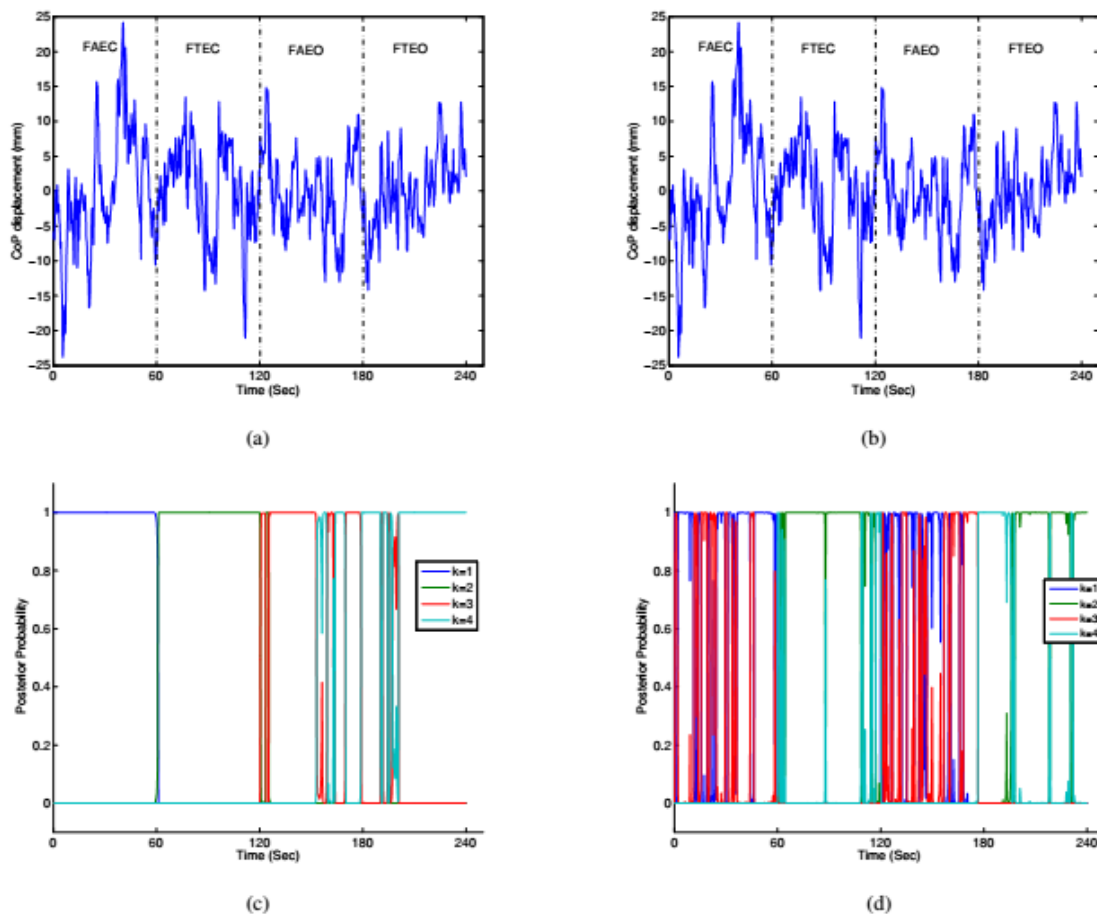


FIGURE 6.3: Results obtained in the case of HMMR (left) and HMM (right) for ML direction with $k=1$: FAEC, $k=2$:FTEC, $k=3$: FAEO, and $k=4$: FTEO.

both AP and ML directions), thus proving that the use of signals from both the AP and ML directions provides more information about the situation of each subject and, consequently, provides results with respect to the one-directional analysis. Fig. 6.4 (a) shows the AP and ML stabilometric signals used for the multiple HMMR model. Fig. 6.4 (b), which illustrates the posterior probabilities obtained with the HMMR method, shows high rates of correct segmentation on all segments. Although the performances obtained using the HMM method are relatively acceptable, they still suffer from important segmentation errors, as shown in fig. 6.4 (c).

Tables 6.1 and 6.2 represent the confusion matrices in the case of HMMR segmentation using AP and ML signals, respectively. It should be noted that the rates of correct segmentation (classification) in ML direction are higher than those in AP direction, except under the last condition (FTEO). One can notice that the classification errors of a given condition with respect to its neighborhood condition present small rates in the ML direction but show relatively high error rates in the AP direction.

TABLE 6.1: Confusion Matrix for AP direction

		Predicted Class			
		FAEC	FTEC	FAEO	FTEO
True Class	FAEC	95.70	4.29	0	0
	FTEC	5.53	72.55	21.91	0
	FAEO	0	25.14	72.05	2.79
	FTEO	0	0	2.24	97.75

TABLE 6.2: Confusion Matrix for ML direction

		Predicted Class			
		FAEC	FTEC	FAEO	FTEO
True Class	FAEC	97.94	2.05	0	0
	FTEC	2.38	96.22	1.38	0
	FAEO	0	4.22	92.11	3.65
	FTEO	0	0	8.49	91.50

TABLE 6.3: Confusion Matrix for both AP and ML directions

		Predicted Class			
		FAEC	FTEC	FAEO	FTEO
True Class	FAEC	100	0	0	0
	FTEC	0	97.83	2.16	0
	FAEO	0	3.31	96.66	0
	FTEO	0	0	2.16	97.82

Table 6.3 shows the confusion matrix obtained for HMMR segmentation for both the AP and ML directions. It shows better results compared to those shown in tables 6.1 and 6.2, where the minimum classification rate is greater than 96%.

TABLE 6.4: Correct classification rates (%) obtained with the different methods

Method	Rate ML (%)	Rate AP (%)	Rate Planar (%)
KNN	51.2	47.1	79.6
CART	46.2	42.6	74.7
RF	51.3	47.2	81.6
HMM	58.2	53.4	72.9
HMMR	94.2	85.2	98.5

Five well-known classification methods were used to assess the performance of the HMMR method for stabilometric signals segmentation : K-nearest neighbours (K-NN), decision tree (CART), random forest (RF) [109–111]. These methods are all supervised classification techniques and require a training process. The true class labels are used as inputs for the training set with the number of segments (groups = 4). After the training

phase, the class labels obtained from the test set are compared with the true labels, and the correct classification rates are calculated with regards to all classifiers.

Table 6.4 gives the correct segmentation (classification) rates using different classification methods with respect to ML and AP directions, both separately and together. The correct classification rates in the AP and ML directions are 85.2% and 94.2%, respectively, for the HMMR method and less than 60% for the remaining methods. The use of multiple inputs (both AP and ML signals) improves the performances of all classifiers. The correct classification rates are 79.6% and 81.6% for K-NN and RF, respectively. The HMMR method gives the best results, with a 98.5% correct segmentation (classification) rate.

In addition to its high performance, the HMMR method is an unsupervised method that does not need data labelling for the segmentation process. Additionally, it does not need any pre-processing tasks, and the model is learned automatically from the raw data.

6.4.2 Segmentation based on feet and visual conditions of PD subjects

TABLE 6.5: Correct classification rates (%) obtained with PD subjects using HMM and HMMR.

Method	Rate (%)	ML	Rate (%)	AP	Rate Planar (%)
HMM	57.3		49.4		63.6
HMMR	87.8		75.7		89.9

Fig. 6.5 shows the segmentation results obtained using multiple inputs (stabilometric signals with respect to both AP and ML directions) for PD subjects. Fig. 6.5 (a) shows an example of a stabilometric signal related to a PD subject in both the AP and ML directions.

TABLE 6.6: Confusion Matrix for both AP and ML directions (Planar) for PD subjects

		Predicted Class			
		FAEC	FTEC	FAEO	FTEO
True Class	FAEC	88.03	11.96	0	0
	FTEC	23.60	74.48	1.90	0
	FAEO	0	5.72	94.27	0
	FTEO	0	0	0	100

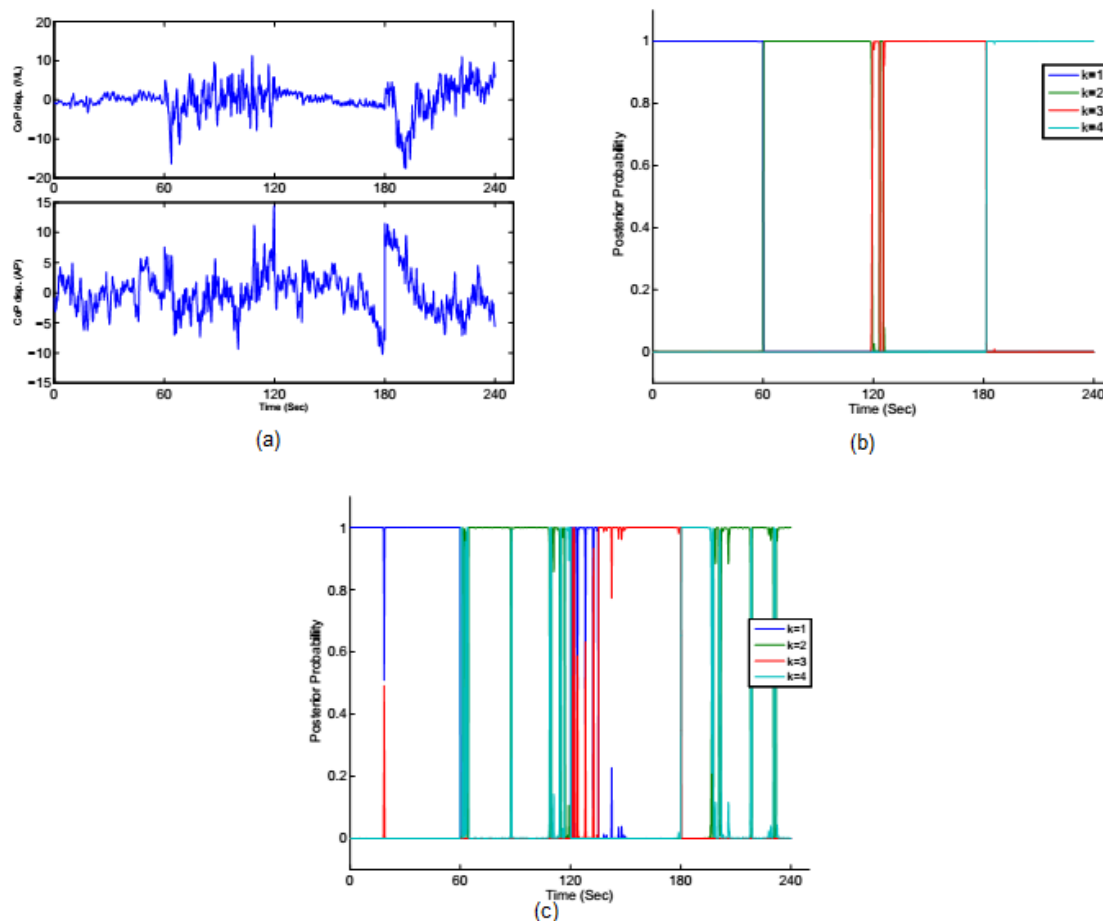


FIGURE 6.4: Results obtained with HMMR (b) and HMM (c) for multi-input AP and ML directions (a) for healthy subjects with $k=1$: FAEC, $k=2$:FTEC, $k=3$: FAEO, and $k=4$: FTEO.

Fig. 6.5 (b) gives the posterior probabilities obtained using the HMMR approach. One can observe relatively high rates of correct segmentation, although there are some errors in the posterior probabilities related to some segments. These results are still satisfactory compared to those obtained with the classical HMM method, which shows important errors in the posterior probabilities (Fig. 6.5 (c)).

Table 6.5 shows the correct classification rates obtained with the ML and AP directions separately as simple inputs and together as multiple inputs. The results obtained with multiple inputs (both ML and AP signals) show better segmentation than does the simple input case with both HMM and HMMR methods.

As we can see, the results obtained with HMMR are better than those obtained with the standard HMM method. For example, HMM and HMMR obtained correct classification rates in the ML direction of 57.3% and 87.8% respectively, in the case of single input

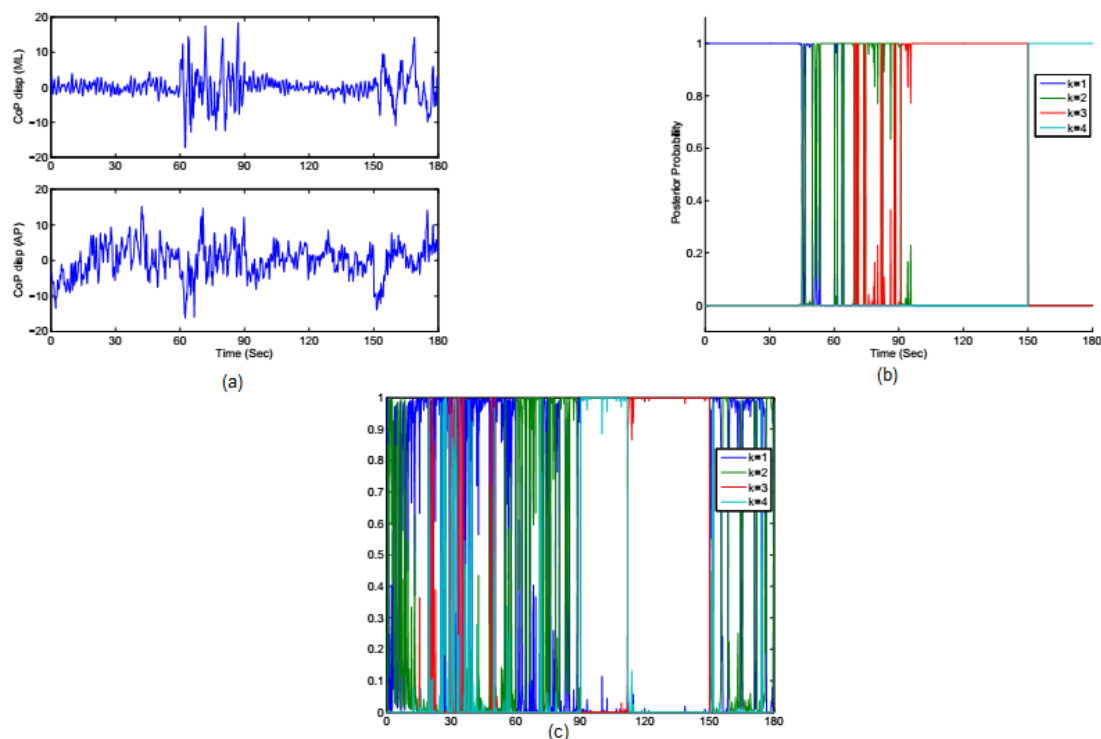


FIGURE 6.5: Results obtained with HMMR (b) and HMM (c) for multi-input AP and ML directions (a) for PD subjects with $k=1$: FAEC, $k=2$:FTEC, $k=3$: FAEO, and $k=4$: FTFO.

(AP or ML directions). They grew to 63.6% and 89.9% respectively with multiple input (ML/AP).

These performances can be compared to those discussed previously for healthy subjects. Note that the HMMR method provides high segmentation rates for healthy subjects (up to 98%) and for PD subjects (up to 89%). This can be explained by the fact that the visual input and foot position have more influence on human stability with healthy subjects. These factors also influence PD subjects but remain relatively limited.

6.5 Conclusion

The human postural system can be affected by several conditions such as visual input and feet position. In this chapter, an automatic segmentation approach of the stabilometric signals is proposed to segment signals under visual and feet conditions. This is achieved to prove whether the HMMR is capable of automatically detecting the variation in structures of signals between these conditions. This approach allows to automatically detect the variation in structures of stabilometric signals between these conditions. The model

is learned in an unsupervised context by maximizing the observed-data log-likelihood via a dedicated expectation-maximization (EM) algorithm. The performances obtained with multiple regression are better than those obtained with simple regression. The HMMR shows satisfactory results for signal segmentation between the used-conditions. The present findings could help clinicians to better understand the motor strategies used by the patients during their orthostatic postures and may guide the rehabilitation process.

Chapitre 7

GENERAL CONCLUSION AND PERSPECTIVES

7.1 Conclusion

This thesis addresses the issue of postural stability analysis. This is a research topic whose results can be exploited in the postural system behaviors analysis, diagnosis of PD subjects, prevention of falls, etc. Four approaches were proposed as contributions of this thesis.

The first approach deals with the human stability analysis in quiet standing using the EEMD method and the stabilogram-diffusion analysis technique. The EEMD method allows to decompose the stabilometric signal into a finite number of elementary signals called IMFs. The stabilogram-diffusion analysis technique is then applied on each IMF to generate the diffusion curve. Each diffusion curve is modeled as a second order system and provides representative features, such as, the gain and CP parameters. These parameters are used to assess the postural stability and to analyze the influence of the visual input, feet position conditions, age and gender on the human stability. The obtained results show a high sensitivity of the extracted parameters under the aforementioned conditions, and more precisely : (1) the human stability under eyes-open condition is higher than under eyes-closed condition ; (2) the human body under feet-apart condition is more stable than under feet-together condition especially, in ML condition ; (3) the young subjects show postural stability higher than elderly subjects with significant differences ; (4) the women subjects show higher postural stability compared to men subjects ; (5) the extracted parameters better characterize the stabilometric signals than the standard parameters used in the literature.

The second approach allows to discriminate between healthy and PD subjects using their stabilometric signals. This approach consists of four steps. In the first step, for each stabilometric signal, the first eight IMFs, obtained from EEMD method, are selected for further processing. In the second step, temporal and spectral characteristics are extracted from raw stabilometric data and their corresponding IMFs. In the third step, a feature selection method is applied to retain the first five relevant characteristics. In the fourth step, four well-known classification methods, including KNN, CART, RF and support vector machine (SVM) are used for the classification task. The obtained results show that the proposed approach is efficient for classifying PD subjects with classification rates up to 96%. The classifiers based on the IMFs data can classify subjects with better performances than those based on raw data. The best results were obtained under

FTEO condition. This can be explained by the fact that under feet together condition, the stability of PD subjects becomes lower, and therefore, PD subjects become more distinguishable from healthy ones.

The third approach is an HMM-based method for differentiating between healthy and PD subjects using their raw stabilometric data. This approach consists of constructing two HMM models : the first model (H-HMM) was constructed using the training healthy subjects data, and the second model (PD-HMM) was learned by the training dataset of PD subjects. Healthy and PD subjects are classified first using either ML or AP stabilometric signals, and then using signals from both ML and AP directions. The classification task of test subjects is carried out as follows : The observation probabilities of each test subject is computed for the H-HMM and PD-HMM models. The highest value between these two probabilities determines the class to which the test subject belongs. The classification performances obtained using this approach are better than those obtained in the previous chapter. The sensitivity and the specificity are 100% and 96.4% respectively, while the overall accuracy is equal to 98.4%.

The last approach addresses the problem of the automatic segmentation of stabilometric signals recorded under four different conditions related to vision and feet position. The Hidden Markov Model Regression (HMMR) approach is used to ensure the segmentation of the stabilometric signals related to the different conditions. The advantage of the used approach relies mainly in its capability to operate in an unsupervised context that avoids data labeling phase that is often time/computation efforts consuming, particularly in the case of massive databases. The segmentation was done based on a multiple HMMR regression process between the different conditions using ML, AP, and ML/AP signals. The HMMR shows excellent results for signal segmentation between the different conditions with up to 98% in terms of overall accuracy. The performances obtained with multiple regression are better than those obtained with simple regression. The outcome of this study may help the clinicians to better understand the motor strategies used by the subjects during quiet standing and may provide a guideline for the rehabilitation process.

7.2 Perspectives

The perspectives resulting from this thesis can be summarized as follows :

- From an algorithmic point of view

1. Extension of the EMD method for bivariate analysis in order to decompose the stabilometric signals in AP and ML directions together.
2. Integration of a selection model in the HMMR-based approach that guarantees the automatic identification of the segment number without any prior knowledge.
3. Extraction of non-linear parameters, such as Lyapunov exponent, sample Entropy, from the IMFs extracted from the stabilometric data, and usage of other machine learning based approaches in the classification task.

- From an application point of view :

1. Classification between healthy/PD, women/men, young/elderly based on gain and CP parameters.
2. Classification between healthy/PD, women/men, young/elderly based on the regression model parameters of segmentation process, proposed in chapter VI. Indeed, other extracted parameters, such as the regression coefficients β , may be considered as potential parameters that may impact the overall classification rate and necessitate further investigations.
3. Applying the used classification approaches in order to discriminate between different levels of PD subjects.
4. Exploring the feasibility of the proposed approaches to characterize human postural stability in the case of dynamic human postures, running and walking activities and gait pathologies.

Bibliographie

- [1] S. Bouisset and J.-L. Duchêne, “Is body balance more perturbed by respiration in seating than in standing posture?.” *Neuroreport*, vol. 5, no. 8, pp. 957–960, 1994.
- [2] C. De Luca, R. LeFever, M. McCue, and A. Xenakis, “Control scheme governing concurrently active human motor units during voluntary contractions,” *The Journal of physiology*, vol. 329, no. 1, pp. 129–142, 1982.
- [3] T. Takeya, “A biofeedback study of postural sway,” *Psychiatry and Clinical Neurosciences*, vol. 30, no. 4, pp. 495–504, 1976.
- [4] K. Imamura, T. Mano, and S. Iwase, “One minute wave of body sway related to muscle pumping during static standing in human,” in *Proc. Of the Xth Internat. Symposium on Disorders of Posture and Gait. FRG : Munchen*, 1990, pp. 2–6.
- [5] F. Spoor, T. Garland, G. Krovitz, T. M. Ryan, M. T. Silcox, and A. Walker, “The primate semicircular canal system and locomotion,” *Proceedings of the National Academy of Sciences*, vol. 104, no. 26, pp. 10 808–10 812, 2007.
- [6] L. Chiari, L. Rocchi, and A. Cappello, “Stabilometric parameters are affected by anthropometry and foot placement,” *Clinical Biomechanics*, vol. 17, no. 9, pp. 666–677, 2002.
- [7] M. S. Redfern, L. Yardley, and A. M. Bronstein, “Visual influences on balance,” *Journal of anxiety disorders*, vol. 15, no. 1, pp. 81–94, 2001.
- [8] D. Abrahamová and F. Hlavacka, “Age-related changes of human balance during quiet stance,” *Physiological Research*, vol. 57, no. 6, pp. 957–964, 2008.
- [9] S. M. Freitas, S. A. Wiczorek, P. H. Marchetti, and M. Duarte, “Age-related changes in human postural control of prolonged standing,” *Gait & posture*, vol. 22, no. 4, pp. 322–330, 2005.

- [10] J. W. Blaszczyk, F. Prince, M. Raiche, and R. Hébert, “Effect of ageing and vision on limb load asymmetry during quiet stance,” *Journal of Biomechanics*, vol. 33, no. 10, pp. 1243–1248, 2000.
- [11] U. Granacher, S. A. Bridenbaugh, T. Muehlbauer, A. Wehrle, and R. W. Kressig, “Age-related effects on postural control under multi-task conditions,” *Gerontology*, vol. 57, no. 3, pp. 247–255, 2010.
- [12] M. L. Callisaya, L. Blizzard, M. D. Schmidt, J. L. McGinley, and V. K. Srikanth, “Ageing and gait variability, a population-based study of older people,” *Age and ageing*, vol. 39, pp. 191–197, 2010.
- [13] B. Amblard and A. Carblanc, “Rôle des informations fovéales et périphériques dans le maintien de l’équilibre postural chez l’homme,” *Agressologie*, vol. 19, pp. 21–28, 1978.
- [14] “<http://www.hftb.org/eye-diseases.html>.”
- [15] D. E. Angelaki and K. E. Cullen, “Vestibular system : the many facets of a multimodal sense,” *Annu. Rev. Neurosci.*, vol. 31, pp. 125–150, 2008.
- [16] M. G. Gaerlan, “The role of visual, vestibular, and somatosensory systems in postural balance,” Ph.D. dissertation, University of Nevada Las Vegas, 2010.
- [17] “<https://www.britannica.com/science/ear>.”
- [18] F. B. Horak, “Postural orientation and equilibrium : what do we need to know about neural control of balance to prevent falls?” *Age and ageing*, vol. 35, pp. 7–11, 2006.
- [19] P. Serra-Añó, L. López-Bueno, X. García-Massó, M. T. Pellicer-Chenoll, and L.-M. González, “Postural control mechanisms in healthy adults in sitting and standing positions,” *Perceptual and motor skills*, vol. 121, no. 1, pp. 119–134, 2015.
- [20] N. W. Mok, S. G. Brauer, and P. W. Hodges, “Hip strategy for balance control in quiet standing is reduced in people with low back pain,” *Spine*, vol. 29, no. 6, pp. E107–E112, 2004.
- [21] B. Colobert, A. Crétual, P. Allard, and P. Delamarche, “Force-plate based computation of ankle and hip strategies from double-inverted pendulum model,” *Clinical biomechanics*, vol. 21, no. 4, pp. 427–434, 2006.

- [22] Y. Kanamiya, S. Ota, and D. Sato, “Ankle and hip balance control strategies with transitions,” in *Proc. of the IEEE International Conference on Robotics and Automation (ICRA 2010)*. Anchorage, USA, May 3, 7, 2010, pp. 3446–3451.
- [23] “quizlet.com/85848481/pta-232-balance-flash-cards/.”
- [24] “ada-posturologie.fr/vierordtdebout.htm.”
- [25] M. Goffredo, M. Schmid, S. Conforto, and T. DAlessio, “A markerless sub-pixel motion estimation technique to reconstruct kinematics and estimate the centre of mass in posturography,” *Medical engineering & physics*, vol. 28, no. 7, pp. 719–726, 2006.
- [26] M. Günther, S. Grimmer, T. Siebert, and R. Blickhan, “All leg joints contribute to quiet human stance : a mechanical analysis,” *Journal of biomechanics*, vol. 42, no. 16, pp. 2739–2746, 2009.
- [27] M. Mancini, A. Salarian, P. Carlson-Kuhta, C. Zampieri, L. King, L. Chiari, and F. B. Horak, “Isway : a sensitive, valid and reliable measure of postural control,” *Journal of neuroengineering and rehabilitation*, vol. 9, no. 1, pp. 59–66, 2012.
- [28] D. Lafond, H. Corriveau, R. Hébert, and F. Prince, “Intrasession reliability of center of pressure measures of postural steadiness in healthy elderly people,” *Archives of physical medicine and rehabilitation*, vol. 85, no. 6, pp. 896–901, 2004.
- [29] T. E. Prieto, J. B. Myklebust, R. G. Hoffmann, E. G. Lovett, and B. M. Myklebust, “Measures of postural steadiness : differences between healthy young and elderly adults,” *IEEE Transactions on Biomedical Engineering*, vol. 43, no. 9, pp. 956–966, 1996.
- [30] B. Maki, P. Holliday, and G. Fernie, “Aging and postural control,” *Journal of the American Geriatrics Society*, vol. 38, no. 1, pp. 1–9, 1990.
- [31] D. Lafond, M. Duarte, and F. Prince, “Comparison of three methods to estimate the center of mass during balance assessment,” *Journal of biomechanics*, vol. 37, no. 9, pp. 1421–1426, 2004.
- [32] D. A. Winter, A. E. Patla, F. Prince, M. Ishac, and K. Gielo-Periczak, “Stiffness control of balance in quiet standing,” *Journal of neurophysiology*, vol. 80, no. 3, pp. 1211–1221, 1998.

- [33] S. S. Hasan, D. W. Robin, D. C. Szurkus, D. H. Ashmead, S. W. Peterson, and R. G. Shiavi, "Simultaneous measurement of body center of pressure and center of gravity during upright stance. part i : Methods," *Gait & posture*, vol. 4, no. 1, pp. 1–10, 1996.
- [34] A. A. Priplata, J. B. Niemi, J. D. Harry, L. A. Lipsitz, and J. J. Collins, "Vibrating insoles and balance control in elderly people," *The Lancet*, vol. 362, no. 9390, pp. 1123–1124, 2003.
- [35] D. L. King and V. M. Zatsiorsky, "Extracting gravity line displacement from stabilographic recordings," *Gait & Posture*, vol. 6, no. 1, pp. 27–38, 1997.
- [36] T. Shimba, "An estimation of center of gravity from force platform data," *Journal of Biomechanics*, vol. 17, no. 1, pp. 53–60, 1984.
- [37] A. Karlsson and H. Lanshammar, "Analysis of postural sway strategies using an inverted pendulum model and force plate data," *Gait & Posture*, vol. 5, no. 3, pp. 198–203, 1997.
- [38] O. Levin and J. Mizrahi, "An iterative model for estimation of the trajectory of center of gravity from bilateral reactive force measurements in standing sway," *Gait & Posture*, vol. 4, no. 2, pp. 89–99, 1996.
- [39] P. Rougier, C. Burdet, I. Farenc, and L. Berger, "Backward and forward leaning postures modelled by an fbm framework," *Neuroscience research*, vol. 41, no. 1, pp. 41–50, 2001.
- [40] Y. Breniere and C. Ribreau, "A double-inverted pendulum model for studying the adaptability of postural control to frequency during human stepping in place," *Biological cybernetics*, vol. 79, no. 4, pp. 337–345, 1998.
- [41] O. Caron, B. Faure, and Y. Brenière, "Estimating the centre of gravity of the body on the basis of the centre of pressure in standing posture," *Journal of biomechanics*, vol. 30, no. 11, pp. 1169–1171, 1997.
- [42] B. J. Benda, P. Riley, and D. Krebs, "Biomechanical relationship between center of gravity and center of pressure during standing," *IEEE Transactions on Rehabilitation Engineering*, vol. 2, no. 1, pp. 3–10, 1994.

- [43] J. Yang, D. Winter, and R. Wells, "Postural dynamics in the standing human," *Biological Cybernetics*, vol. 62, no. 4, pp. 309–320, 1990.
- [44] D. A. Winter, "Overall principle of lower limb support during stance phase of gait," *Journal of biomechanics*, vol. 13, no. 11, pp. 923–927, 1980.
- [45] F. Horak and A. Kuo, "Postural adaptation for altered environments, tasks, and intentions," in *Biomechanics and neural control of posture and movement*. Springer, 2000, pp. 267–281.
- [46] W. McIlroy and B. Maki, "Task constraints on foot movement and the incidence of compensatory stepping following perturbation of upright stance," *Brain research*, vol. 616, no. 1, pp. 30–38, 1993.
- [47] S. Moore, D. Rushmer, S. Windus, and L. Nashner, "Human automatic postural responses : responses to horizontal perturbations of stance in multiple directions," *Experimental brain research*, vol. 73, no. 3, pp. 648–658, 1988.
- [48] F. Scoppa, R. Capra, M. Gallamini, and R. Shiffer, "Clinical stabilometry standardization : basic definitions–acquisition interval–sampling frequency," *Gait & posture*, vol. 37, no. 2, pp. 290–292, 2013.
- [49] W. McIlroy and B. Maki, "Preferred placement of the feet during quiet stance : development of a standardized foot placement for balance testing," *Clinical Biomechanics*, vol. 12, no. 1, pp. 66–70, 1997.
- [50] D. A. Winter, "Human balance and posture control during standing and walking," *Gait & posture*, vol. 3, no. 4, pp. 193–214, 1995.
- [51] A. V. Alexandrov, A. A. Frolov, F. Horak, P. Carlson-Kuhta, and S. Park, "Feedback equilibrium control during human standing," *Biological cybernetics*, vol. 93, no. 5, pp. 309–322, 2005.
- [52] E. Mira, "Improving the quality of life in patients with vestibular disorders : the role of medical treatments and physical rehabilitation," *International journal of clinical practice*, vol. 62, no. 1, pp. 109–114, 2008.
- [53] D. A. Winter, A. E. Patla, S. Rietdyk, and M. G. Ishac, "Ankle muscle stiffness in the control of balance during quiet standing," *Journal of Neurophysiology*, vol. 85, no. 6, pp. 2630–2633, 2001.

- [54] C. Maurer, T. Mergner, B. Bolha, and F. Hlavacka, “Vestibular, visual, and somatosensory contributions to human control of upright stance,” *Neuroscience letters*, vol. 281, no. 2, pp. 99–102, 2000.
- [55] T. Mergner, C. Maurer, and R. Peterka, “A multisensory posture control model of human upright stance,” *Progress in brain research*, vol. 142, pp. 189–201, 2003.
- [56] R. Peterka, “Sensorimotor integration in human postural control,” *Journal of neurophysiology*, vol. 88, no. 3, pp. 1097–1118, 2002.
- [57] L. Chiari, L. Rocchi, and A. Cappello, “Stabilometric parameters are affected by anthropometry and foot placement,” *Clinical Biomechanics*, vol. 17, no. 9, pp. 666–677, 2002.
- [58] S. Nejc, R. Jernej, S. Loeffler, and H. Kern, “Sensitivity of body sway parameters during quiet standing to manipulation of support surface size,” *Journal of sports science & medicine*, vol. 9, no. 3, pp. 431–438, 2010.
- [59] S. Ramdani, B. Seigle, J. Lagarde, F. Bouchara, and P. L. Bernard, “On the use of sample entropy to analyze human postural sway data,” *Medical engineering & physics*, vol. 31, no. 8, pp. 1023–1031, 2009.
- [60] O. Caron, P. Fontanari, J. Cremieux, and F. Joulia, “Effects of ventilation on body sway during human standing,” *Neuroscience letters*, vol. 366, no. 1, pp. 6–9, 2004.
- [61] S. G. Brauer, Y. R. Burns, and P. Galley, “A prospective study of laboratory and clinical measures of postural stability to predict community-dwelling fallers,” *The Journals of Gerontology Series A : Biological Sciences and Medical Sciences*, vol. 55, no. 8, pp. M469–M476, 2000.
- [62] R. W. Baloh, K. M. Jacobson, K. Beykirch, and V. Honrubia, “Static and dynamic posturography in patients with vestibular and cerebellar lesions,” *Archives of Neurology*, vol. 55, no. 5, pp. 649–654, 1998.
- [63] L. Rocchi, L. Chiari, and A. Cappello, “Feature selection of stabilometric parameters based on principal component analysis,” *Medical and Biological Engineering and Computing*, vol. 42, no. 1, pp. 71–79, 2004.

- [64] H. Amoud, H. Snoussi, D. Hewson, and J. Duchêne, “Univariate and bivariate empirical mode decomposition for postural stability analysis,” *EURASIP Journal on Advances in Signal Processing*, vol. 2008, no. 1, pp. 1–11, 2008.
- [65] H. Amoud, M. Abadi, D. J. Hewson, V. Michel-Pellegrino, M. Doussot, and J. Duchêne, “Fractal time series analysis of postural stability in elderly and control subjects,” *Journal of NeuroEngineering and Rehabilitation*, vol. 4, no. 1, pp. 12–23, 2007.
- [66] J. J. Collins and C. J. De Luca, “The effects of visual input on open-loop and closed-loop postural control mechanisms,” *Experimental Brain Research*, vol. 103, no. 1, pp. 151–163, 1995.
- [67] —, “Open-loop and closed-loop control of posture : a random-walk analysis of center-of-pressure trajectories,” *Experimental brain research*, vol. 95, no. 2, pp. 308–318, 1993.
- [68] —, “Random walking during quiet standing,” *Physical review letters*, vol. 73, no. 5, pp. 764–767, 1994.
- [69] J. A. O. Carneiro, T. E. G. Santos-Pontelli, J. F. Colafêmina, A. A. O. Carneiro, and E. Ferriolli, “Analysis of static postural balance using a 3d electromagnetic system,” *Brazilian journal of otorhinolaryngology*, vol. 76, no. 6, pp. 783–788, 2010.
- [70] H. Tanaka, M. Nakashizuka, T. Uetake, and T. Itoh, “The effects of visual input on postural control mechanisms : an analysis of center-of-pressure trajectories using the auto-regressive model.” *Journal of human ergology*, vol. 29, no. 1/2, pp. 15–25, 2000.
- [71] J. W. Blaszczyk, “The use of force-plate posturography in the assessment of postural instability,” *Gait & posture*, vol. 44, pp. 1–6, 2016.
- [72] A. A. Priplata, J. B. Niemi, J. D. Harry, L. A. Lipsitz, and J. J. Collins, “Vibrating insoles and balance control in elderly people,” *The Lancet*, vol. 362, no. 9390, pp. 1123–1124, 2003.
- [73] D. C. Gravelle, C. A. Laughton, N. T. Dhruv, K. D. Katdare, J. B. Niemi, L. A. Lipsitz, and J. J. Collins, “Noise-enhanced balance control in older adults,” *Neuroreport*, vol. 13, no. 15, pp. 1853–1856, 2002.

- [74] A. Gabell, M. Simons, and U. Nayak, "Falls in the healthy elderly : predisposing causes," *Ergonomics*, vol. 28, no. 7, pp. 965–975, 1985.
- [75] P. Overstall, A. Exton-Smith, F. Imms, and A. Johnson, "Falls in the elderly related to postural imbalance." *Br Med J*, vol. 1, no. 6056, pp. 261–264, 1977.
- [76] D. Prudham and J. G. Evans, "Factors associated with falls in the elderly : a community study." *Age and Ageing*, vol. 10, no. 3, pp. 141–146, 1981.
- [77] A. Khasnis, R. Gokula *et al.*, "Romberg's test." *Journal of postgraduate medicine*, vol. 49, no. 2, p. 169, 2003.
- [78] D. A. Winter, "Human balance and posture control during standing and walking," *Gait & posture*, vol. 3, no. 4, pp. 193–214, 1995.
- [79] P. Cordo and L. M. Nashner, "Properties of postural adjustments associated with rapid arm movements," *Journal of neurophysiology*, vol. 47, no. 2, pp. 287–302, 1982.
- [80] J. S. Frank and M. Earl, "Coordination of posture and movement," *Physical therapy*, vol. 70, no. 12, pp. 855–863, 1990.
- [81] J. Błaszczuk, R. Orawiec, D. Duda-Kłodowska, and G. Opala, "Assessment of postural instability in patients with parkinsons disease," *Experimental Brain Research*, vol. 183, no. 1, pp. 107–114, 2007.
- [82] L. Rocchi, L. Chiari, A. Cappello, and F. B. Horak, "Identification of distinct characteristics of postural sway in parkinson's disease : a feature selection procedure based on principal component analysis," *Neuroscience letters*, vol. 394, no. 2, pp. 140–145, 2006.
- [83] M. A. McVey, A. P. Stylianou, C. W. Luchies, K. E. Lyons, R. Pahwa, S. Jernigan, and J. D. Mahnken, "Early biomechanical markers of postural instability in parkinson's disease," *Gait & posture*, vol. 30, no. 4, pp. 538–542, 2009.
- [84] F. B. Horak, D. Dimitrova, and J. G. Nutt, "Direction-specific postural instability in subjects with parkinson's disease," *Experimental neurology*, vol. 193, no. 2, pp. 504–521, 2005.

- [85] B. Schoneburg, M. Mancini, F. Horak, and J. G. Nutt, "Framework for understanding balance dysfunction in parkinson's disease," *Movement disorders*, vol. 28, no. 11, pp. 1474–1482, 2013.
- [86] G. Kerr, S. Morrison, and P. Silburn, "Coupling between limb tremor and postural sway in parkinson's disease," *Movement Disorders*, vol. 23, no. 3, pp. 386–394, 2008.
- [87] A. Frenklach, S. Louie, M. M. Koop, and H. Bronte-Stewart, "Excessive postural sway and the risk of falls at different stages of parkinson's disease," *Movement Disorders*, vol. 24, no. 3, pp. 377–385, 2009.
- [88] J. W. Błaszczyk and R. Orawiec, "Assessment of postural control in patients with parkinsons disease : sway ratio analysis," *Human movement science*, vol. 30, no. 2, pp. 396–404, 2011.
- [89] J. C. Menant, M. D. Latt, H. B. Menz, V. S. Fung, and S. R. Lord, "Postural sway approaches center of mass stability limits in parkinson's disease," *Movement Disorders*, vol. 26, no. 4, pp. 637–643, 2011.
- [90] L. Palmerini, L. Rocchi, S. Mellone, F. Valzania, and L. Chiari, "Feature selection for accelerometer-based posture analysis in parkinson's disease," *IEEE Transactions on Information Technology in Biomedicine*, vol. 15, no. 3, pp. 481–490, 2011.
- [91] B. Brewer, S. Pradhan, G. Carvell, and A. Delitto, "Feature selection for classification based on fine motor signs of parkinson's disease," in *Proc. Of the 31th Annual International Conference of the IEEE Engineering in Medicine and Biology Society (EMBC'09)*. Minneapolis, Minnesota, 2009, pp. 214–217.
- [92] M. Zok, C. Mazzà, and A. Cappozzo, "Should the instructions issued to the subject in traditional static posturography be standardised?," *Medical engineering & physics*, vol. 30, no. 7, pp. 913–916, 2008.
- [93] W. McIlroy and B. Maki, "Preferred placement of the feet during quiet stance : development of a standardized foot placement for balance testing," *Clinical Biomechanics*, vol. 12, no. 1, pp. 66–70, 1997.

- [94] M. G. Carpenter, J. S. Frank, D. A. Winter, and G. W. Peysar, "Sampling duration effects on centre of pressure summary measures," *Gait & posture*, vol. 13, no. 1, pp. 35–40, 2001.
- [95] N. E. Huang, Z. Shen, S. R. Long, M. C. Wu, H. H. Shih, Q. Zheng, N.-C. Yen, C. C. Tung, and H. H. Liu, "The empirical mode decomposition and the hilbert spectrum for nonlinear and non-stationary time series analysis," in *Proceedings of the Royal Society of London A : Mathematical, Physical and Engineering Sciences*, vol. 454, no. 1971. The Royal Society, 1998, pp. 903–995.
- [96] G. Rilling, P. Flandrin, P. Goncalves *et al.*, "On empirical mode decomposition and its algorithms," in *Proc. Of the IEEE-EURASIP workshop on nonlinear signal and image processing*, vol. 3, 2003, pp. 8–11.
- [97] G. Rilling, "Décompositions modales empiriques. contributions à la théorie, l'algorithme et l'analyse de performances," Ph.D. dissertation, Ecole normale supérieure de lyon, 2007.
- [98] O. Niang, É. Deléchelle, and J. Lemoine, "A spectral approach for sifting process in empirical mode decomposition," *IEEE Transactions on Signal Processing*, vol. 58, no. 11, pp. 5612–5623, 2010.
- [99] N. E. Huang *et al.*, "Introduction to the hilbert-huang transform and its related mathematical problems," *Hilbert-Huang transform and its applications, interdisciplinary mathematical sciences*, vol. 5, pp. 1–24, 2005.
- [100] Z. Wu and N. E. Huang, "Statistical significance test of intrinsic mode functions," *Hilbert-Huang Transform and Its Applications*, pp. 107–127, 2005.
- [101] J.-C. Nunes and E. Deléchelle, "Empirical mode decomposition : Applications on signal and image processing," *Advances in Adaptive Data Analysis*, vol. 1, no. 01, pp. 125–175, 2009.
- [102] M. Blanco-Velasco, B. Weng, and K. E. Barner, "Ecg signal denoising and baseline wander correction based on the empirical mode decomposition," *Computers in biology and medicine*, vol. 38, no. 1, pp. 1–13, 2008.

- [103] S. Li, W. Zhou, Q. Yuan, S. Geng, and D. Cai, "Feature extraction and recognition of ictal eeg using emd and svm," *Computers in biology and medicine*, vol. 43, no. 7, pp. 807–816, 2013.
- [104] H. Liang, Q.-H. Lin, and J. Chen, "Application of the empirical mode decomposition to the analysis of esophageal manometric data in gastroesophageal reflux disease," *IEEE Transactions on Biomedical Engineering*, vol. 52, no. 10, pp. 1692–1701, 2005.
- [105] J. Guo, S. Qin, and C. Zhu, "The application of energy operator demodulation approach based on emd in mechanical system identification," in *Proc. Of the 19th IEEE International Conference Mechatronics and Machine Vision in Practice (M2VIP 2012)*, 2012, pp. 80–85.
- [106] Z. Wu and N. E. Huang, "Ensemble empirical mode decomposition : a noise-assisted data analysis method," *Advances in adaptive data analysis*, vol. 1, no. 01, pp. 1–41, 2009.
- [107] N. Enriquez, "A simple construction of the fractional brownian motion," *Stochastic Processes and their Applications*, vol. 109, no. 2, pp. 203–223, 2004.
- [108] B. B. Mandelbrot and J. W. Van Ness, "Fractional brownian motions, fractional noises and applications," *SIAM review*, vol. 10, no. 4, pp. 422–437, 1968.
- [109] T. Cover and P. Hart, "Nearest neighbor pattern classification," *IEEE transactions on information theory*, vol. 13, no. 1, pp. 21–27, 1967.
- [110] L. Breiman, J. Friedman, C. J. Stone, and R. A. Olshen, *Classification and regression trees*. CRC press, 1984.
- [111] L. Breiman, "Random forests," *Machine learning*, vol. 45, no. 1, pp. 5–32, 2001.
- [112] ———, "Bagging predictors," *Machine learning*, vol. 24, no. 2, pp. 123–140, 1996.
- [113] V. Vapnik, *The nature of statistical learning theory*. Springer-Verlag, 1995.
- [114] L. E. Baum, T. Petrie, G. Soules, and N. Weiss, "A maximization technique occurring in the statistical analysis of probabilistic functions of markov chains," *The annals of mathematical statistics*, vol. 41, no. 1, pp. 164–171, 1970.

- [115] L. R. Rabiner, “A tutorial on hidden markov models and selected applications in speech recognition,” *Proceedings of the IEEE*, vol. 77, no. 2, pp. 257–286, 1989.
- [116] A. J. Viterbi, “Error bounds for convolutional codes and an asymptotically optimum decoding algorithm,” *IEEE Transactions on Information Theory*, vol. 13, no. 2, pp. 260–269, 1967.
- [117] M. Fridman, “Hidden markov model regression,” Ph.D. dissertation, Graduate School of Arts and Sciences, University of Pennsylvania, 1993.

List of Publications

Journals :

- K. Safi, S. Mohammed, F. Attal, Y. Amirat, M. Khalil, J-M Gracies and E. Hutin, "Automatic Segmentation of Stabilometric Signals using Hidden Markov Model Regression", Accepted on *IEEE Transactions on Automation sciences and Engineering*, (Dec 2016).
- K. Safi, S. Mohammed, I-M. Albertsen, E. Delechelle, Y. Amirat, M. Khalil, J-M. Gracies, E. Hutin, "Automatic Analysis of Human Posture Equilibrium using Empirical Mode Decomposition", Accepted on *Signal, Image, and Video Processing journal*, (Jan. 2017).

International Conferences :

- K. Safi, A. Diab, I-M. Albertsen, E. Hutin, S. Mohammed, M. Khalil, Y. Amirat, "Non-linear analysis of human stability during static posture", in *Proc. Of the International Conference on Advances in Biomedical Engineering (ICABME 2015)*, Beirut, Lebanon, pp. 285-288, 2015.
- K. Safi, F. Attal, S. Mohammed, M. Khalil, Y. Amirat, "Physical activity recognition using inertial wearable sensors. A review of

- supervised classification algorithms”, in *Proc. Of the International Conference on Advances in Biomedical Engineering (ICABME 2015)*, Beirut, Lebanon, pp. 313-316, 2015.
- K. Safi, E. Hutin, S. Mohammed, M. Albertsen, E. Delechelle, Y. Amirat, M. Khalil, J-M. Gracies, ”Human Static Postures Analysis using Empirical Mode Decomposition”, in *Proc. Of the IEEE 38th Annual International Conference on Engineering in Medicine and Biology Society (EMBC 2016)*, Florida, USA, pp. 3765-3768, 2016.
 - K. Safi, S. Mohammed, F. Attal, M. Khalil, Y. Amirat, ”Recognition of different daily living activities using Hidden Markov Model Regression”, *Accepted to appear in Proc. Of the 3rd Middle East Conference on Biomedical Engineering (MECBME16)*, Beirut, Lebanon, pp. 16-19, 2016.
 - K. Safi, I-M. Albertsen, E. Hutin, E. Delechelle, S. Mohammed, M. Khalil, Y. Amirat, J-M. Gracies, ”The Effect of Feet Position on the Human Stability during Static Postures”, in *Proc. Of the 21th LAAS International Science Conference (LAAS’15)*, 2015.